

**RECONSTRUCTION OF THE PHYSICAL
VOLCANOLOGICAL PROCESSES AND
PETROGENESIS OF THE 3.5GA
WARRAWOONA GROUP PILLOW BASALT
OF THE WARRALONG GREENSTONE
BELT, PILBARA CRATON WESTERN
AUSTRALIA**

Thomas Frederick David Spring

Bachelor of Applied Science (Geology)

Submitted in fulfilment of the requirements for the degree of

Master of Applied Science (Geoscience)

School of Earth, Environment and Biological Science

Faculty of Science and Engineering

Queensland University of Technology

2017

Abstract

The formation of Earth's continental crust initiated in the early Archean and has continued to the present day. In the early Archean, the Earth was substantially hotter than the present day leading to dramatically different tectonic processes. Early Archean tectonic processes have to be inferred from the rare well-preserved remnants of Archean crust. Models for the formation of Archean crust include large scale mantle melting associated with mantle plumes to generate thick basaltic to ultramafic crust. This crust then undergoes partial melting and internal differentiation to more felsic compositions.

The Pilbara craton provides an ideal area for research into the Archean crust, with some of Earth's oldest crust being preserved in relatively low strain and low metamorphosed greenstone belts. The volcanic cycles preserved in the greenstone belts of the Paleoproterozoic East Pilbara Terrane of the Pilbara craton represent the type example of plume-derived volcanism in the early Earth.

Here I investigate the lithostratigraphy, volcanology and depositional environment of a volcanic and sedimentary succession ascribed to the Warrawoona group of the East Pilbara Supergroup from the Eastern Warralong Greenstone belt of the East Pilbara Terrane. In addition, I investigate the petrogenesis of well-preserved basaltic samples from the pillow basalt sequence ascribed to the Mt Ada Basalts in the study area.

While the greenstone succession is significantly dismembered by at least three deformation events, it is possible to piece together a coherent stratigraphy that was deposited in a deep water environment with cherts, turbidites and vesicle free pillow basalts. The Mount Ada basaltic unit exclusively consists of pillow basalts implying low effusion rates.

The Mt Ada pillow basalts contain abundant leucocratic globules, here referred to as ocelli. I demonstrate that the ocelli represent a liquid immiscibility feature rather than either sperulitic crystallisation or magma mingling between a mafic melt and a felsic melt. The geochemistry of the Mt Ada pillow basalts demonstrate low Th/Nb ratios that are consistent either with derivation from a hydrated mantle source or crustal contamination.

The association of low effusion rate pillow lavas and deep-water cherts suggest that this section of the Warralong greenstone belt formed in a relatively low energy environment distal from major sediment sources and with low rates of volcanism. This is not consistent with the predictions of a plume source for the Mt Ada basalts.

Table of Contents

Abstract.....	i
Table of Contents.....	iii
List of Figures.....	v
Statement of Original Authorship.....	ix
Acknowledgements.....	x
Chapter 1: Introduction	13
Chapter 2: Background Geology	17
Geological Setting.....	17
Implications and Aims	26
Chapter 3: Methodology.....	29
Mapping, Logging and Volcanology Observations	29
Petrology.....	30
Sample preparation for geochemistry	31
Loss on ignition.....	31
X-Ray Fluorescence (XRF) – Major Element Analysis	32
Inductively Coupled Plasma Mass Spectroscopy – Trace Element Analysis	32
Electron Probe Microanalysis	32
Melts Modelling.....	33
Chapter 4: Stratigraphic Architecture of the Warralong Greenstone Belt.....	35
Lithostratigraphy and Facies Analysis.....	38
Yellow Meta-Chert	38
Eastern Pillowed Meta-Basalt.....	39
Eastern Psammite.....	39
Eastern Chert.....	41
Central Pillowed Meta-Basalt	43
Western Psammite	49
Western Chert	51
Western Pillow basalt Unit	52
Gabbro Intrusions.....	53
Deformation	53
Chapter 5: Geochemistry	56
Alteration	56
Host Basalts Major Elemental Oxides versus LOI.....	56
Ocelli Major Element and LOI Variation	58
Whole Rock Elemental Data.....	60
Microprobe Analysis.....	67
Chapter 6: Discussion	69
Stratigraphy and Emplacement Processes.....	69

Depositional Environment	73
Petrogenesis of ocelli bearing basalts	74
Petrogenesis of ocelli	75
Petrogenesis of Central Pillow Basalt Unit	79
Volcanic Conditions.....	81
Geodynamics of the Archaean	83
Chapter 7: Conclusions	87
Bibliography	91
Appendices 101	
Appendix A Sample Locations	101
Appendix B High MgO vs Lower MgO Basalt Sample Locations.....	102
Appendix C LOI Results of Basalts and Ocelli from the Eastern Warralong green stone belt	103
Appendix D Trace Element Composition of Basalts and Ocelli from the Eastern Warralong green stone belt (ppm).	105
Appendix E Major Element Composition of Basalts and Ocelli from the Eastern Warralong green stone belt (w%)	109
Appendix F Micro Probe analysis of host basalts and ocelli from the Eastern Warralong green stone belt (ppm)	110

List of Figures

Figure 1. Geological map of the Pilbara Craton displaying the different terranes and basins; black box denotes the location of the Warralong Greenstone belt that represents the research area for this project; adapted from Hickman 2012.	18
Figure 2. Stratigraphic sequence from East Pilbara terrane (modified from Hickman, 2012)	21
Figure 3. Recorded unit of the Eastern portion of the Warralong Greenstone belt (Van Kranendonk et al., 2004a), compared to the currently accepted stratigraphy of the Warrawoona group. Modified from Hepple (2014).	24
Figure 4a. Research area of the WGB highlighted by red box; exert from Western Australia Geological map 2856: Western Australian Geological Survey 1:100 000 (Van Kranendonk et al., 2004a)	25
Figure 4b. Lithology Key; exert from Western Australia Geological map 2856: Western Australian Geological Survey 1:100 000 (Van Kranendonk et al., 2004a)	26
Figure 5. Digital field map of the Warralong Greenstone Belt, denoting the structural observations and outcrops mapped during field work.	36
Figure 6. Stratigraphic representation of the Warralong Greenstone Belt showing distribution of pillow sizes in the best preserved sections.	37
Figure 7: Hand specimen of Yellow Chert (TS-26).....	39
Figure 8. Stereonet plot of tilted bedding planes within the Eastern Psammite and Eastern Chert.....	41
Figure 9. Photomicrograph taken of TS-24-1-14 and example of the eastern Psammite taken at low magnification in plain polarised light (left) and cross polarised light (right). Image shows an example of the typical mineralogy and textures observed within the Eastern meta-sediment. The rock consists of Silicified volcanoclastic clasts with common vesicles and pseudomorphs after plagioclase in quartz/barite cement. (Image width = 31 mm)	41
Figure 10. Image showing gradational contact between the Eastern Psammite and the Eastern Chert.....	42
Figure 11. Image of fractured red chert, by secondary white quartz veins.....	42
Figure 12. Photomicrograph of thin-section TS-27-1-14, an example of thin-sections observed from the eastern chert unit. Image taken at low magnification with transmitted plain polarised light (left) and cross polarised light (right). The rock is formed out of predominantly microcrystalline quartz that has been brecciated	

by vein quartz, the black minerals are hematite and in rare case magnetite (Image width = 31 mm).....	43
Figure 13. Figure A shows a set of stacked pillows with carbonated inter pillowed hyaloclastite between pillows and circled hyaloclastite. Image B is an example of a pillow with multiple cavities, as a results from multiple pulses of lava through the pillow. Cavities denoted by white out line and pillow extent denoted by black outline. (Rock hammer 30cm)	44
Figure 14. Stereonet of planar flow tops of pillows and flow tubes within pillows, taken from outcrops within the mapping area.	45
Figure 15. Ocelli size as a percentage of pillows measured. (Locations shows in appendix B)	46
Figure 16. Ocelli abundance as a percentage of pillows measure. (Locations shows in appendix B)	46
Figure 17. Image of cut surface of sample TS-37-1-14. The image shows the quenched rim of the pillowed basalt as well as evidence of possible multiple flows and disseminated ocelli (2 to 5 mm).	47
Figure 18. Photomicrograph taken at low magnification of whole thin section photomosaic of sample TS-2 in (A) plane polarised light and (B) cross polarised light, with 2 ocelli in a basaltic matrix. The basaltic matrix is alteration due to low-grade metamorphism, dominated by primary pyroxene in an altered matrix predominantly made up of chlorite, calcite and quartz. The image also shows a preserved ocellis and the distinct boundary between it and the host basalt. The ocelli samples have similar mineralogy with preserved primary pyroxenes in a more altered matrix dominated by chlorite and carbonate.	48
Figure 19. Stereonet of sedimentary layering of the western sedimentary unit.....	49
Figure 20. Image of western meta-sediments, note the repetitive sequence of sandstone, mudstones and cherts. Image shows medium-fine grained sandstone topped with fine-grained mudstone and cherts in part. (Rock hammer ~30cm long) Location 20°49'17.7"/119°30'51.4".....	50
Figure 21. Microscopic image taken at low magnification with transmitted polarised light (left) and transmitted cross polarised light (right). Image shows the typical mineralogical observed within the sandstone beds from the Western meta-sedimentary unit. (Image width = 31 mm) The Image shows a number of small clasts of finely microcrystalline quartz in a recrystallized silica rich matrix with earthy secondary iron oxides and hematite.....	51
Figure 22, Image of unit E, thinly laminated red, black and white cherts at base, with large veins of secondary white chert crosscutting bedding and running along bedding. (Rock hammer ~30cm) location E20°49'16.7" N119°31'03.5".....	52

Figure 23. Stereonet of the S1 foliation within and around lozenges.	54
Figure 24. Stereonet of fault foliation from the D3 deformation event listed.....	55
Figure 25. Elemental oxide wt% for host basalt versus LOI. Note that although wt% values for LOI increase the values for SiO ₂ , Al ₂ O ₃ , TiO ₂ and P ₂ O ₅ , are very constant, whereas the values for FeO, CaO and MgO become more scattered at higher (>5%) LOI.	57
Figure 26. Elemental oxide wt% for host basalt (green triangles) and corresponding ocelli samples (red squares) 343-1, 344-2, TS-2- 1, TS-31-1 and JDK-69 versus LOI.	58
Figure 27. TAS diagram used for classifying volcanic rock types based on geochemical analysis (after Le Bas et al., 1986, Fig 2). This diagram is typically used to determine rock types of fresh unweathered and unaltered rocks; however the rocks within the research area have undergone some alteration and weathering. Smithies (2007) data from the Mount Ada Basalts analysed form other greenstone belts have been plotted for comparison.....	60
Figure 28. Basalt classification for samples with available major element analysis. Recreated from Viljoen et al. (1982) and recalculated as anhydrous. Smithies (2007) data from the MAB have been plotted for comparison.	61
Figure 30. Harker diagrams showing the chemical variation observed in the host basalt and ocelli. Diagram A, C and E are examples of the host basalts versus ocelli in relation to smithies (2007) data. Diagrams B, D and F are examples of trace element segregation between the different host basalts and ocelli samples.	63
Figure 30. REE diagram normalised to chondrite showing the enrichment of REE in the Ocelli as well as the higher proportion of light REE enrichment.	64
Figure 31. Trace element diagram normalised to N MORB Sun & McDonough (1989), showing variations in trace elements across the samples.	65
Figure 32. Host basalt and ocelli elements ppm versus MgO. Note that both the host basalts and the ocelli samples are enriched in Cr and Ni (ppm).	65
Figure 33. Zr/Nb vs Nb/Th shows a hydrated mantle signature in both the host basalts and ocelli samples (Condie, 2015). HM = Hydrated Mantle, DM = Depleted Mantle and EM = Enriched Mantle.	66
Figure 34. Pyroxene Classification Ternary Diagram, showing the Clinopyroxenes tested in both the Ocelli and Host basalt plot together. Three samples were selected for their well preserved pyroxenes in both the ocelli and the host basalt, TS- 2-1, TS-31-1 and 344-2.	67

Figure 35. Harker diagrams showing the chemical variation observed in the host basalt and ocelli within the remnant pyroxenes compared to modern volcanic settings. Note the overlapping geochemical result for the ocelli and host basalts. MORB and Oceanic Plateau data obtained from PetDB (http://www.earthchem.org/petdb)	68
Figure 36. Figure taken from Gregg and Fink 1995; showing influence of cooling rate, slope and flow rate on submarine morphology.	72
Figure 37. Photomicrograph of supercooling spherulitic textures forming within ocelli as presented by Monecke et al. (2004), scale bare 1 mm.....	76
Figure 38. Digital mosaic image of ocelli bearing samples in plane polarised light (A & B) TS-334-1 where (B) is a close up of the ocelli host contact and (C & D) JDK 69 where (D) is a close up of the ocelli host contact. The images show the ocelli and host basalt relationship with very distinct rims. Both the host basalt and the ocelli contain pyroxene micro-phenocrysts. The preserved magmatic texture in the ocelli are not consistent with spherulitic textures.	77
Figure 39. Multi elemental spider diagram of combined trace elements normalised to MORB, the defined negative and positive anomalies noted within the individual melts is consistent when compared to the combined elemental spider diagram.	81
Figure 40. Archean mantle temperatures from a modelling and petrology perspective. Mantle temperatures from studies by Puchtel et al (2013) and Connolley et al. (2011) using protocols from both McKenzie and Bickle (1988) and Herberg and Asimow (2008) compared to Korenagas (2006) model for ambient mantle temperature and the recorded liquidus temperatures from the Warralong Greenstone belt.....	83

Statement of Original Authorship

The work contained in this thesis has not been previously submitted to meet requirements for an award at this or any other higher education institution. To the best of my knowledge and belief, the thesis contains no material previously published or written by another person except where due reference is made.

QUT Verified Signature

Signature:

Date: March 2017

Acknowledgements

David Murphy, for instilling a love and fascination for the Pilbara that I will keep with me for the rest of my life. For taking that, and creating the opportunity for me to do research with fantastic people. Thanks for helping through the many difficult and often trying stages of this research, and for believing in my ability as a geologist to complete it.

Jessica Trofimovs for providing detailed and constructive reviews of my drafts, especially in relation to litho-stratigraphy and volcanological emplacement.

I would like to thank all the biogeosciences academic and technical staff at Queensland University of Technology for their generosity, passion and assistance. To name a few of those who have been of massive help: Courtney Innes, David Gust and Tony Raftery.

Fieldwork would not have been possible without the help of the Western Australia Geological Survey who provided the field equipment including a field ready 4WD, camping and safety equipment. I experienced their efficiency and generosity when learning practical recovery skills for 4x4 driving and supplying the vehicle. Particular thanks needs to be made to Arthur Hickman also of the Western Australia Geological Survey for offering his wealth of knowledge and experience in our endeavours.

I would like to acknowledge the laboratory staff at the Queensland University of Technology for their dedication to their work and for their time teaching me laboratory methods and procedures, and the long hours spent running my samples. In

particular I would like to thank Tri Nguyen, Sunni Hu and Irina Kinaev for being on the receiving end of many a question and staying long after-hours to run my samples.

To Daniel Wiemer, for your patience in explaining to me some of the most obvious geological field observations and helping me get through 5 weeks of the most gruelling field experience I have ever had. For letting me bounce ideas and analysis off you. To Shoshanna and Ali for helping us through the field work.

To my darling wife Tatiana, I could not have completed this without your patience and your keen eye when reading drafts. You kept me going and believing I could finish my research.

To my company and employer, for allowing me the flexibility and time to complete this personal goal.

Chapter 1: Introduction

Earth's earliest history is poorly understood, with processes during this time leading to the only known inhabited planet in the Universe. Understanding and explaining how the Earth's early crust formed is important when trying to determine how the Earth has evolved (Harrison et al., 2008; Harrison, 2009; Cawood et al., 2013; Kemp et al., 2015b; Nebel et al., 2014a).

Approximately 60-70% of the present volume of continental crust formed during the Archean (Cawood et al., 2013; Hawkesworth et al., 2013), however, less than 10% of current outcropping crust consists of Archean-aged rocks (Griffin et al., 2004; Cawood et al., 2013). This is due to crustal reworking, whereby old crust is reworked and recycled during plate tectonics Wilson cycles.

Archean crust has been dominantly preserved as granite-greenstone terranes in variably preserved states around the globe (Furnes et al., 2015). Such terranes have been studied in Australia, South Africa, North America, South America, Asia, Europe and Canada, (Condie, 1981; Furnes et al., 2011; Hickman, 2012; Dostal and Mueller, 2013; Furnes et al., 2013; Kröner et al., 2013; Puchtel et al., 2013; Hepple, 2014; Van Kranendonk et al., 2015). Granite-greenstone terranes are characterized by dome-and-keel structures, where volcanic and sedimentary rocks are wedged between dome-shaped granite-gneiss-pegmatitic structures (Marshak et al., 1992), and are a classic map pattern seen in Archean terranes (Van Kranendonk et al., 2004b). There are two main components that make up granite-greenstone terranes, one being granitoid bodies that are often near synchronous with the emplacement of the second component, the Greenstone belts, which are dominated by metamorphosed supercrustal volcanics and sediments (Kröner et al., 2013).

Such granite-greenstone terranes provide the only direct evidence for early crustal forming tectono-thermal processes (Van Kranendonk, 2001; Van Kranendonk et al., 2001; Van Kranendonk et al., 2004b; Smithies et al., 2005; Van Kranendonk et al., 2007; Hickman and Resources, 2008; Cawood et al., 2013; Hawkesworth et al., 2013; Nebel et al., 2014a). As research into this area has progressed, two main theories have been suggested to explain the formation of these Archaean terranes. The uniformitarian theory suggests that the granite-greenstone terranes and their associated dome-and-keel structures are the result of a tectonic environment similar to today's plate-tectonic-style geodynamics (Hickman, 1974; Glikson, 2013; Wyman, 2013). The second theory favours vertical processes that are responsible for whole-crustal volcanic resurfacing, similar to what has been observed on present-day Venus (Anhaeusser, 1975; Van Kranendonk and Collins, 1998; Smithies et al., 2005; Kloppenburg et al., 2001; Van Kranendonk et al., 2002; Hickman, 2004; Van Kranendonk et al., 2004b; Hickman et al., 2010b; Hickman, 2012;).

That komatiites, which are ultramafic magmas (Arndt et al., 2008), are preserved in most Archean granite-greenstone terranes (Campbell et al., 1989; Grove and Parman, 2004; Arndt et al., 2008; Dostal, 2008) indicates that the formation of these terranes included processes that could generate very high degree partial melts of the mantle (Condie, 1981; Furnes et al., 2011; Dostal and Mueller, 2013; Furnes et al., 2013; Kröner et al., 2013; Puchtel et al., 2013;).

Komatiite magmatism require above ambient mantle temperatures such as deep mantle derived plumes. Ambient mantle temperature in the Archean has been suggest to be ~1680°C (Arndt, 1977; Campbell et al., 1989; Arndt and Nisbet, 2012; Puchtel et al., 2013; Leverington, 2014; Sossi et al., 2016) while the komatiites of the Barberton have been suggested to have formed from melting temperatures of

~1740°C to 1830°C (Furnes et al., 2011; Robin-Popieul et al., 2012; Kröner et al., 2013; Puchtel et al., 2013;).

Komatiites in the Early Archean have been heavily studied, although they form a minority of the rock types preserved (Polat and Kerrich, 2000; de Wit, 2004; Dostal, 2008; Hickman and Resources, 2008). Most Archean Greenstone belts are dominated by basaltic rocks of tholeiitic to high magnesium basalt origin (Furnes et al., 2015) commonly including ocelli bearing pillow basalts, and are often interbedded with felsic and sedimentary sequences (Polat and Kerrich, 2000; Van Kranendonk et al., 2002; de Wit, 2004; Grove and Parman, 2004; Dostal, 2008; Hickman and Resources, 2008; Dostal and Mueller, 2013; Furnes et al., 2013; Nebel et al., 2014a) .

The East Pilbara Terrane (EPT), Western Australia, has an age range of 3.80-2.83 Ga (Hickman, 2012) and contains low metamorphic grade (lower greenschist facies) and low strain granite-greenstone associations. The EPT is therefore an ideal area to conduct research on Earth's Archean crust. While many research papers have presented different models for the formation of the EPT (Zegers et al., 1996; Van Kranendonk and Collins, 1998; Kloppenburg et al., 2001; Van Kranendonk et al., 2001; Van Kranendonk and Australia, 2001; Van Kranendonk et al., 2002; Van Kranendonk et al., 2004b; Van Kranendonk et al., 2008; Hickman, 2008, 2009, 2012; Hickman and Resources, 2008; Hickman et al., 2010b), there is a significant lack of research into the primary processes of emplacement such as eruption styles, the origin of ocelli in pillow basalts, lateral continuity of volcanic stratigraphy and their implications for melting dynamics in the Archean. This project will focus on a section of near continuous stratigraphic sedimentary and ocelli bearing pillow basalt volcanic sequence within the Eastern Warralong Greenstone Belt (EWGB) that is assigned to the Warrawoona Group of the East Pilbara Supergroup (Van Kranendonk

et al., 2001; Hickman and Resources, 2008) to determine the possible deposition environments, emplacement mechanisms and basaltic petrogenesis. Petrogenetic constraints from geochemical data obtained from lava flows within the EWGB coupled with physical volcanology and morphological analysis will be used to determine the depositional environment. Emplacement processes and depositional environmental conditions (such as water depth and volcanic effusion rate) can be constrained by analysing the vesiculation of pillow basalt (Moore, 1965; Jones, 1969; Furnes et al., 2011) and the volume percentage of pillow lava versus massive/sheet flow lava distribution (Griffiths and Fink, 1992b; Gregg and Fink, 1995; White et al., 2002; Furnes et al., 2011). Geochemical analysis as well as petrology will be used to determine the petrogeneses and mechanisms of formation for the central pillow basalt unit and the associated ocelli. This will allow for a comparison with available data for comparison with other Warrawoona Group successions in other EPT Greenstone belts.

Chapter 2: Background Geology

Geological Setting

The Archean Pilbara Craton is located in the north of Western Australia and consists of five segmented terranes ranging in age from 3.80 Ga. to 2.83 Ga (Figure 1). The terranes include the Regal Terrane, Karratha Terrane, Sholl Terrane, East Pilbara Terrane (EPT) and Kurrana Terrane (Figure 1); (Hickman, 1981; Hickman, 1983, 2012; Smithies et al., 2009; Smithies, 2007; Van Kranendonk et al., 2004a; Van Kranendonk et al., 2008). The EPT is one of the Earth's oldest preserved crustal fragments and consists of areas of both high and low-strain and high and low-grade metamorphic outcrops. Unlike other Archean terranes, the EPT has not been substantially reworked by late Archean or Proterozoic metamorphic events. Early interpretations of the evolution of the crust in the EPT were based on the lithostratigraphy, and were a result of detailed systematic mapping undertaken by the Geological Survey of Western Australia (GSWA) during the 1970's (Hickman, 1981; Hickman, 1983; Van Kranendonk et al., 2004a; Van Kranendonk et al., 2004b). In 1995, another major mapping project was launched by the GSWA called the Pilbara Craton Mapping Project (PCMP) and resulted in numerous publications from 2002 onward (Van Kranendonk et al., 2002; Smithies et al., 2003; Hickman, 2004; Smithies et al., 2005; Van Kranendonk, 2006; Smithies, 2007; Van Kranendonk et al., 2007; Hickman and Resources, 2008; Smithies et al., 2009). The nomenclature of the EPT lithostratigraphy has been changed and updated several times since the publication of Hickman's original paper, with current nomenclature derived from Hickman's 2012 paper.

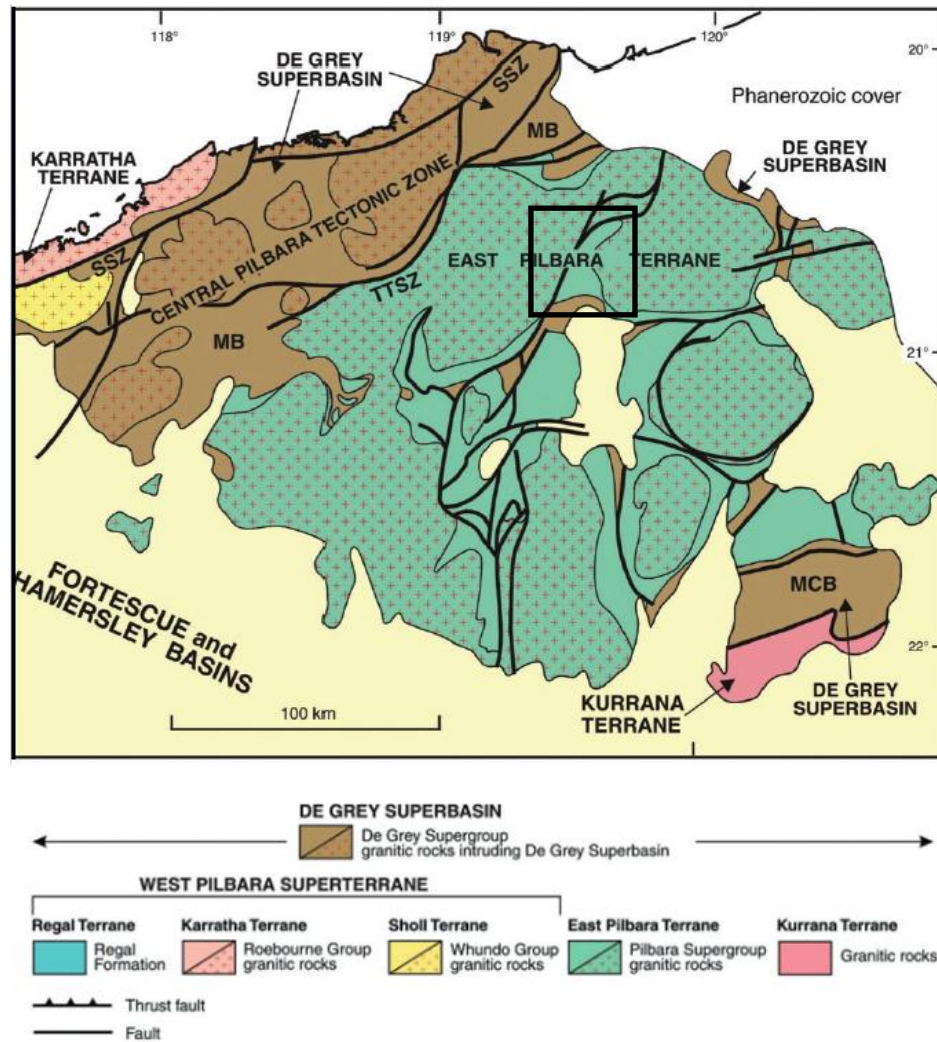


Figure 1. Geological map of the Pilbara Craton displaying the different terranes and basins; black box denotes the location of the Warralong Greenstone belt that represents the research area for this project; adapted from Hickman 2012.

The Pilbara Craton is composed of crust that formed 3.80 – 2.83 Ga, and underlies most of the north-western part of Western Australia (Hickman, 2011; Hickman, 2012; Van Kranendonk et al., 2002). Geophysical data suggests that only 30% of the crust that form the Pilbara craton is exposed with the rest concealed by the overlying 2.78 – 2.45 Ga rock formations of the Fortescue and Hamersley Basin (Hickman, 2012). Geochemical and geochronological data suggests that the Pilbara Craton was initiated 3.80 – 3.55 Ga (Hickman, 2012; Hickman et al., 2010b; Hickman et al., 2011; Smithies et al., 2003; Smithies, 2007; Van Kranendonk et al., 2002; Van Kranendonk et al., 2007), however this very early crust of the Pilbara Craton is very

rarely exposed. The Warrawagine Granitic Complex, Duffer Formation and the Shaw Granitic Complex contain evidence of pre 3.58 Ga xenoliths/enclaves. Rare detrital zircons dated between 3.55-3.8 Ga have been analysed from the De Grey Supergroup, Mallina Basin and the Mosquito Creek basin (Hickman, 2012; Kemp et al., 2015b; Nelson, 2000, 2001, 2005; Smithies et al., 2009; Van Kranendonk et al., 2007). The East Pilbara Terrane (3.53 – 3.22 Ga), is thought to cover an area of about 100 000 km² although much of it does not outcrop (Van Kranendonk, 2001; Van Kranendonk et al., 2004a; Van Kranendonk, 2006; Yuan, 2015). The EPT has undergone six stages of regional deformation (D1-D6). These deformation events include: D₁ deformation and metamorphism due to synvolcanic extension deformation as well as associated local tilting of the Coonterunah Group and Talga Talga Sub group (3.490 – 3.410 Ga), D₂ deformation and metamorphism as well as uplift and erosion during diapirism (3.3 Ga), D₃ deformation and metamorphism due to partial convection overturn and intrusion of the Strelley Granite causing a suite of growth faults (3.24 Ga), D₄ Deformation of much of the North Pilbara resulting in the formation of the northerly striking Lalla Rookh-Western Shaw structural corridor and deposition of the De Grey Group, D₅ Sinistral shearing on north-northeast–striking zones affected the northwestern EPT (2.89 Ga) and D₆ uplift and erosion with a the unconformably overlying Fortescue Group (Van Kranendonk and Collins, 1998; Van Kranendonk et al., 2002; Van Kranendonk, 2010; Van Kranendonk et al., 2015).

The EPT displays a characteristic dome-and-keel map pattern (Figure 1 and 2), of domal granitoid complexes that are flanked by metamorphosed volcano-sedimentary rocks known as greenstone belts. The EPT consists of eight Granitic Complexes (known as the domes): Carlindi, Mount Edgar, Yilgalong, Muccan, Corunna Downs,

Shaw, Warrawagine along with Yule. Between these domes are twenty greenstone belts: Pilbara Well, Cheearra, Wodgina, Abydos, Pincunah, East Strelley, Soanesville, Panorama, North Shaw, Emerald Mine greenstone complex, Tambina greenstone complex, Western Shaw, Coongan, Kelly, Mcphee, Mount Elsie, Marble Bar, Doolena Gap, Warralong and Goldsworthy. The granitoid complexes form anticlinal domes with diameters of 35-120 km (Van Kranendonk, Collins, et. al. 2004), which make up the majority of the exposed EPT. These are thought to be genetically related to the volcanic successions within the greenstone belts. The greenstone belts represent synclinal tracts of steeply dipping to overturned meta-volcano-sedimentary rocks from the Pilbara Supergroup and the greenstone belts commonly contain Mesoarchean sedimentary and volcanic rocks in the synclinal axis.

The Pilbara Supergroup has been mapped in eighteen of the twenty Greenstone belts in the EPT, with the other two, Wodgina and Cheearra, consisting of Mesoarchean formations (Hickman, 2009; Hickman, 2008, 2012; Van Kranendonk et al., 2004a; Van Kranendonk et al., 2002). It is split into three main sub-groups (as well as a number of unassigned groups); these litho-stratigraphic groups are separated by two regional erosional unconformities at 3.43 Ga and 3.27 Ga. From the oldest to youngest these are Warrawoona Group (3.53-3.43 Ga), Kelly Group (3.42-3.32 Ga) and Sulphur Springs Group (3.27-3.23 Ga) - Figure 3.

The Warrawoona and Kelly Groups have been recognised across 13 of the Greenstone belts, and have previously been used to establish that the volcanic successions were not deposited in separate basins or narrow linear belts as they are represented now, but were deposited in a large sedimentary basin (Hickman, 2011; Hickman, 2012; Hickman, 2008; Van Kranendonk, 2006). It is suggested that the

EPT was formed as one large volcanic plateau overlying older crust, with an average thickness estimated between 15 to 20 km (Hickman, 2008; Hickman, 2011; Hickman, 2012; Hickman et al., 2010b; Van Kranendonk, 2006; Van Kranendonk et al., 2007). However, the Warrwoona Group is rarely seen to outcrop in thickness greater 1 km with the exception of the North Pole Dome (Brown et al., 2006) and the Marble Bar greenstone belts (Hickman, 2008; Van Kranendonk, 2006).

The Warrwoona Group is further split into four subgroups: the Coonterunah Subgroup (3.53-3.5 Ga), Talga Talga Subgroup (3.5-3.47 Ga), Coongan Subgroup (3.47-3.45 Ga) and Salgash (3.4-3.42 Ga). The Coongan Subgroup, the focus of this thesis, contains two formations known as the Mount Ada Basalt (MAB) and the Duffer Formation (Hickman, 2009; Hickman, 2008; Hickman et al., 2010a; Hickman et al., 2011; Hickman and Resources, 2008; Van Kranendonk, 2006; Van Kranendonk et al., 2004a; Van Kranendonk et al., 2004b; Van Kranendonk et al., 2002; Van Kranendonk and Pirajno, 2004; Van Kranendonk et al., 2007) (Figure 2).

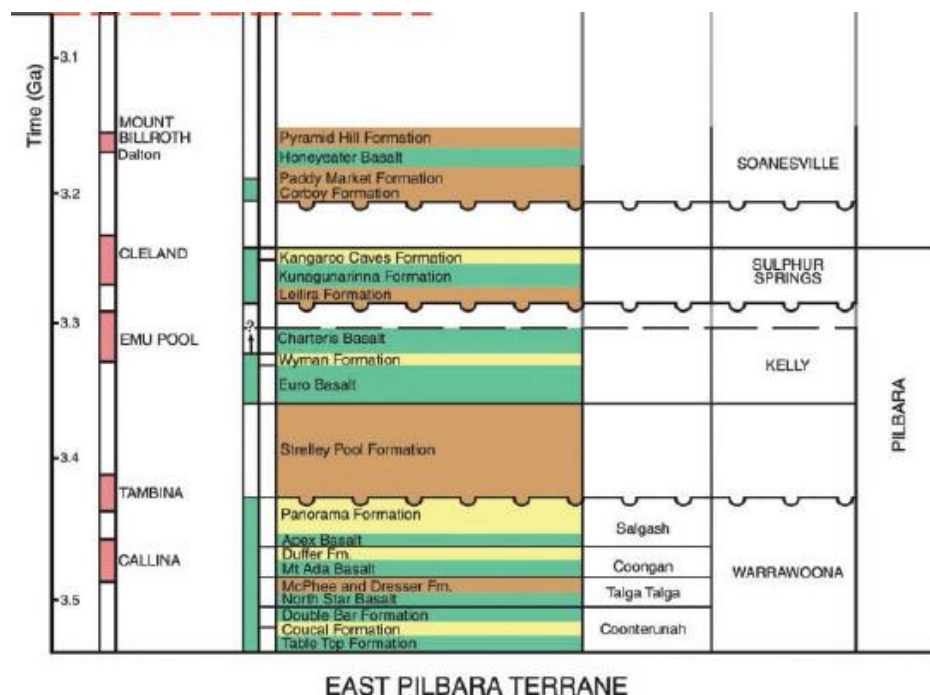


Figure 2. Stratigraphic sequence from East Pilbara terrane (modified from Hickman, 2012)

The MAB has previously been described as 2000-2500 m of interbedded dominantly pillowed metabasalts, metamorphosed pyroxene spinifex-textured komatiitic basalts, and thin horizons of metasedimentary chert and felsic volcanoclastic rocks (Van Kranendonk, 2010). Numerous sills of dolerite and gabbro also intrude into the formation. The MAB has been well preserved and mapped in six Greenstone belts including Panorama, North Shaw, Coongan, Marble Bar, Warralong and Doolena Gap Greenstone belts. Weakly metamorphosed basalt forms the bulk of MAB, and contains common pillows and inter-pillow hyaloclastite (Van Kranendonk, 2010; Van Kranendonk et al., 2004a). It has been shown to conformably overlie either the McPhee Formation or the Dresser Formation of the Talga Talga subgroup in different Greenstone belts and to be conformably overlain by and interbedded with the Duffer Formation.

Warralong Greenstone Belt

There are two distinct components to the Warralong Greenstone Belt, the western succession and the eastern succession that is separated by a significant exposure gap. This study concentrates on the Eastern Warralong Greenstone Belt (EWGB). The EWGB consists of a steeply dipping succession of metavolcanic and metasedimentary rocks of the Pilbara Supergroup (Van Kranendonk, 2010; Van Kranendonk et al., 2004a). The EWGB is preserved between the Muccan and Carlindi Granite complexes (Hickman, 2012; Van Kranendonk et al., 2002). This belt is then unconformably overlain by the De Grey Superbasin to the south (Hickman, 2012; Van Kranendonk et al., 2002).

The stratigraphy of the southern EWGB, the focus of this study, is poorly constrained with no geochronological control. The stratigraphic units within the EWGB have been correlated with similar lithological units in the adjacent Greenstone belts during

large scale geological surveys undertaken by the GSWA (Figure 3). Because of this there is no current research specifically related to the EWGB, it is however rarely mentioned in the GSWA annual reviews. Due to the regional scale of previous studies it was noted that there was a number of observed units had previously not been assigned to the East Pilbara Supergroup stratigraphy or observed as well as assigned to incorrect units. The most eastern units in the EWGB have been correlated to two different units, the McPhee Formation in the south, and the Mount Ada Basalts to the North (Figure 3) (Van Kranendonk, 2010; Van Kranendonk et al., 2004a). As part of the McPhee Formation the eastern chert unit was described as “Grey and white layered chert, and minor felsic tuff, jasper, and limonitic chert; metamorphosed” and as part of the Mount Ada Basalts it was described as “Chert; Generally white, grey and blue-black layered; locally massive blue-grey; weakly metamorphosed” (Figure 3).

The ~1km thick central pillowed meta-basalt unit (Figure 4) is correlated with the Mount Ada Basalt, part of the Coongan Subgroup (Van Kranendonk, 2010). They have previously been described as Komatiitic basalt; commonly pillowed; local pyroxene spinifex texture; weakly metamorphosed (Figure 4b). The Western Psammite unit is correlated with the Duffer Formation and it is described as a volcanogenic sandstone with cherty siltstone tops, carbonated cemented, tubiditic and weakly metamorphosed (Figure 4). The last outcrop forming the end of the research area is the western Chert unit and has previously been mapped as the “Marble Bar Chert Member” part of the Tower Formation, describing it as a grey, white and red layered chert; weakly metamorphosed (Figure 4).

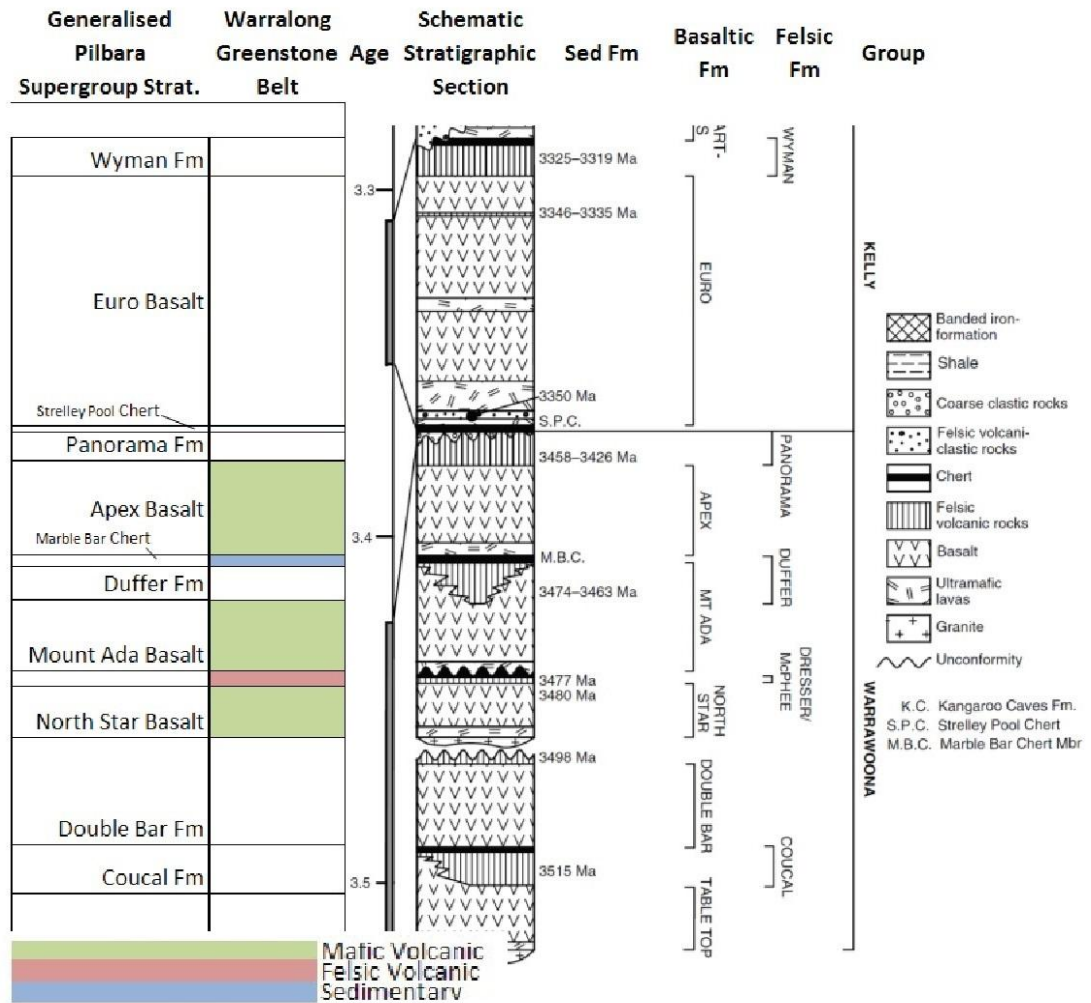
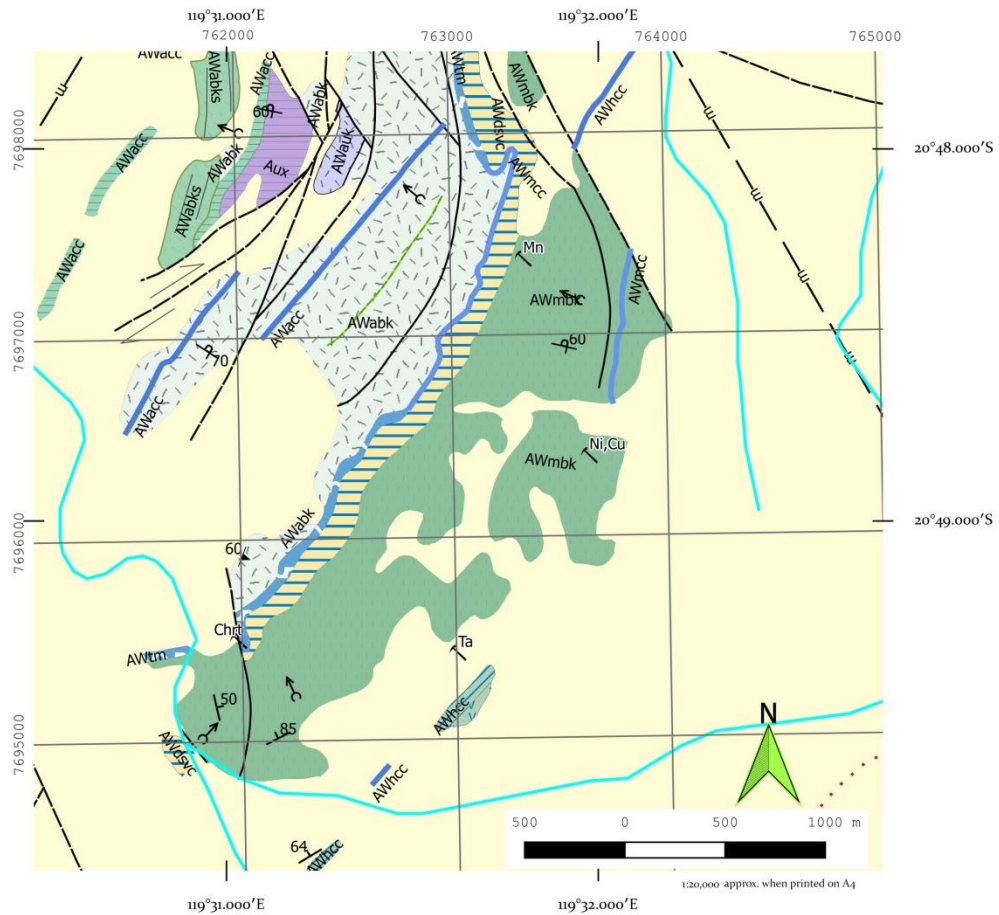


Figure 3. Recorded unit of the Eastern portion of the Warralong Greenstone belt (Van Kranendonk et al., 2004a), compared to the currently accepted stratigraphy of the Warrawoona group. Modified from Hepple (2014).



- | | | | |
|-----------|---|---|--------------------|
| + | Bedding showing strike vertical dip | ⊗ | Abandoned mine |
| ├ | Bedding showing strike and inclined dip | ↖ | Mineral occurrence |
| └ | Bedding overturned | — | Watercourse lines |
| ↑ | Pillow structure way up | | |
| ▲ | Metamorphic Foliation | | |
| — | Fault exposed | | |
| - - - | Fault concealed | | |
| - m - | Fault concealed, derived from aeromagnetic data | | |
| → | Fault relative displacement | | |
| — | Bedding, showing strike of bedding | | |
| · · · · · | Aeromagnetic lineament | | |
| — | Lineament - undefined | | |

Digital data sourced from Dept. of Mines and Petroleum, West Australia. 1:100000 Geological Map - Coongan (2856) 1st Ed. 2004

Coordinate System: GDA 1994 MGA Zone 50
 Projection: Transverse Mercator
 Datum: GDA 1994



Figure 4a. Research area of the WGB highlighted by red box; exert from Western Australia Geological map 2856: Western Australian Geological Survey 1:100 000 (Van Kranendonk et al., 2004a)

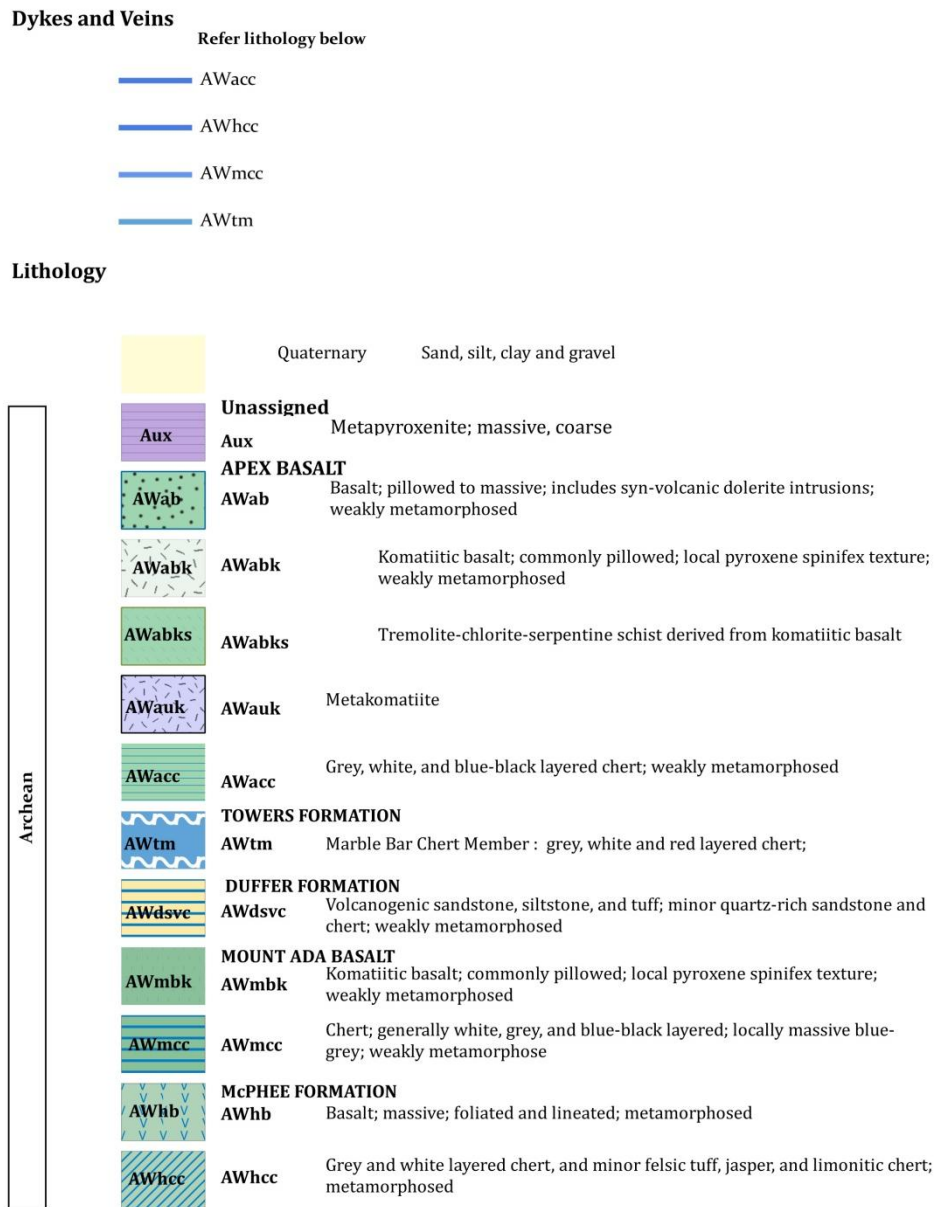


Figure 4b. Lithology Key; excerpt from Western Australia Geological map 2856: Western Australian Geological Survey 1:100 000 (Van Kranendonk et al., 2004a)

Implications and Aims

Of the 20 Greenstone belts in the EPT, only a small number have received significant attention from the geological community. A number of research papers have tried to determine the appropriate units present in a small number of greenstone belts; Marble bar, (Hickman et al., 2010a; Van Kranendonk et al., 2001); Doolena Gap, (Hepple, 2014, Wiemer et al., 2016); and North Shaw, (Van Kranendonk and

Morant, 1997); Western Warralong (Sugitani et al., 2015)) and some papers have tried to determine magmatic petrogenesis (Hickman et al., 2011; Smithies et al., 2003; Smithies et al., 2009; Smithies et al., 2005, 2007). Although much work has been done the models for the early evolution of the EPT are still poorly constrained.

This study aims to answer the following:

- What was the emplacement process, depositional environment and petrogenetic processes of the near continuous stratigraphic sequence preserved within the Eastern Warralong Greenstone Belt?
- What are the petrogenesis and process that led to the formation of the central basalt units and ocelli within the Eastern Warralong Greenstone Belt?
- To add to the discussion on the formation of the East Pilbara Craton.

Chapter 3: Methodology

This section provides an overview of the field and geochemical analysis techniques utilised within this study.

Mapping, Logging and Volcanology Observations

The study area is located in the Eastern Warralong Greenstone belt in the North East of the Pilbara Craton and consists of a 9 km² focus area with 1200 m interrupted stratigraphy exposure in which detailed mapping was undertaken (Figure 2 & 3). The study area was chosen as it represents a low grade metamorphosed and low deformation sequence of the Coongan Subgroup basalts and has areas of well-preserved pillow basalts. This area is bound by lack of exposure to the south and east, with outcrops from the Muccan Dome to the east and De Grey group metasediments to the south. To the west a chert unit ascribed to the Marble Bar Chert Formation was used to demarcate the western extent of the study area.

Measurements of pillow sizes and flow orientations were undertaken in areas that had well preserved pillows. Pillow height and width were measured, and for best practice measurements were taken at right angle to flow directions to ensure that measurement accurately reflected pillow sizes. Where this was not possible, the orientation of the surface used to measure was taken to determine what axes the measurements related to, and was then restricted to a measurement area of 5 m by 10 m. A visual estimation of leucocratic globules (ocelli) abundance and size was also recorded for every pillow that was measured. Ocelli are centimetre to millimetre in diameter ellipsoidal inclusions within basalt (Polat et al., 2007; Polat et al., 2008; Polat et al., 2009). Where flow tubes were present, dip azimuths were taken to help

determine direction of flow, as well as the orientation of the tops of pillows parallel to flow direction.

With the aid of google earth images and GPS, detailed mapping was undertaken in the research area (Figure 7). This was used to produce a stratigraphic log of the units outcropping within the Greenstone belt, including physical volcanological and sedimentological features. Orientation of younging directions and layering within the pillow basalts and sediments were recorded with the aid of a Freiberg Geological Compass to determine original deposition sequences and position, taken as dip and dip direction. Declination of $+1^{\circ}35'$ was taken into consideration and all measurements are to true north. Foliations and lineations within the pillow basalt units were also recorded in addition to relative timing, to determine the minimum number of deformation events.

Rock samples were collected from the EWGB, with particular focus on the basalt units, previously mapped as Mount Ada Basalt. Eighty-five samples were collected from all outcropping units, and the sample sites were chosen as to where the best primary textures could be seen in outcrop. A sledge hammer was used to break off a sample of rock, from which the innermost portion of the pillow was sampled, in addition to outer rims where appropriate. Each sample was individually packed in a cloth or plastic bag to reduce contamination in the field. All samples were shipped to the Queensland University of Technology (QUT) Banyo Pilot Plant Precinct for geochemical and petrographic analysis. Sample locations are shown in Appendix A.

Petrology

Samples from 58 locations were prepared as polished thin sections at the Queensland University of Technology (QUT) Banyo Pilot Plant Precinct for use under a transmitted, cross-polarised and reflected light petrographic microscope.

Sample preparation for geochemistry

Twenty six rock samples that showed primary magmatic mineralogy and/or primary magmatic texture were cut into slabs ~2.5cm thick using a diamond-bonded steel saw. The cut edges were then sanded using a silicon-carbide wet and dry sandpaper to reduce contamination from the saw. Slabs were wrapped in plastic samples bags to reduce contamination and were then further broken down into sand size pieces using a sledgehammer. The small pieces were cleaned in an ultrasonic bath in deionized water to remove dust covering. The sand sized pieces were handpicked to avoid obvious alteration of veins and any cut surfaces to reduce contamination. All samples that contained ocelli chips and host basalt were segregated out and, where there was enough ocelli present within the sample, were analysed separately. The crushed samples were pulverized in an agate mill until the suitable particle size was obtained. Due to the hardness (approximately 7 on Mohs scale of mineral hardness) and elemental composition (mainly SiO₂ or quartz), agate is an ideal material to use to reduce the level of impurities introduced into the sample during grinding (C.F. Allaby, 2008).

Loss on ignition

Loss on ignition (LOI) analysis was carried out on 31 samples at the Institute of Future Environments – Central Analytical Research Facility (IFE CARFS) following standard operating procedures. This test was used to help determine which samples the least amount of alteration. Basalt samples that had LOI values of less than 5 were chosen for trace and major element analysis. The ocelli samples that corresponded to the host sample with a LOI value less than 5 were also included for analysis.

X-Ray Fluorescence (XRF) – Major Element Analysis

Major element analysis was carried out on 10 host basalt samples and 5 ocelli samples. Each sample was made into a glass disk using as LeIVeo Fluxer at the IFE CARF. 0.87 g of the sample was combined with 6.67g of dried (at 105°C) flux in a platinum crucible and melted in a furnace at 850°C before being transferred into a platinum disk mould. The XRF analysis was completed on the SPECTRO XEPOS 03 Energy Dispersive X-ray Fluorescence (ED-XRF) Spectrometer using a Pd X-ray tube at 50W. The W-2, GSP-2, AVG-2, BCR-2, DNC-1a, DTS-2b, Dunite, Norite, Pyroxenite, Syenite standards were analysed for calibration.

Inductively Coupled Plasma Mass Spectroscopy – Trace Element Analysis

Trace and rare earth elements (REE) analysis was carried out on the 15 samples at IFE CARF QUT on an Agilent 8800 Inductively Coupled Plasma Mass Spectrometer (ICP-MS) coupled to a Mass Hunter Workstation. A Triple quad-pole mass spectrometer, capable of trace metal analysis down to parts per trillion was used. For sample preparation and analysis refer to standard operating procedures by Hu and Kineav (2013). This uses a multielement internal standard and is calibrated against a number of standards.

Electron Probe Microanalysis

A mineralogical investigation was carried out by a field emission electron probe micro analyser (JEOL EPMA JXA-8530F) equipped with five wave-length dispersive spectrometers (WDS) at the IFE CARF QUT. Backscattered electron images were used to guide the analysis on target positions of minerals. A 3 μ defocused beam was operated for analysis at an acceleration voltage of 15 kV with a beam current of 20 nA and a take-off angle of 40°. The measured X-ray

intensities were corrected by the ZAF method using the standard calibration of synthetic standards with various diffracting crystals, as follows: all Astimex mineral standards for, jadeite for Na, diopside for Mg, Si and Ca, plagioclase (An65) for Al, apatite for P, celestite for S and Sr, orthoclase for K, rutile for Ti, Cr Oxide synthetic for Cr, rhodonite for Mn, hematite for Fe, barite for Ba, pentlandite for Ni and willemite for Zn. Elemental X-ray by spectrometer using crystals: Na, K α (5,TAPH), Mg, K α (5,TAPH), Al, K α (3, TAP), Si, K α (3, TAP), P, K α (2,PETL), S, K α (2,PETL), K, K α (2,PETL), Ca, K α (2,PETL), Ti, K α (4,LIFH), Cr, K α (4,LIFH), Mn, K α (4,LIFH), Fe, K α (4,LIFH), Ba, L β (4,LIFH), Sr, L α (2,PETL), Ni, K α (4,LIFH) and Zn, K α (4,LIFH).

Melts Modelling

The petrogenesis of the different basalts was modelled using the program pHMELTS (Ghiorso and Sack, 1995; Smith and Asimow, 2005). This software uses a SiO₂-TiO₂-Al₂O₃-Fe₂O₃-MnO-MgO-CaO-Na₂O-K₂O-P₂O₅-H₂O-SO₃ system and a thermodynamic database to calculate liquidus and mineral-melt relationships. The user sets the thermodynamic parameters such as pressure (bar), water content (wt.%) and the relative oxidation state (xO₂) of the magma that is being modelled.

Chapter 4: Stratigraphic Architecture of the Warralong Greenstone Belt

This chapter presents the results from field observations, stratigraphic correlation and petrographic analysis of the units observed in the field. The stratigraphy is described from southeast to northwest, based on the observation that younging is consistently to the west.

The eastern portion of the Warralong Greenstone belt consists of interbedded sedimentary and volcanic units, dominated by a central pillowed meta-basalt unit that covers over 75% of the study area. Within the research area, five different units have been defined. A description of the mapped units and their justification for definition as individual units is provided below in stratigraphic order from oldest to youngest. Petrology was then used to validate these defined units.

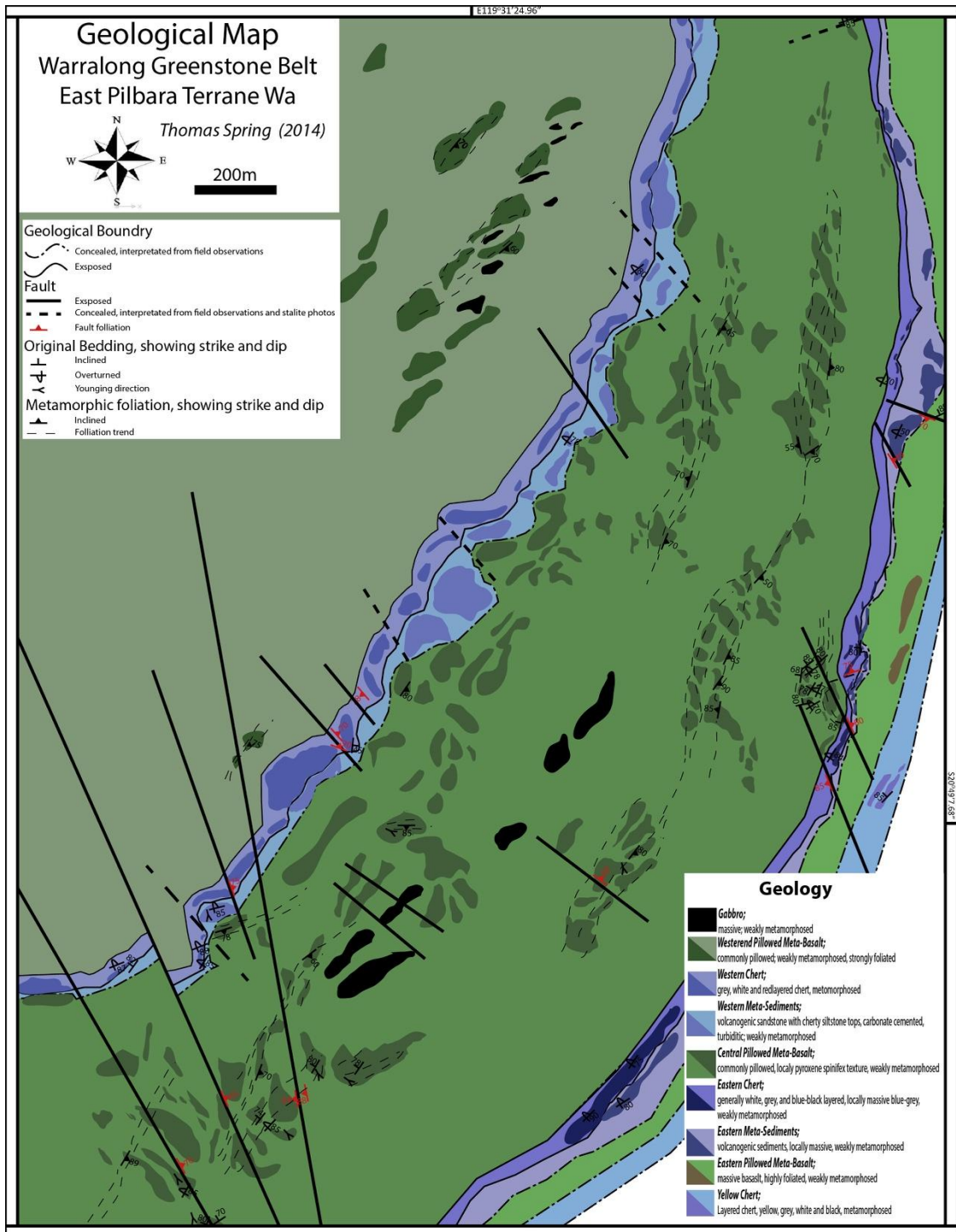
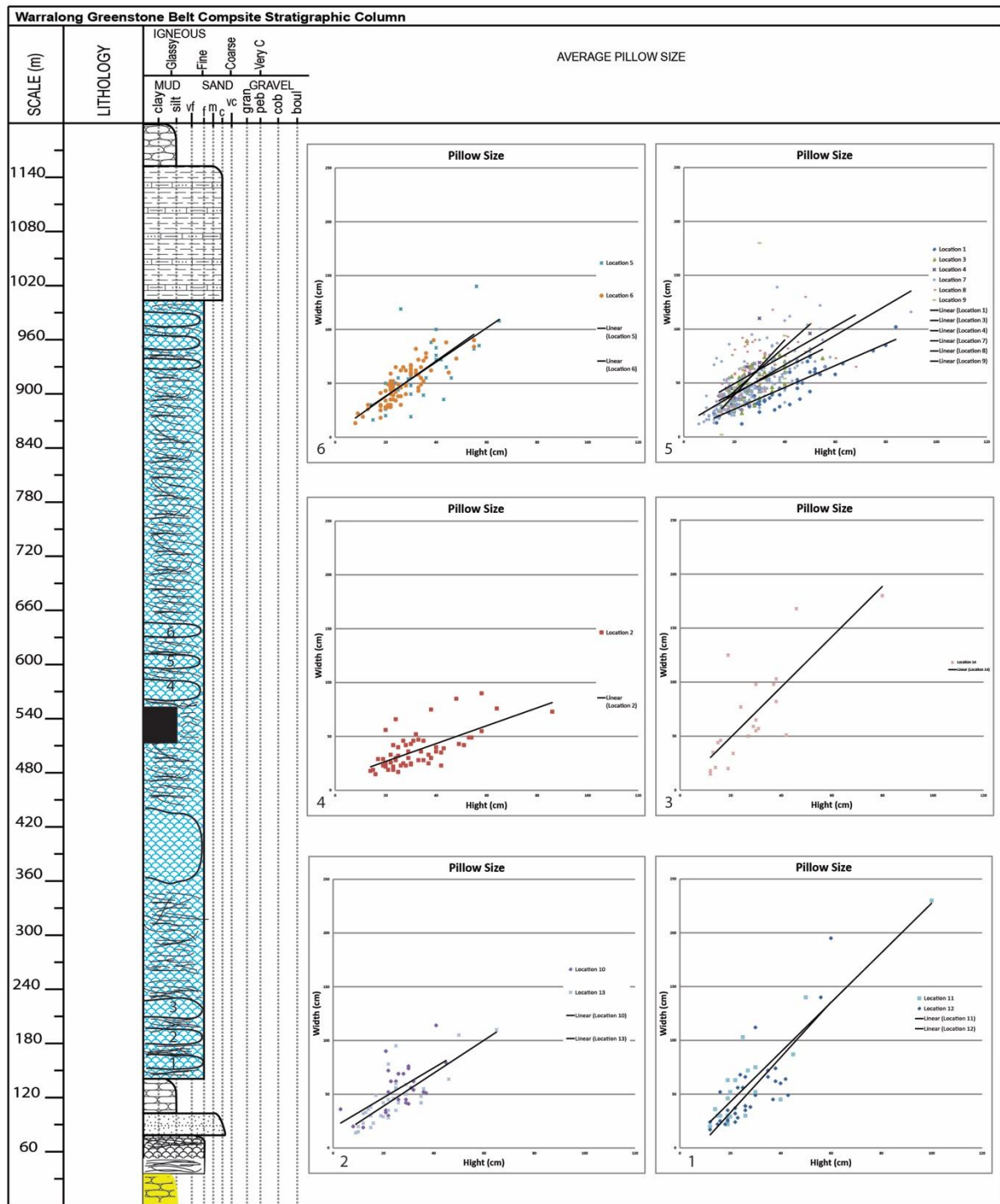


Figure 5. Digital field map of the Warralong Greenstone Belt, denoting the structural observations and outcrops mapped during field work.




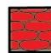




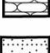
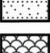
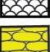

-  **Gabbro;**
massive weakly metamorphosed
-  **Western Chert;**
Grey, white and red layered chert, metamorphosed
-  **Western Meta-Sediments;**
volcanogenic sandstone with cherty siltstone tops, carbonated cemented, turbiditic weakly metamorphosed
-  **Central Pillowed Meta-Basalt;**
Commonly pillowed, local pyroxene spinifex texture, weakly metamorphosed
-  Areas of high shearing and foliation where no coherent outcrop was observed
-  **Eastern Chert;**
Grey, white and blue-black layered locally massive blue grey, weakly metamorphosed
-  **Eastern meta-sediments;**
Volcanogenic sediments, locally massive, weakly metamorphosed
-  **Eastern Pillowed Meta-Basalt;**
Massive basalt, highly foliated, weakly metamorphosed
-  **Yellow Chert;**
Layered chert, yellow, grey, white and black, metamorphosed
-  Areas within highly foliated zones where outcrop was preserved

Figure 6. Stratigraphic representation of the Warralong Greenstone Belt showing distribution of pillow sizes in the best preserved sections.

Lithostratigraphy and Facies Analysis

Yellow Meta-Chert

The most south-eastern outcrops (Figure 7 and Figure 8; 20°49'6.50"S: 119°32'0.95"E), which are the first outcrops to the west of a significant exposure gap between the Warralong Greenstone belt and the Muccan Granitoid Complex, represent the south eastern margin of the Warralong Greenstone belt. These outcrops consist of one large continuous outcrop (20 m x 30 m) with a smaller outcrop (2 m x 5 m) a short distance to the north of the larger outcrop. The larger of these outcrops contained a 30 cm recessive bed where the outcrop had been weathered out along strike. The bedding of the unit has a dip and dip direction of 135/85°. This unit consists of yellow (figure 7) silica rich amorphous layers (30%) with interbedded grey (10%), white (10%) and black (30%) silica rich cryptocrystalline layers, as well as grey friable altered clay rich layers (20%). Each layer of cryptocrystalline silica also contains some fine laminations in places, no cross bedding or sedimentary structures to suggest younging direction were observed. True thickness of the unit was calculated as 20 m, with individual beds of the silica rich cryptocrystalline rock ranging from 5 cm to 30 cm, and interbedded highly altered clay rich beds 5 cm thick. Interpreted original sedimentary layering is highlighted by the colour changes within and from the yellow, grey, white and black cryptocrystalline silica rich rocks. Petrographically the yellow cryptocrystalline layers consist of recrystallised microcrystalline quartz. SEM analysis indicated that the samples contained abundant 10-20 µm zircons.



Figure 7: Hand specimen of Yellow Chert (TS-26)

Eastern Pillowed Meta-Basalt

To the West of the yellow meta-chert are four individual lozenge shaped outcrops that range from 10 m to 20 m thick and 50 m to 100 m wide (Figure 7 and Figure 8). No direct contact between the Yellow Meta-Chert and the Eastern pillowed meta-basalt units was observed in the field. The two outcrops to the North East are outside of the mapped area shown in Figure 7. The outcrops predominantly consist of elongated deformed pillow shaped basalts with minor highly foliated basalts. Between the outcrops there are rare centimetre to meter-sized outcrops of highly foliated basalt, often covered by dense scrub or spinifex and float material.

Eastern Psammite

The Eastern Psammite unit is laterally extensive and represents the base of the continuous stratigraphy of the Eastern Warralong Greenstone belt. The unit has exposures up to 20 m in thickness; the contact between the sedimentary unit and the underlying basalts is not observed. This unit can be traced laterally for the entire mapping area (Figure 7), with major breaks in exposed outcrop in parts up to 500 m. The outcrop can be broken into three main continuous outcrops with the first occurring in the south, consisting of an area 5 m x 40 m. There is then a major exposure gap of 500 m before another section of smaller outcrops ranging from 1 m

to 10s of metres in size along strike. After another exposure gap of 100 m, there is a large outcrop in the northern end of the mapping area, this outcrop is much thicker than the other outcrops up to 20 m in true thickness. Some smaller outcrops were also observed towards the very north of the mapping area and further north outside of the mapping area.

The Eastern Psammite unit consists of a light grey to medium grey lightly altered sandstone with red oxidation in patches with sub-angular to angular grains and medium to coarse-grained sandstone. A medium grained sample from the unit petrographically displays sub-rounded to sub-angular clasts of silicified volcanoclastic clasts with common vesicles and pseudomorphs after plagioclase with minor limonite/goethite from weathering in quartz/barite rich matrix (Figure 10). This unit is predominantly massive with little internal layering. Where preserved, this consisted of planar sedimentary layering and fining of grains size to the west. No definitive younging indicator was observed. Preserved bedding ranged from 2 cm to 5 cm and has been tilted to $\sim 124/75^\circ$ (Figure 9).

An overprinting secondary microcrystalline fabric, a result of recrystallization from metamorphism, is observed with overprinting hematite and ilmenite often hosted within the relic grains. The protolith for this unit would have been described as medium grained sandstone that has now been completely recrystallized, thus destroying the original mineralogy and texture. This sandstone unit has not been previously mapped or described in any formations within the Warrawoona Group.

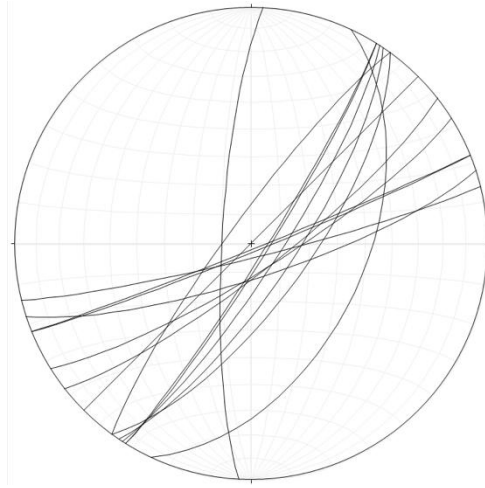


Figure 8. Stereonet plot of tilted bedding planes within the Eastern Psammite and Eastern Chert.

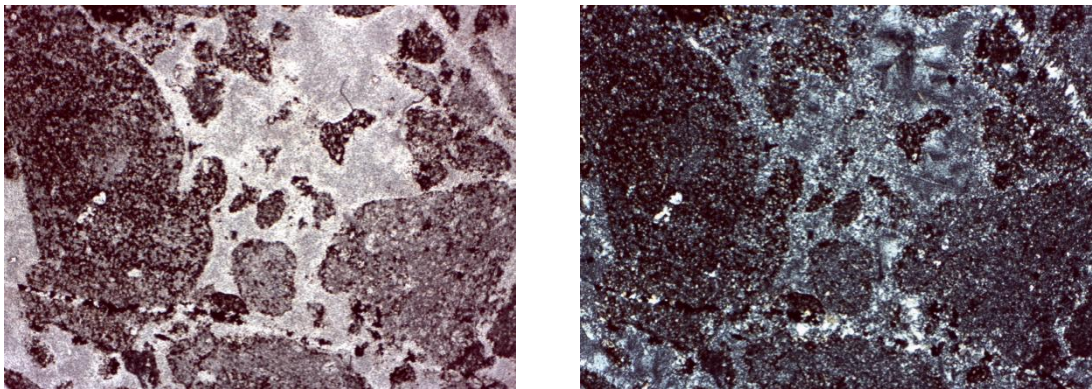


Figure 9. Photomicrograph taken of TS-24-1-14 and example of the eastern Psammite taken at low magnification in plain polarised light (left) and cross polarised light (right). Image shows an example of the typical mineralogy and textures observed within the Eastern meta-sediment. The rock consists of Silicified volcaniclastic clasts with common vesicles and pseudomorphs after plagioclase in quartz/barite cement. (Image width = 31 mm)

Eastern Chert

Lying conformably on top of the Eastern Psammite unit is the Eastern chert unit, with a gradational transition zone between the two units consisting of intercalated sediments and cryptocrystalline silica rich layers (Figure 11). The unit consists of layers exposed in parts up to 10 m thick consistently to the west of the Eastern sedimentary unit outcrops. This unit can be traced laterally for the entire mapping area (Figure 7) and was observed to extend significantly further to the north of the mapping area as well as previously mapped by the GSWA (Van Kranendonk, 2010). The cryptocrystalline silica rich layers show varying thickness laterally, ranging from half a metre to 10 m in thickness.



Figure 10. Image showing gradational contact between the Eastern Psammite and the Eastern Chert.



Figure 11. Image of fractured red chert, by secondary white quartz veins.

Original sedimentary layering has been preserved with different coloured layers of white, red, blue, grey and black chert observed. These individual layers range from 5 cm to 30 cm thick, with the white and black cryptocrystalline silica rich layers predominantly forming in thicker layers than the rest. As seen in Figure 12 and 13, the chert has been fractured in parts resulting in angular fragments of chert within a quartz-veined rock, veins have trace amounts of opaque oxides. The bedding has been tilted near vertical ($135/90^{\circ}$) (Figure 9); the strike varies by up to 30 degrees. Petrographically the Eastern Chert unit consists of a range of cherts, consisting of predominantly finely layered micro to cryptocrystalline quartz (Figure 13). The layers of reddish chert (Jasper) have an increased concentration of hematite and magnetite than the other layers. The darker layers of black chert could denote areas that contain carbonaceous matter, however this is unconfirmed.

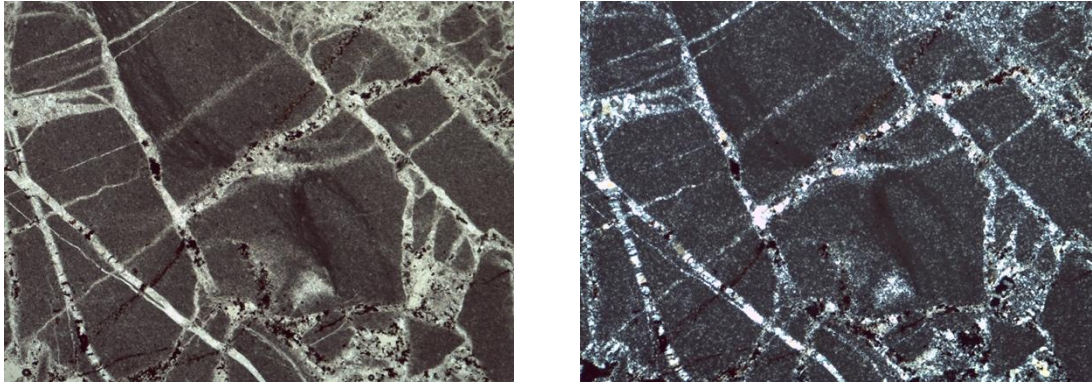


Figure 12. Photomicrograph of thin-section TS-27-1-14, an example of thin-sections observed from the eastern chert unit. Image taken at low magnification with transmitted plain polarised light (left) and cross polarised light (right). The rock is formed out of predominantly microcrystalline quartz that has been brecciated by vein quartz, the black minerals are hematite and in rare case magnetite (Image width = 31 mm)

Central Pillowed Meta-Basalt

The Central Pillowed Meta-Basalt unit is the most extensive and thickest unit within the mapped area (Figure 7). A conformable contact was observed between the Central Pillow Meta-Basalt and the Eastern Chert in one locality, whereas a number of conformable contacts are observed with the overlying Western Psammite. The unit covers a 3.6 km² area of the field site, with a maximum possible thickness of 1200 m. However, this unit outcrops as a number of segmented “lozenge like” outcrops, with a total outcrop thickness (and possible minimum thickness) of 600 m, disregarding any possible lateral or horizontal structural movements. Individual lozenges range from a 5 m by 5 m outcrop to a 50 m by 200 m outcrop (Figure 6). Where basalts are exposed they outcropped as pillow structures, no massive sheet flows are observed. The pillows range in size from 15 x 15 to 110 x 80 cm (Figure 8) with no obvious trends with stratigraphic height. Often, multiple fine-grained/chilled pillow rims are preserved within individual pillows (Figure 13). Multiple pillow cavities are preserved in some pillows as well, that extend into the pillows with a rounded bottom section and flat top denoting the up direction within the pillow (Figure 13B). Inter pillow hyaloclastite is preserved throughout the Greenstone belt, preserved with infilling carbonate (calcite and on occasion siderite) cement (Figure 13 A).

Hyaloclastite ranges from white, grey to black and consists of “glassy” shards of now carbonate altered basalt, ranging from micro-shards to larger debris-like shards. No vesicles were observed within the pillow basalt of the central pillowed meta-basalt unit or the hyaloclastite.

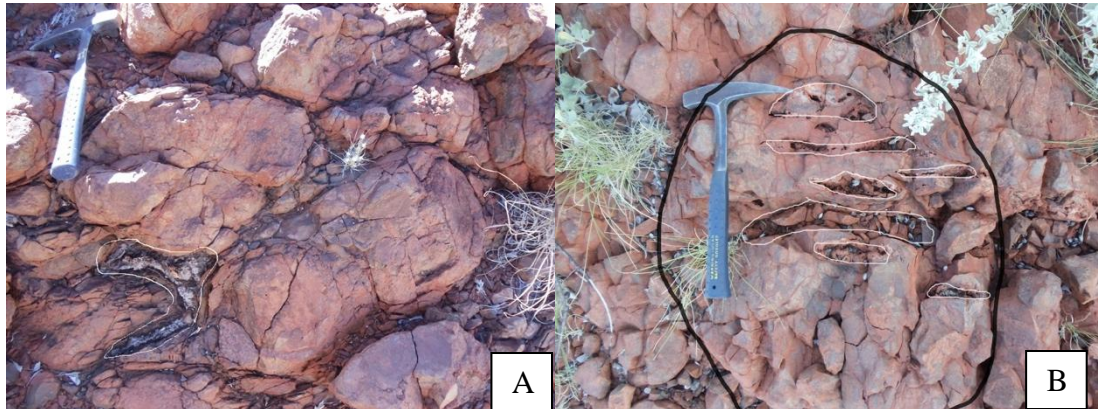


Figure 13. Figure A shows a set of stacked pillows with carbonated inter pillowed hyaloclastite between pillows and circled hyaloclastite. Image B is an example of a pillow with multiple cavities, as a results from multiple pulses of lava through the pillow. Cavities denoted by white out line and pillow extent denoted by black outline. (Rock hammer 30cm)

Where outcrop is well-preserved, orientation of primary flow tops and flow tubes within pillows could be determined with an average strike of 220° and dip of 78° (Figure 14). Pillow tops are characterised by their flat surface and the bottom of pillows are characterised by the nipple or tear drop shape, formed when being emplaced. Throughout the central pillowed meta-basalt unit, there is no evidence of breaks in the volcanic sequence such as interbedded sedimentary units or erosional contacts.

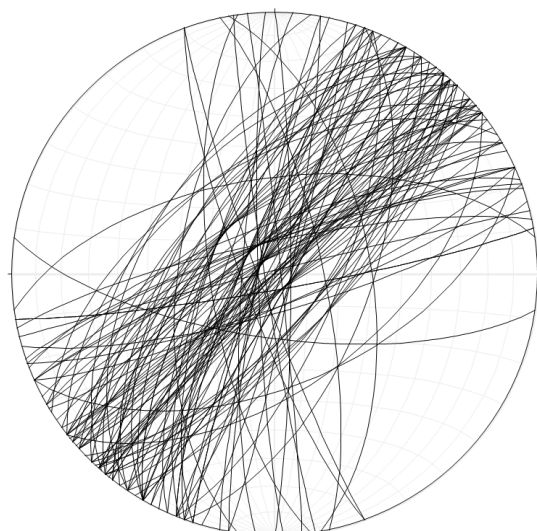


Figure 14. Stereonet of planar flow tops of pillows and flow tubes within pillows, taken from outcrops within the mapping area.

Leucocratic Globules

Leucocratic globules, referred to as ocelli (Appel et al., 2009; Coish et al., 1982; Foley, 1984; Polat et al., 2007; Polat et al., 2008; Polat et al., 2009), can be seen within all the pillowed meta-basalts. The ocelli vary in both size (2 mm to 100 mm) (Figure 16) and abundance (from no ocelli, very rare <5%, rare >5 % to <15 % moderate >15 % to <30 %, abundant >30 % < 45% and very abundant >45% of pillow) throughout the Greenstone belt (Figure 18). The majority of the measured ocelli fall within a range of 2 mm to 10 mm in size and in most of the pillows occur moderately (10-20%) abundant to abundant (20-40%) (Figure 15 & 16). The ocelli are much lighter in colour than the host basalt, from an off cream to a pale green colour, and have typically sub-spherical to spherical shapes (Figure 17 & 18). Larger well-preserved ocelli can often show zoning within them, with darker centres and lighter rims. The ocelli are often preferentially weathered out of the host basalt, suggesting that they are more susceptible to weathering. The contact between the host basalt and ocelli is commonly sharp both on a macro and micro scale, but in altered samples can be wavy or diffusive. Within the pillows the ocelli are disseminated throughout (Figure 17), with a small proportion of pillows showing a preference of ocelli to form in the rims of the pillows.

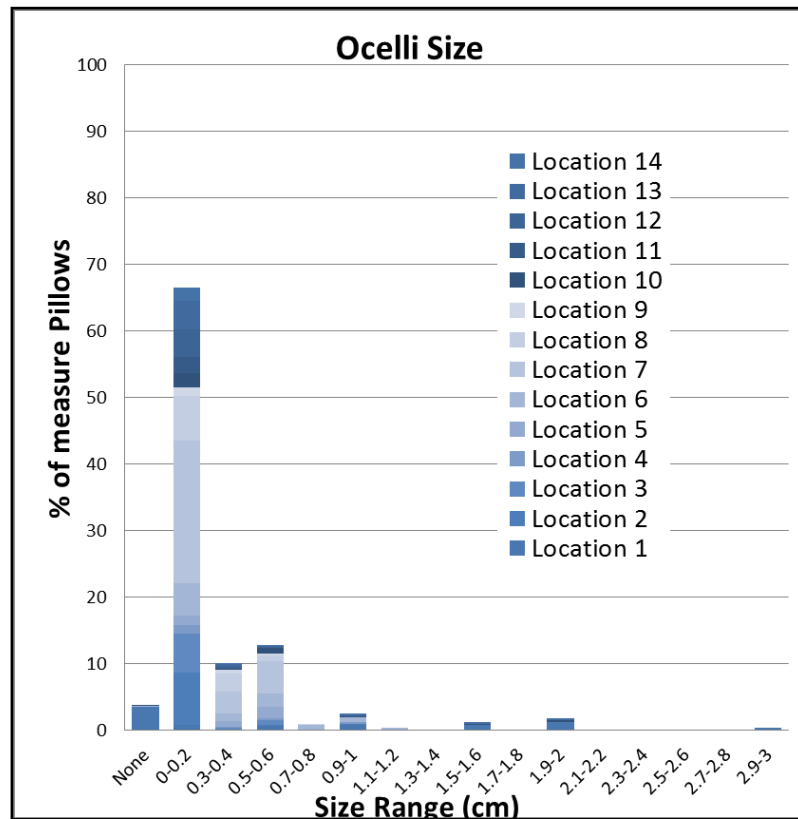


Figure 15. Ocelli size as a percentage of pillows measured. (Locations shows in appendix B)

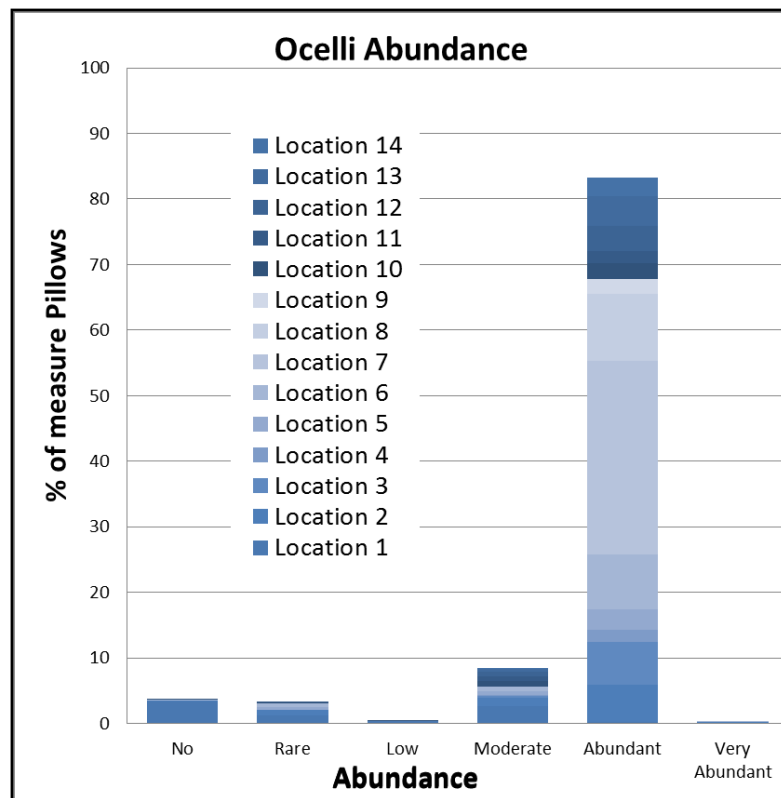


Figure 16. Ocelli abundance as a percentage of pillows measure. (Locations shows in appendix B)



Figure 17. Image of cut surface of sample TS-37-1-14. The image shows the quenched rim of the pillowed basalt as well as evidence of possible multiple flows and disseminated ocelli (2 to 5 mm).

Between outcrops of the Central Pillowed Meta Basalt there are often valleys with dense spinifex and meta-basaltic float, covering rare exposure of centimetre-scale outcrops of highly foliated basalt (foliations average is $124/75^0$), which appeared to preserve no primary structures.

Petrographically the freshest samples can be subdivided into the host basalt and the leucocratic ocelli. The host basalt can be described as a hypocrySTALLINE meta-basalt with rare acicular pyroxenes. The majority of samples are dominated by secondary alteration and metamorphic minerals including chlorite, actinolite, epidote and carbonate reflecting lower greenschist facies metamorphism. Rare samples, predominantly from the south-west outcrops, contain preserved primary magmatic clinopyroxene, spinel, albitised plagioclase and pseudomorphs after olivine (Figure 19). Minor amounts of quartz and calcite are seen as cross cutting veins. The ocelli

have the same micro phenocryst assemblage as the host basalt, however the matrix consists of predominantly calcite (Figure 19).

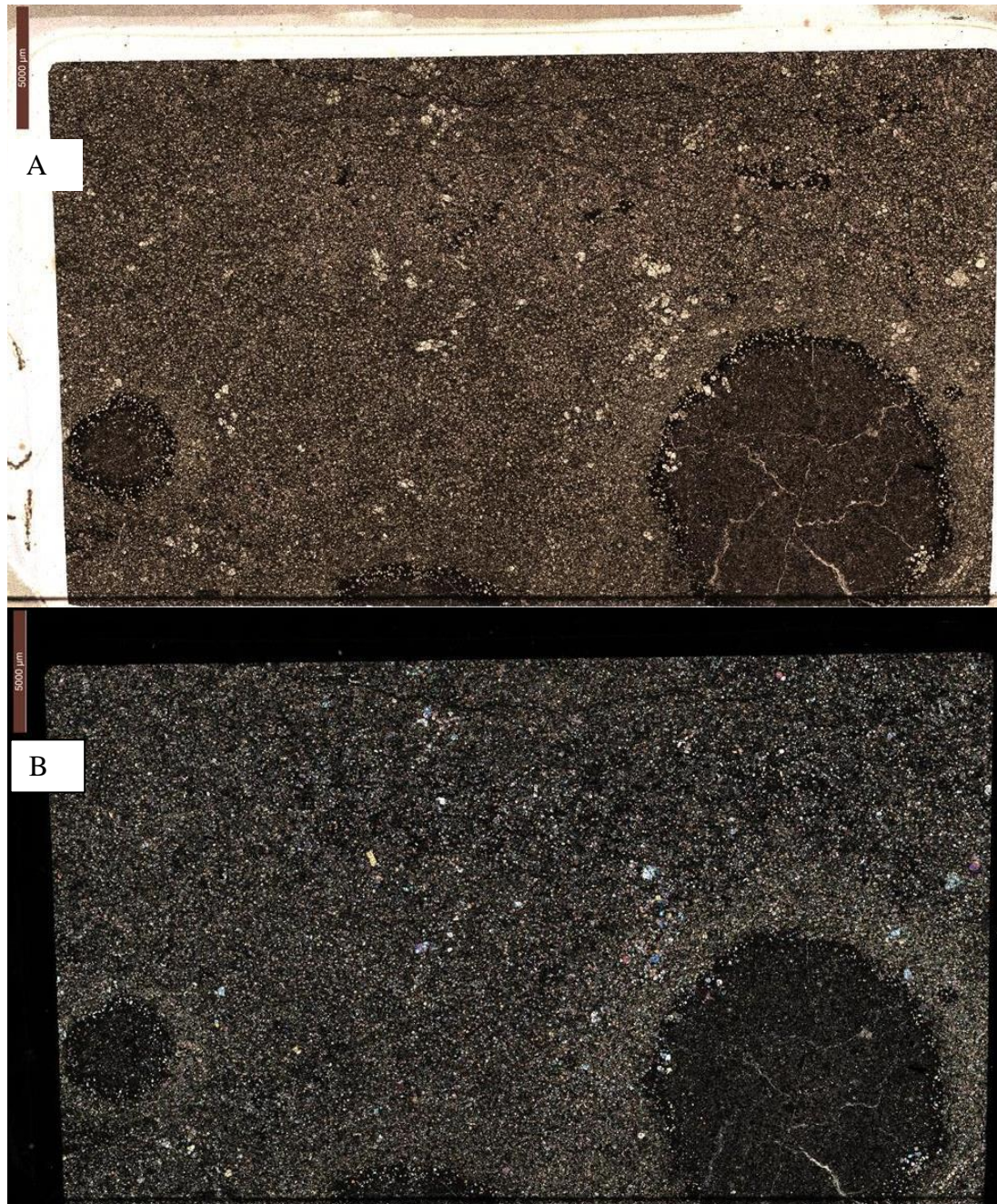


Figure 18. Photomicrograph taken at low magnification of whole thin section photomosaic of sample TS-2 in (A) plane polarised light and (B) cross polarised light, with 2 ocelli in a basaltic matrix. The basaltic matrix is alteration due to low-grade metamorphism, dominated by primary pyroxene in an altered matrix predominantly made up of chlorite, calcite and quartz. The image also shows a preserved ocellis and the distinct boundary between it and the host basalt. The ocelli samples have similar mineralogy with preserved primary pyroxenes in a more altered matrix dominated by chlorite and carbonate.

Western Psammite

Lying conformably (with a straight contact and no erosion evident) on top of the central Pillowed Basalt unit is the Western Psammite unit. This unit is laterally continuous, flanking the western boundary of the mapping area, however, has sections of no outcrops ranging from the metre to scale to tens of metres (Figure 7).

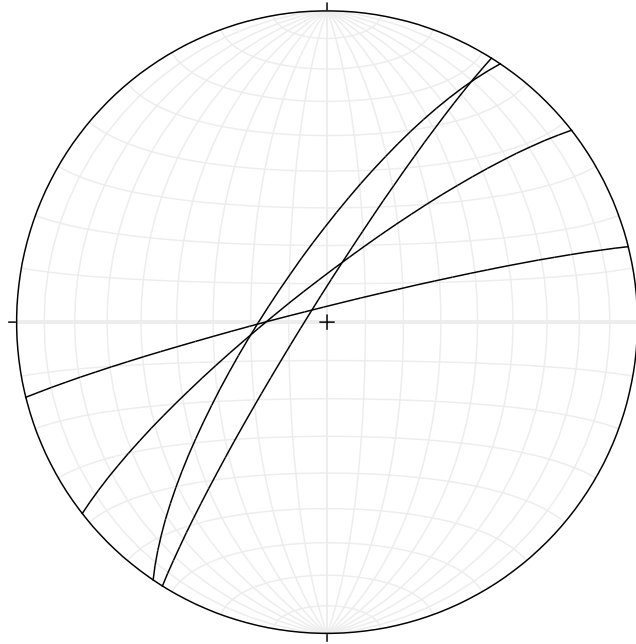


Figure 19. Stereonet of sedimentary layering of the western sedimentary unit.

It was observed to range from ~2 meters to ~5 metres thick over most of the map area and in three major outcrops thickens to up to ~50 metres, with individual beds 10 to 15 cm thick. The unit consists of a repeated sedimentary sequence of sandstone, mudstone and cryptocrystalline silica rich layers (Figure 20). The layers, which are between 5 and 15 cm in thickness, consist of a medium to fine grained sandstone at the base that grades up into a very fine siltstone then into a cryptocrystalline silica (Figure 20). Cross trough bedding can be seen preserved in some sandstone beds, while little to no sedimentary structures are preserved within

the fine grained siltstone and cryptocrystalline silica rich rock. Where sedimentary features were preserved in the siltstone, they consisted of planar laminations.

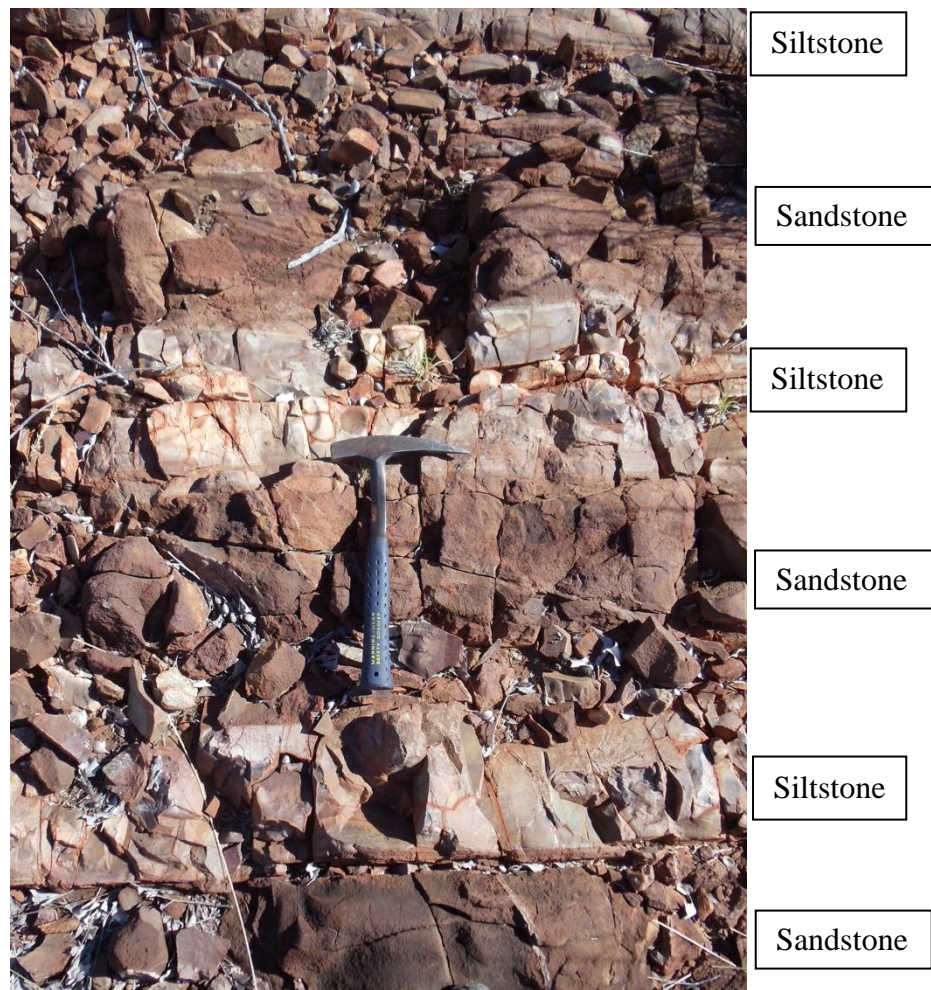


Figure 20. Image of western meta-sediments, note the repetitive sequence of sandstone, mudstones and cherts. Image shows medium-fine grained sandstone topped with fine-grained mudstone and cherts in part. (Rock hammer ~30cm long) Location 20°49'17.7"/119°30'51.4".

This unit can be described petrographically as poorly sorted, sub-angular to sub-rounded, grading from fine-medium grained to very fine grained lithic sandstone, with sub-rounded to sub angular mudstone and amorphous silica rich layers interbedded (Figure 21). Remanent rock clasts consist of finely crystallized cryptocrystalline quartz. 10-15% opaque oxides and earthy secondary iron oxides can be seen throughout the matrix (Figure 21).

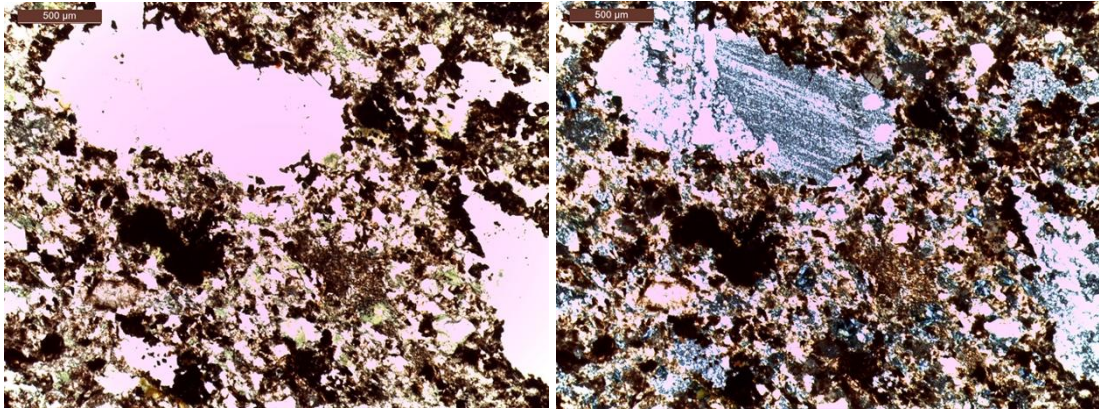


Figure 21. Microscopic image taken at low magnification with transmitted polarised light (left) and transmitted cross polarised light (right). Image shows the typical mineralogical observed within the sandstone beds from the Western meta-sedimentary unit. (Image width = 31 mm) The Image shows a number of small clasts of finely microcrystalline quartz in a recrystallized silica rich matrix with earthy secondary iron oxides and hematite.

Western Chert

The Western Psammite has a conformable contact with a ~20 metre thick chert unit (Figure 7 and Figure 8). The unit consistently outcrops to the west of the Western Psammite near-continuously along the western flank of the map. The Western Chert unit consists of thinly laminated (1-5 cm) interbedded red and white very fine grained to cryptocrystalline silica rich layers. The layers show fine laminations but no other evident sedimentary structures. Layer parallel quartz veining has separated original layering as well as brecciated the rock by cross cutting quartz veining as seen in Figure 22.

Petrographically, the Western Chert unit consists of finely microcrystalline quartz with secondary quartz veining. Similar to macro scale, on the micro scale primary sedimentary features, such as laminations, have been preserved, however many of the laminations have been fractured by secondary quartz veining, running both cross cutting and layer parallel.



Figure 22, Image of unit E, thinly laminated red, black and white cherts at base, with large veins of secondary white chert crosscutting bedding and running along bedding. (Rock hammer ~30cm) location E20⁰49'16.7" N119⁰31'03.5".

Western Pillow basalt Unit

The western pillow basalt unit outcrops in a number of individual lozenge shaped outcrops that range from 10 m to 20 m thick and 50 m to 100 m wide (Figure 7 and Figure 8). No direct contact between the western chert and the western pillowed meta-basalt units was observed in the field. The outcrops predominantly consist of elongated deformed pillow shaped basalts with minor highly foliated basalts. Between the outcrops there are rare centimetre to meter-sized outcrops of highly foliated basalt, often covered by dense scrub or spinifex and float material.

Gabbro Intrusions

Cross cutting through the central basalt unit as well as in a number of other places outside of the research area, are a series of discordant coarse grained mafic bodies that are referred to here as a single mafic intrusive unit (Figure 7 and Figure 8). This unit is observed as six oblong massive outcrops within the central pillowed metabasalt unit. Other smaller discordant mafic bodies were observed to the northwest. These mafic bodies are distinguished from the surrounding pillow basalts because of their massive structure and coarse grain size. The contact between the pillow basalts and the massive mafic bodies was not observed. Outcrops formed in massive sill-like structures and ranged from 5 to 10 m by 20 to 30m. Within the Central Basalt Unit the intrusions occur at a consistent level within the stratigraphy and appear to be of similar mineralogy. Petrographically this unit consists of predominately fresh plagioclase and primary preserved pyroxenes with rare relic olivine now altered to chlorite, actinolite and carbonate.

Deformation

Within the research area, the Warralong Greenstone belt has undergone significant deformation. The original stratigraphy has been tilted (D_1) vertically to sub-vertically with an average strike of 50° (Figure 9). Consistent younging indicators throughout the eastern Warralong Greenstone belt indicate that the units are younging from SE to NW. Outcrop is sparse in the east, consisting of disconnected north to northeast trending lozenges of metasediments and meta-basalts. Outcrop increases to the west with a higher density of basaltic lozenges followed by near continuous outcrop of meta-sedimentary sequence and chert. To the west of the chert unit outcrop again diminishes.

The meta-basalt lozenges are decimetre in size. The lozenges are cut by metre sized foliated shear bands and rare centimetre sized inter-lozenge outcrops preserve a dominantly north south trending secondary foliation (S_2) (Figure 5). This foliation shows two orientations with the dominant orientation being 80/137 and a second orientation 85/062 clearly indicating that the foliation has been folded (D_2). The D_2 fold can be traced by the outcrop of lozenges and sheared foliated inter-lozenge outcrops in the west and north of the study area.

North-west south-east trending faulting (Figure 6) and associated shearing has also been mapped over printing earlier foliations, and is ascribed the third deformation (D_3) event.

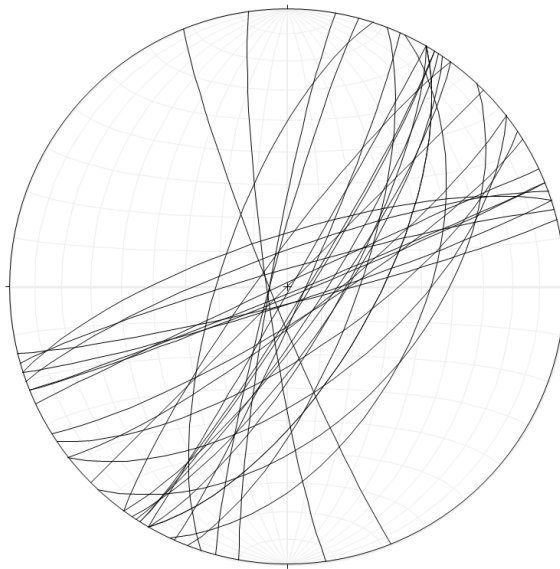


Figure 23. Stereonet of the S1 foliation within and around lozenges.

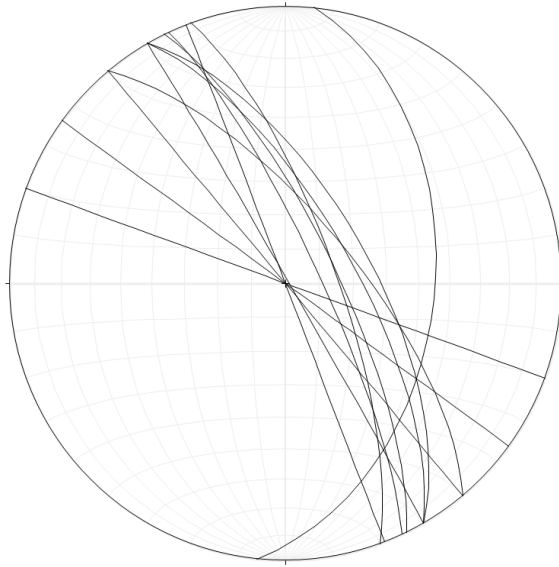


Figure 24. Stereonet of fault foliation from the D3 deformation event listed.

Chapter 5: Geochemistry

Samples from the Central Basalt Unit that contained primary magmatic minerals and/or preserved primary magmatic textures were chosen for major element and Loss On Ignition (LOI) analysis (Appendix B). The majority of the samples analysed (26) represented purely the host basaltic components. In addition, for 5 samples, where ocelli were sufficiently large to separate from the host basalt and primary magmatic minerals were present, the ocelli component was analysed. Based on the results of these analyses, fifteen samples were chosen for further trace chemistry (Appendix D) analysis. All samples analysed were taken from pillow basalts with ocelli.

Alteration

All of the central basalt unit samples have been affected by alteration and therefore potential element mobility. Here LOI was used as an index of alteration because LOI has been shown to increase with hydrothermal alteration (Duzgoren-Aydin et al., 2002).

Host Basalts Major Elemental Oxides versus LOI

SiO₂, Al₂O₃, TiO₂ and P₂O₅ show limited variation with LOI in the host basalt suggesting limited mobility for these elements during alteration (Figure 24). FeO, CaO and MgO show little variation at LOI <5% but significant scatter at higher LOI. High MgO and low MgO trends are observed in LOI versus MgO. The tight cluster of samples from both these trends at low LOI likely indicates that the trends are not related to alteration but rather reflect primary magmatic variation. Interestingly, SO₃, which is often associated with alteration, shows limited variation at LOI <5%. Both

K_2O and Na_2O show significant scatter even at low LOI, indicating that even the best preserved samples have undergone mobility of these elements.

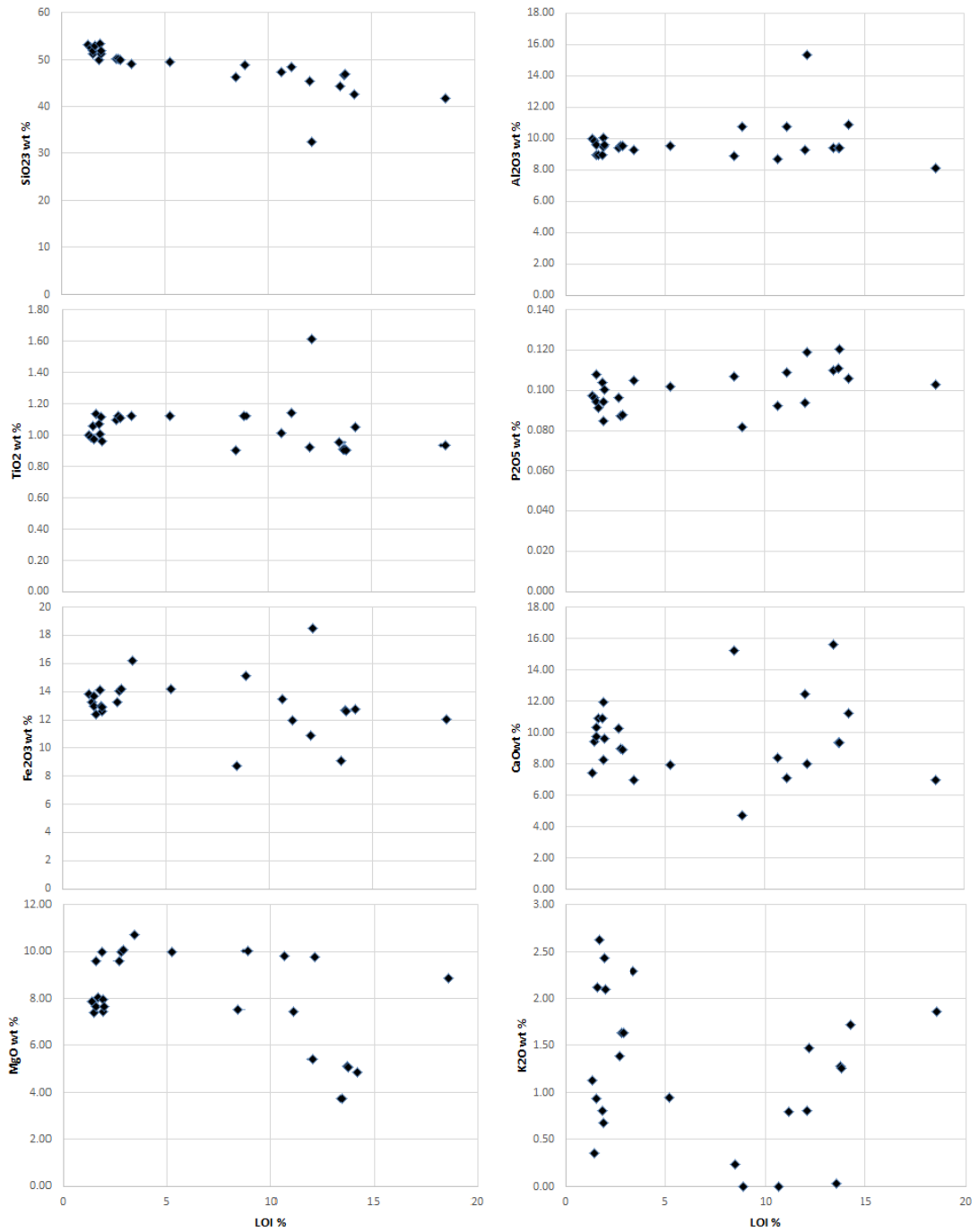


Figure 25. Elemental oxide wt% for host basalt versus LOI. Note that although wt% values for LOI increase the values for SiO_2 , Al_2O_3 , TiO_2 and P_2O_5 , are very constant, whereas the values for FeO , CaO and MgO become more scattered at higher (>5%) LOI.

Ocelli Major Element and LOI Variation

The ocelli samples all have consistently higher LOI than their host basalt. Of the major oxide elements, only TiO_2 shows insignificant variation between both ocelli and host basalts. Al_2O_3 , P_2O_5 , Na_2O and SO_3 are all significantly enriched in the ocelli relative to the host basalts. SiO_2 is mostly enriched in the ocelli, except at high LOI. MgO , MnO and FeO are significantly depleted in the ocelli samples relative to the host basalt. The ocelli show a positive correlation between LOI and CaO ($R^2=0.99$). The increased presence of CaO is consistent with petrographic observation of carbonate within the ocelli (Chapter 4, Petrology of the Central Basalt Unit). K_2O shows no coherent variation in the ocelli similar to the host basalts.

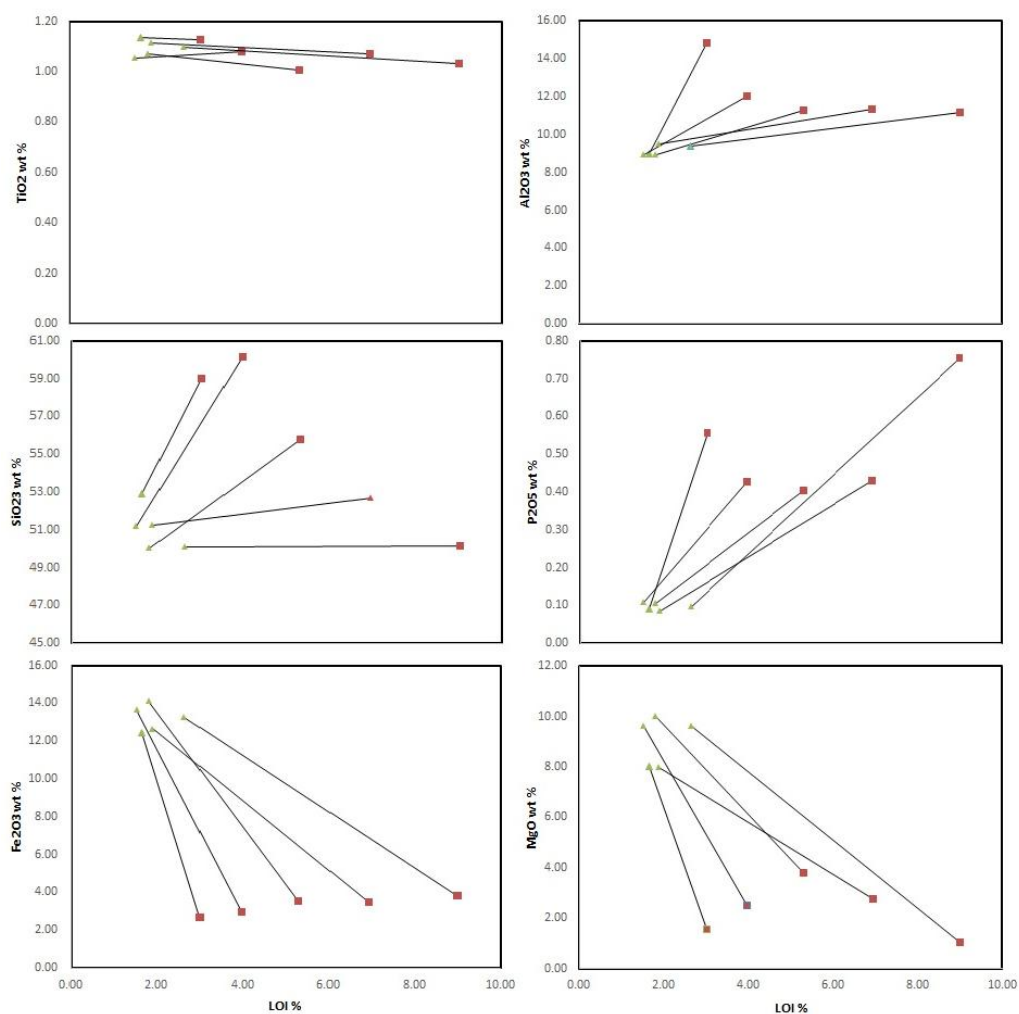


Figure 26. Elemental oxide wt% for host basalt (green triangles) and corresponding ocelli samples (red squares) 343-1, 344-2, TS-2-1, TS-31-1 and JDK-69 versus LOI.

Based upon the observation that host basalt samples with LOI of less than 5% show limited variation in major elements, except K₂O and Na₂O, twelve host basalts of less than 5% LOI and ocelli extracted from them were analysed for trace element chemistry.

Whole Rock Elemental Data

Classifying Archean rocks based on geochemistry can be challenging because all Archean rocks are altered to varying degrees. The Total Alkali Silica (TAS) diagram (Figure 26) plots the host basalt as basalt to basaltic-andesite; however both Na_2O and K_2O have clearly been affected by alteration. Because of this the ternary diagram (Figure 27) by Viljoen et al. (1982) is used, with the host basalt plotting as komatiitic basalt. The range of MgO concentration of 8 to 10 wt% classifies the host basalt as high Mg basalts. The host basalt samples all have moderate to low Mg# of 36 to 51 and plot along the classic tholeiite crystallisation trend toward high FeO content (Figure 27).

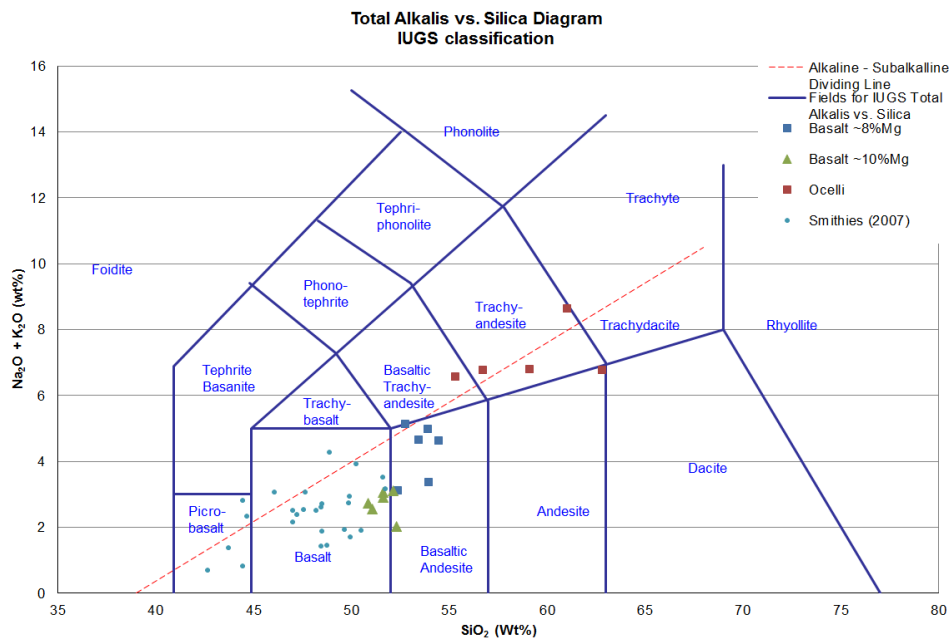


Figure 27. TAS diagram used for classifying volcanic rock types based on geochemical analysis (after Le Bas et al., 1986, Fig 2). This diagram is typically used to determine rock types of fresh unweathered and unaltered rocks; however the rocks within the research area have undergone some alteration and weathering. Smithies (2007) data from the Mount Ada Basalts analysed from other greenstone belts have been plotted for comparison.

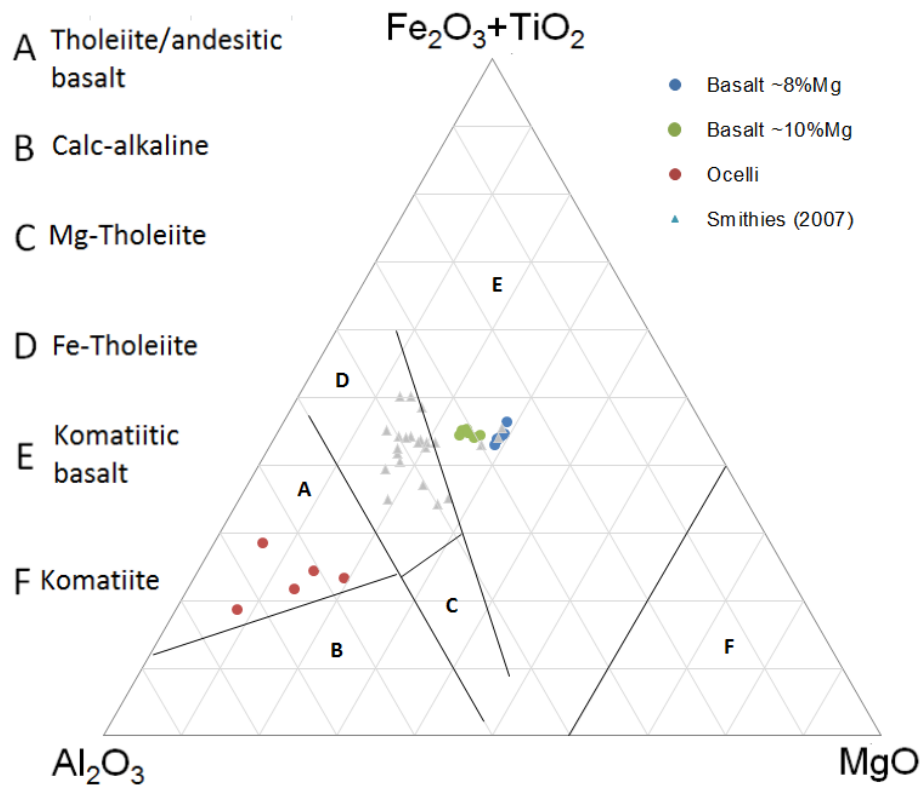


Figure 28. Basalt classification for samples with available major element analysis. Recreated from Viljoen et al. (1982) and recalculated as anhydrous. Smithies (2007) data from the MAB have been plotted for comparison.

The host basalts demonstrate two groupings of MgO wt% concentration of around 8% and 10%. The lower MgO basalt group are all located throughout the stratigraphic middle of the central basalt unit and the higher grouped MgO are all located together near the central eastern boundary of the central pillow basalt unit (Appendix B). Ocelli chemistry does not vary between the higher and lower magnesium groups. This MgO bimodal distribution shows that there are at least two geochemically distinct components within the central basalt unit, which were not identifiable in the field or petrographically.

When comparing the two different basalt units, it can be seen that they form tight coherent clusters (Figure 29), which is also evident in the ocelli. The samples are plotted against MgO, as it best differentiates the two host basalt as well as the ocelli. There is a positive correlation with Fe_2O_3 and MgO, with Fe_2O_3 having values ranging from 12.7 to 16.8 wt%, and the ocelli sample values ranging from 2.7 to 3.8

wt%. P_2O_5 is seen to be depleted in both the host basalts, with no comparable difference between the two. These host basalt results are similar to those found by Smithies (2007) in the Mount Ada formation within the Marble Bar Greenstone belt (Figure 29). In all samples both ocelli and host basalts show slight enrichment in TiO_2 when compared to similar samples taken from the Mount Ada basalts in the Pilbara region (Smithies, 2007). The host basalts have moderately silicic ($SiO_2 = 50.8$ wt% to 54.4 wt%), and while the ocelli samples also fall within moderately silicic, they do have a higher comparable silica content than the host basalts ($SiO_2 = 59.1$ wt% to 62.8 wt%).

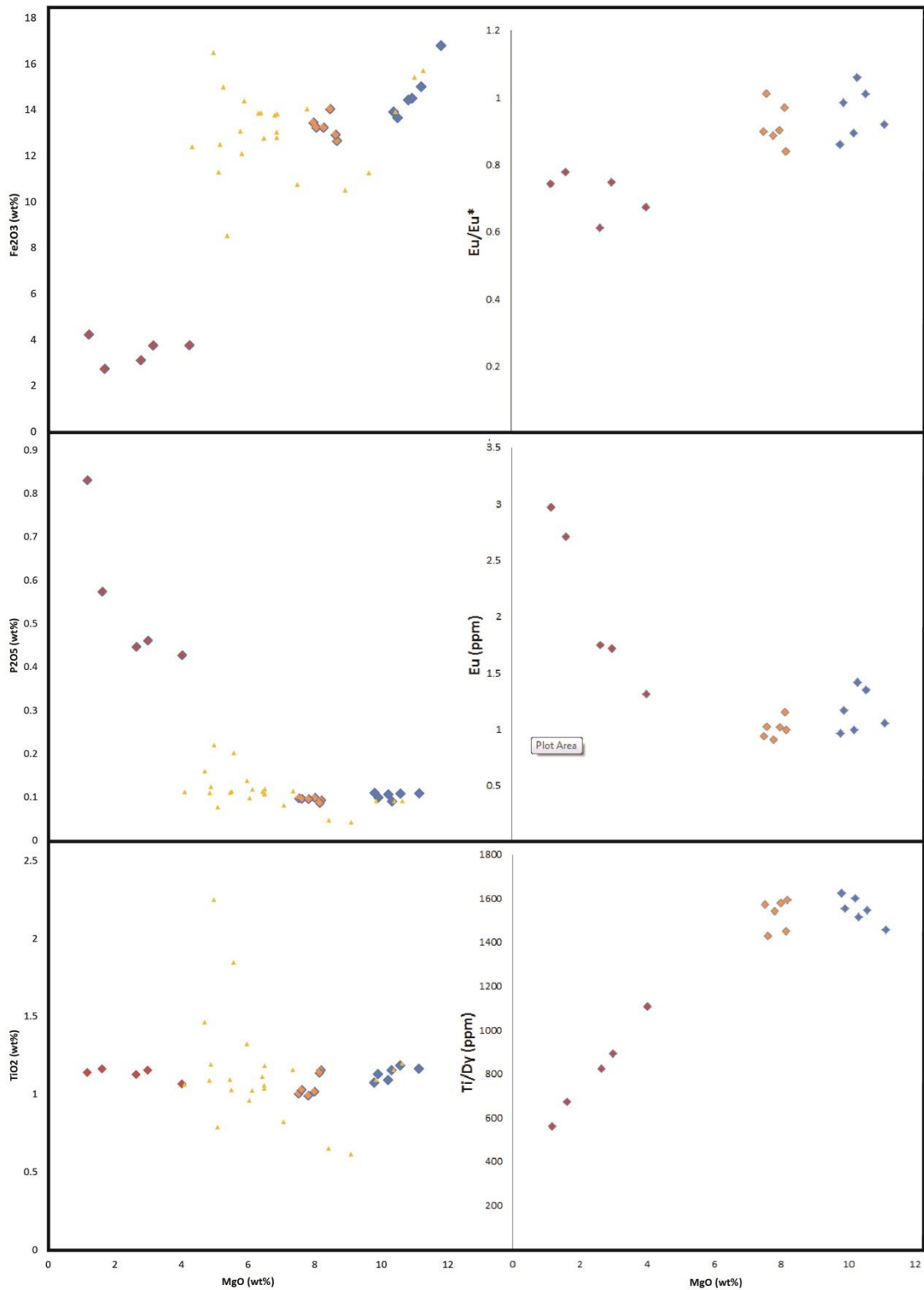


Figure 29. Harker diagrams showing the chemical variation observed in the host basalt and ocelli. Diagram A, C and E are examples of the host basalts versus ocelli in relation to smithies (2007) data. Diagrams B, D and F are examples of trace element segregation between the different host basalts and ocelli samples.

The chondrite normalized rare earth element pattern (Figure 30) shows that all of the host basalt samples have slight LREE enrichment with La/Yb of 2.7 ± 0.6 (Sun and McDonough, 1989). The ocelli samples are significantly enriched in all REE relative to the host basalts and are further enriched in LREE with La/Yb of 6.7 ± 0.9 . The host basalts have minor Eu anomalies ($\text{Eu}/\text{Eu}^* 0.92 \pm 0.06$), whereas the ocelli have significant negative Eu anomalies ($\text{Eu}/\text{Eu}^* 0.71 \pm 0.07$).

The host basalts show an almost flat HREE chondrite normalised pattern with a Gd/Yb 1.36 ± 0.06 , while the ocelli samples have higher Gd/Yb 1.73 ± 0.1 .

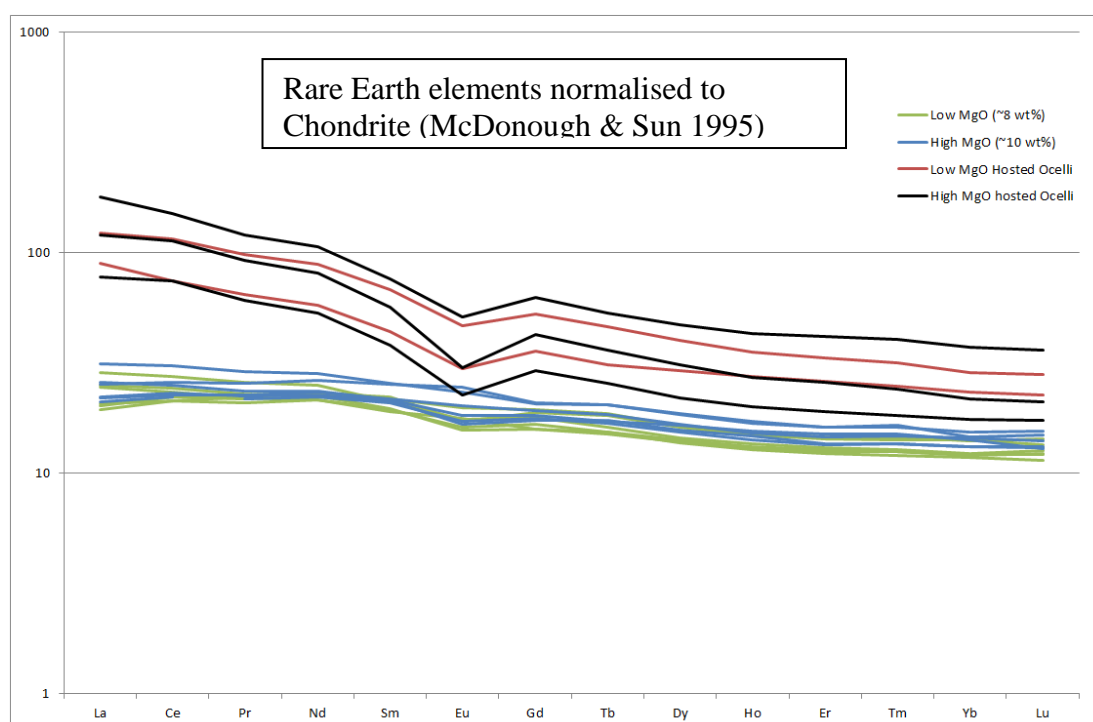


Figure 30. REE diagram normalised to chondrite showing the enrichment of REE in the Ocelli as well as the higher proportion of light REE enrichment.

The N-MORB normalised multi element spider diagram (figure 31) shows that Cs, Rb and Ba have a scattered distribution in both host basalts and ocelli. The host basalts have positive anomalies in U and Pb and negative anomalies in Sr, Ti, Nb and Ta. The ocelli show negative anomalies in Nb, Ta, Ti, Zr, Sr, Eu and Hf. When ocelli

are compared to the host basalts they are indistinguishable in relation to Sr, Zr, Hf, Ti, Nb and Ta, all of which are high field strength or large-ion lithophile elements.

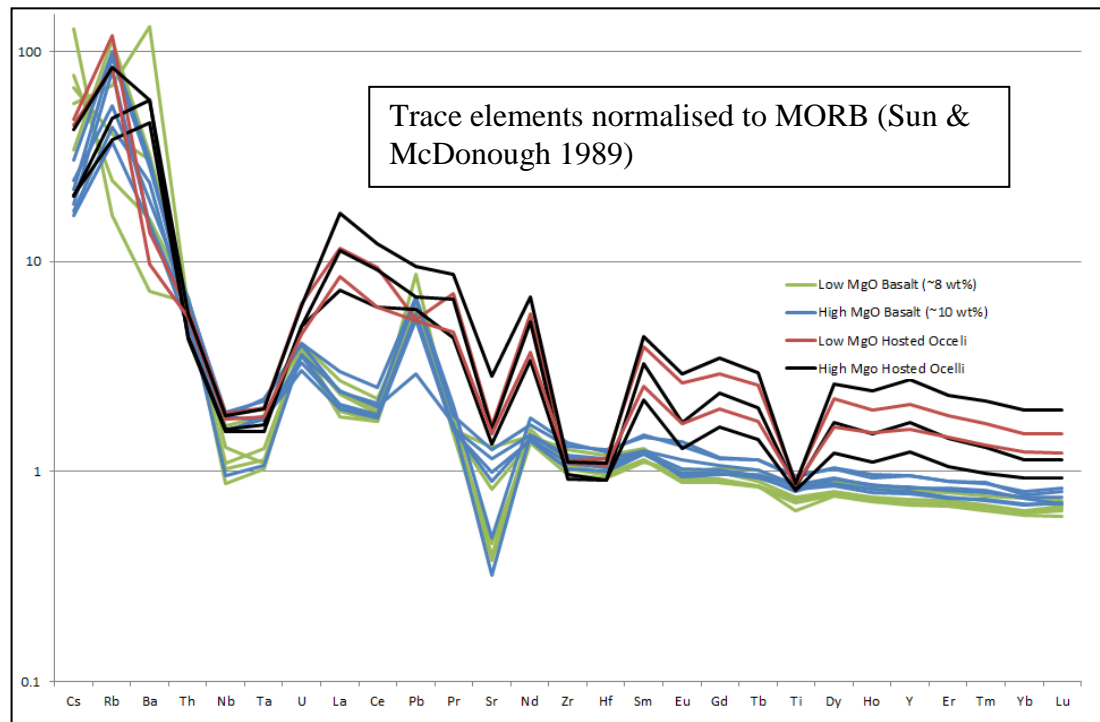


Figure 31. Trace element diagram normalised to N MORB Sun & McDonough (1989), showing variations in trace elements across the samples.

The host basalts show enrichment in Ni and Cr, well above MORB values. The host basalt also shows a slight increase in Cr and Ni with increasing MgO, a typical fractional crystallisation trend. The ocelli samples also show relatively high Ni and Cr. However, the Ni concentrations are lower than the two host basalt types while the Cr values are indistinguishable. (Figure 32).

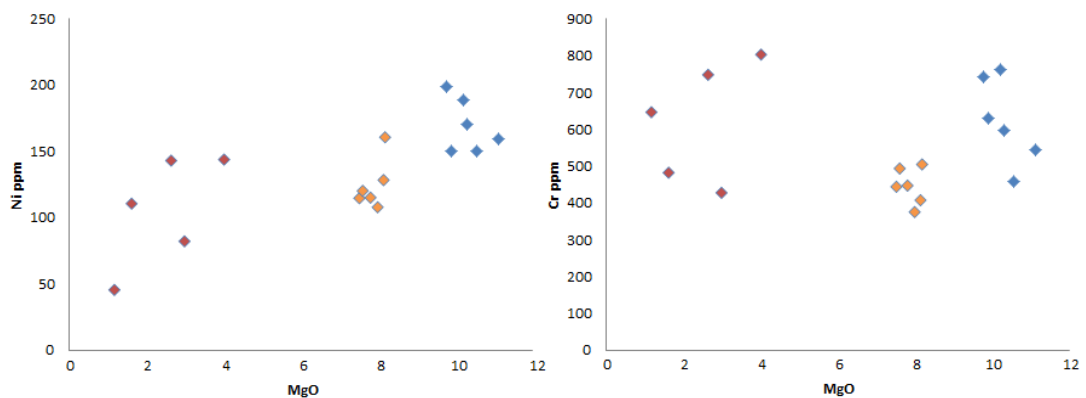


Figure 32. Host basalt and ocelli elements ppm versus MgO. Note that both the host basalts and the ocelli samples are enriched in Cr and Ni (ppm).

The depletions in Nb shown in Figure 31 are reflected in the low Nb/Th with both the host basalt and ocelli samples falling within the field of a hydrated mantle source (Condie, 2015) (Fig. 33). The host basalts and ocelli samples have low Nb/Th ratio when compared to N-MORB. With MORB average of 19.4 compared to the high MgO basalt 3.3-6.2, low MgO basalts 1.8-4.9 and ocelli 6.2-7.0.

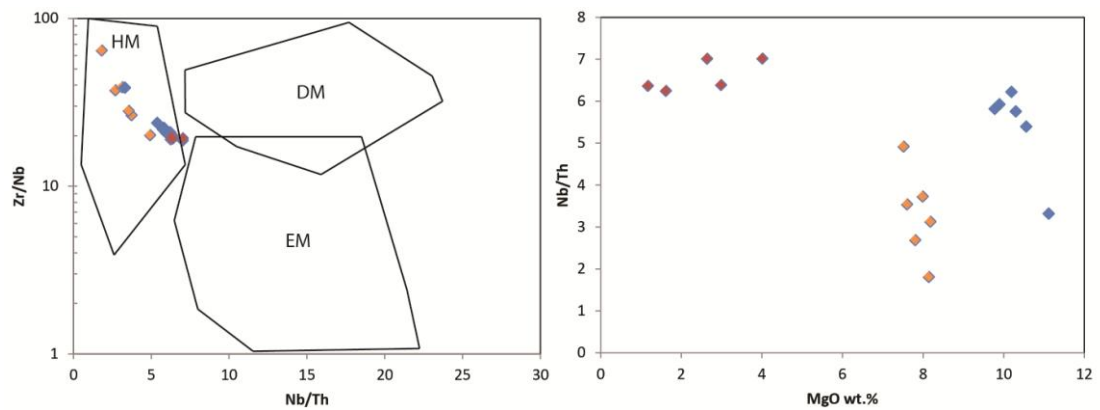


Figure 33. Zr/Nb vs Nb/Th shows a hydrated mantle signature in both the host basalts and ocelli samples (Condie, 2015). HM = Hydrated Mantle, DM = Depleted Mantle and EM = Enriched Mantle.

Microprobe Analysis

Microprobe analysis (Appendix E) was used to compare preserved pyroxenes within the host basalt and the ocelli samples. Three samples were selected for analysis for their well-preserved large pyroxene crystals in both host basalts and ocelli. Both the centres and the rims of the pyroxenes were analysed. The one type of pyroxenes that was identified in both the host basalts and the ocelli sample was Augite ($\text{Wo}_{0.31-0.42}\text{En}_{0.37-0.56}\text{Fs}_{0.11-0.22}$). A comparison of the different elements was done between the host basalts and ocelli samples, with no discernible difference between them.

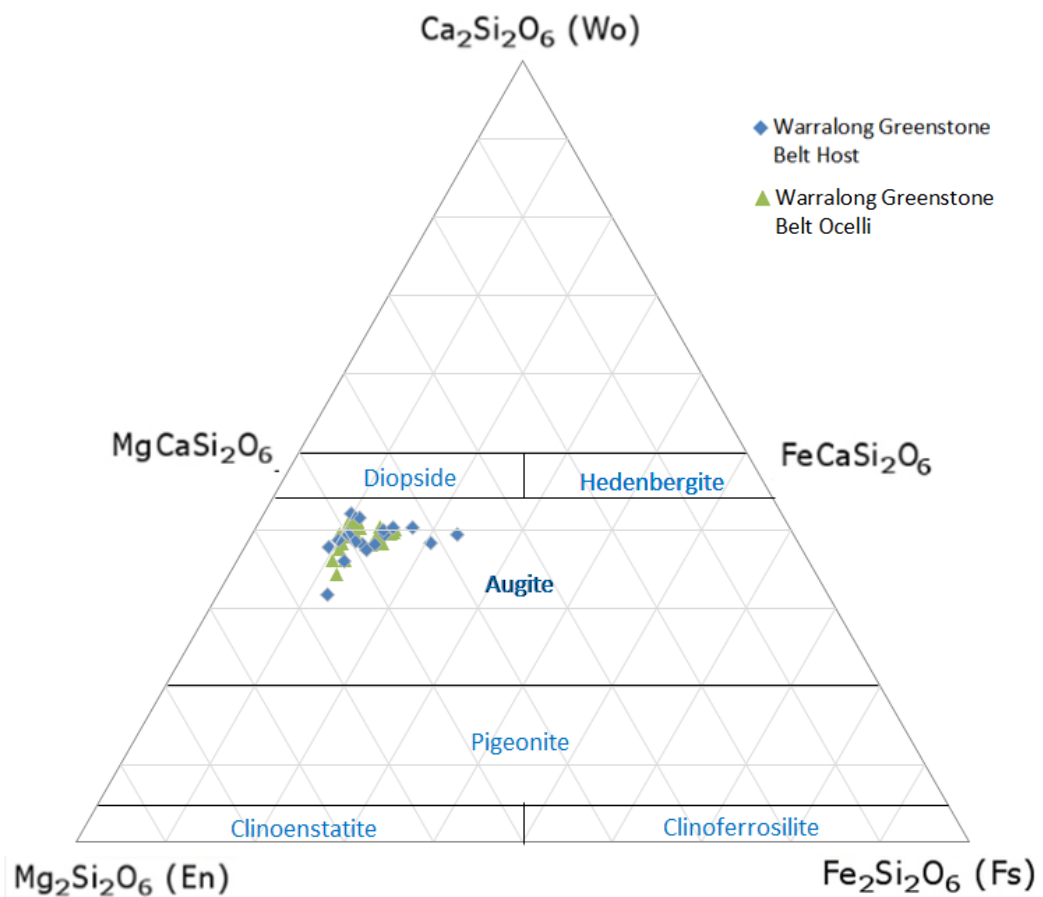


Figure 34. Pyroxene Classification Ternary Diagram, showing the Clinopyroxenes tested in both the Ocelli and Host basalt plot together. Three samples were selected for their well preserved pyroxenes in both the ocelli and the host basalt, TS-2-1, TS-31-1 and 344-2.

For all elements within the pyroxenes, both the host basalt and the ocelli samples lay on the same trend. Comparison of the results with pyroxene data from MORB and

oceanic plateau data (Figure 34) indicate that the Warralong pyroxenes are indistinguishable from MORB pyroxenes, however, with slightly lower Al_2O_3 at a given MgO.

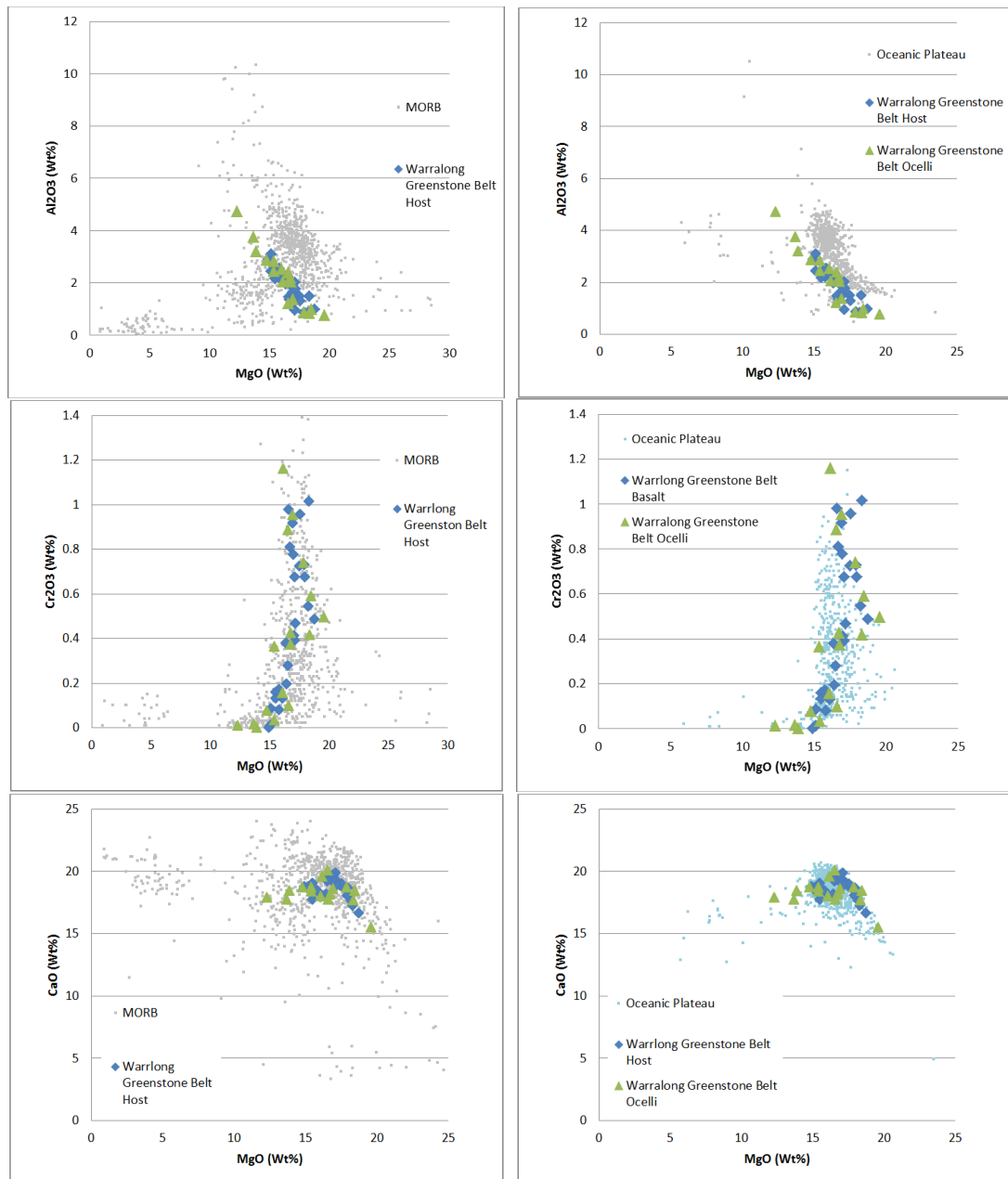


Figure 35. Harker diagrams showing the chemical variation observed in the host basalt and ocelli within the remnant pyroxenes compared to modern volcanic settings. Note the overlapping geochemical result for the ocelli and host basalts. MORB and Oceanic Plateau data obtained from PetDB (<http://www.earthchem.org/petdb>)

Chapter 6: Discussion

The Eastern Section of the Warralong Greenstone Belt has undergone at least three deformation events. These deformation events include tilting of original stratigraphy and at least two faulting and/or folding events. The tilting of volcano-sedimentary stratigraphy to its now sub-vertical orientation, could be associated with emplacement of the Muccan Granitoid dome. Despite these deformation events, areas of low strain are present throughout the eastern Warrawong Greenstone belt and these areas preserve primary stratigraphic, sedimentological and volcanological features. Younging indicators, such as pillow tops, suggest that the stratigraphy gets consistently younger towards the north-west. There is no structural or stratigraphic indication of structural repetition.

Stratigraphy and Emplacement Processes

The eastern yellow chert unit consists of alternating chert and friable recessive clay rich layers. The association of cryptocrystalline quartz and abundant 10-20 μ m zircon in the yellow chert sample indicates that the chert formed possibly from a combination of precipitation from silica rich fluid and volcanic derived air fall material that included zircons. While the recessive clay rich layers could possibly be volcanic ash fall as previously suggested (Van Krenandonk, 2010). This unit was not observed to be in contact with any of the other units in the Eastern Warralong Greenstone belt and therefore cannot be consider as part of the more coherent stratigraphy.

West of the yellow chert, the next unit is the Eastern pillowed meta-basalt, which outcrops as isolated small lozenges. The Eastern pillowed meta-basalt unit consists

of deformed pillow basalts, none of the observed outcrops show the contact between it and the other units in the Eastern Warralong Greenstone belt and therefore cannot be incorporated into a coherent stratigraphy. The observed outcrops consisted of only pillowed basalt, from emplacement under-water.

The Eastern Psammite represents the first unit that can be incorporated into a coherent stratigraphic succession of the EWGB, as it has a conformable contact with the overlying Eastern Chert unit. The protolith was most likely a well sorted silica rich lithic sandstone. Some of the clast observed are dominantly microcrystalline quartz (chert), while the abundant secondary Fe oxides likely represent the alteration products of mafic components. The unit represents a succession of laminated sandstones beds, interbedded with barite rich horizons. Barite bearing sediments in Archean Supercrust have been suggested to occur from either primary precipitates from seawater (Satkoski et al., 2016) or reworking of barite precipitate beds (Sugitani et al., 2006).

The Eastern sedimentary unit has a gradational transition into the overlying conformable Eastern chert unit, which consists of finely laminated layers of chert. However within the Eastern sedimentary unit, the shape of the grains range from sub-rounded to rounded suggesting that the clasts in mineral grains were transported by tractional flow processes and were not deposited close to the original source. The contact between the Eastern sedimentary unit and the Eastern chert is gradational with the Eastern meta-sedimentary unit finely grading upward and intercalating with the Eastern chert unit.

Previous studies have suggested three main mechanisms associated with the formation of chert in the Archean: precipitation from seawater, biogenic deposition and hydrothermal precipitation (Kato and Nakamura, 2003; Sugitani, 1992; van den

Boom et al., 2007). The Eastern chert unit at the base of the studied stratigraphy is interpreted to have been originally hydrothermal precipitation and sedimentary in nature. The laminations, both parallel to strike and conformable to the contact with the underlying meta-sedimentary unit are remnant sedimentary features. The chert unit can be traced along the eastern boundary of the Warralong Greenstone belt and therefore is a single unit. This unit is overlain conformably by younger basalt and therefore is prescribed to the Mount Ada Basalt formation. Many cherts have been associated with the Mount Ada basalts in different Greenstone belts, and are thought to represent periods of low effusion rates or breaks in volcanic activity (Van Kranendonk, 2010; Van Kranendonk et al., 2004a).

The Central pillowed meta-basalt unit forms the largest portion of the research area, composed entirely of pillowed basalts lying conformably on top of the Eastern chert unit. Although the contact was only observed in a small number of outcrops, it was seen to lie conformably above the chert. Pillowed basalts are evidence of subaqueous volcanism (Gregg and Fink, 2000; Jones, 1969; Rakovan, 2005; Wells et al., 1979). On Earth today the greatest amount of basaltic lava is emplaced on the sea floor, however most of this volcanism occurs at depth within the ocean (Griffiths and Fink, 1992a). Despite efforts to observe deep-sea eruptions in action (Baker et al., 1999; Chadwick Jr et al., 1991; Haymon et al., 1991), there is still a lack of direct observation of active deep submarine flows. However shallow submarine flows have been directly observed in areas such as Hawaii and the Mariana arc (Chadwick et al., 2008; Tribble, 1991), helping to broaden the knowledge on submarine flows. Because of this lack of in situ observations of deep marine emplacement, flow parameters have to be determined through laboratory experiments and, due to this, emplacement parameters are predominantly inferred from the resulting flow

morphology (Figure 31). Five lava flow morphologies for basaltic emplacement in subaqueous environments have been identified from laboratory testing (Figure 36). These include pillows, lobate sheets, lineated sheets, ropery sheets and jumble sheets (Gregg and Fink, 1995; Gregg and Fink, 2000; Griffiths and Fink, 1992b). Experiments conducted have suggested that changes in the morphology can be attributed to variations in eruption temperature, effusion rate, viscosity, and crystallinity (Ballard et al., 1979; Bonatti and Harrison, 1988; Gregg and Fink, 1995; Griffiths and Fink, 1992b). Within the EWGB, only pillow basalts are observed, suggesting a high cooling rate, in conjunction with a low slope and low effusion/flow rate (Gregg and Fink, 1995).

Laboratory morphology	Submarine morphology	Ψ 0° min	Cooling rate	Slope	Flow rate
pillows	pillows		↑	↓	↓
	lobate sheets				
rifts	lineated sheets	3			
folds	ropy sheets	10			
levees	jumbled sheets	30			

Figure 36. Figure taken from Gregg and Fink 1995; showing influence of cooling rate, slope and flow rate on submarine morphology.

The western meta-sedimentary unit consists of a repetitive sequence of graded fine-grained sandstones and mudstones with interbedded cherts. The sedimentary sequence has been sorted by grain size and density, with coarser grains being overlain by finer grained particles. This would suggest water saturated turbulent flow (Bouma, 1962; Bouma, 1964). The angular nature of the clasts could be attributed to being in close to proximity to the source material.

Sitting conformably on top of the western meta-sedimentary unit is the western chert unit, observed in a number of outcrops in the southern part of the EWGB. The

western chert unit has similar characteristics as the eastern chert unit, with laminations, both parallel to strike and conformable to the contact with the underlying western meta-sedimentary unit. The western chert unit has the same emplacement mechanism as the eastern and is interpreted to have been originally hydrothermal precipitation and sedimentary in nature.

Depositional Environment

The Eastern meta-sedimentary unit rock clasts and mineral grains were transported by tractional flow processes, however the depositional environment of this unit cannot be further constrained, as primary sedimentary morphologies have not been preserved. Primary bedding structures preserved within the overlying Eastern chert unit suggest deposition in a low energy environment below wave base. This, coupled with the presence of underlying sedimentary sequences, could suggest that both units were deposited in the same environment, transitioning from a higher energy process that formed the Eastern meta-sediment to a low energy process of the Eastern chert.

The lack of vesiculation in the pillow basalts observed both in outcrop and from petrographic analysis suggest that the lava flows in the EWGB was either emplaced in deep water (Jones, 1969; Moore, 1965) where vesiculation is suppressed due to pressure proximal to the site of eruption or that the lavas lost their volatile load due to long transport from a distal eruption site. These two possibilities cannot be tested without knowledge of the proximity to the vent site or the volatile content of the lavas. High effusion rates favour sheet/massive flows, whereas low effusion rates favour pillow formation (Gregg and Fink, 2000; Rakovan, 2005; Wells et al., 1979). Topography and cooling rate influence pillow morphology, with pillow formation associated with fast cooling and no slopes (Furnes, et al., 2011). The presence of only pillowed basalt flows, and the conformably bounding fine-grained sediments,

suggest that basalts were ubiquitously emplaced in a locally flat-lying marine environment with locally low effusion rate resulting in increased cooling rate (Furnes et al., 2011; Gregg and Fink, 1995; Griffiths and Fink, 1992b; White et al., 2002).

The Western meta-sediment unit lies conformably above the central basalt unit, and consists of repeated cycles of mudstones and siltstones. A lack of significant deposits of coarse-grained sediments, in addition to the sub-angular to sub-rounded grain morphology suggests that the unit was deposited medially to distally to the source. Sitting conformably above the Western meta-sediments is the Western chert unit, which is interpreted to have been originally sedimentary in nature due to the presence of primary sedimentary structures, parallel strike and conformability to the underlying sediments. The Western chert unit would have been deposited in a similar environment to that of the Eastern chert unit, possibly in a low energy deep marine environment.

Petrogenesis of ocelli bearing basalts

The geochemical data obtained in this study from the central basalt unit indicates that there is a variation in composition of the pillow lavas with stratigraphy (appendix b). The samples with relatively low MgO occur to the east and west while the samples with relatively high MgO occur through the central part of the unit as seen in appendix B. The near identical trace element systematics between the two groups (Figure 30 and 31) indicate that they represent a cogenetic lava suite with variation caused by variation in fractional crystallisation. The ocelli and host basalt were analysed separately to determine the relationship between the two. Once defined, the host-ocelli relationship then allows for the petrogenesis of the central basalt unit to be elucidated upon.

Petrogenesis of ocelli

Ocelli occur in many Archean basaltic rocks (Sandstå et al., 2011) and there have been several different processes proposed for formation of ocelli within basalt, including supercooling spherulitic process (Clay et al., 2013; Fowler et al., 2002; Fowler et al., 1987; Gudin et al., 2012; Monecke et al., 2004), incorporation of immiscible crustal melt (Appel et al., 2009; Gudin et al., 2012; Polat et al., 2009) and fractional crystallisation liquid immiscibility (Gélinas et al., 1976; Philpotts, 1982; Philpotts, 1979; Philpotts, 2008; Sandstå et al., 2011; Veksler et al., 2007).

The petrographic evidence within the pillowed basalt has shown that rapid cooling has taken place in the form of long acicular and radiating pyroxene. The petrography shows no evidence of spherulitic textures in the ocelli. Spherulitic textures are typically represented as radial intergrowth of plagioclase and pyroxene needles (Figure 37). No such textures are observed within the ocelli's of all the samples (Figure 17, 38). Petrographically the ocellis show similar mineral textures as the host basalts suggesting similar rates of crystallisation.

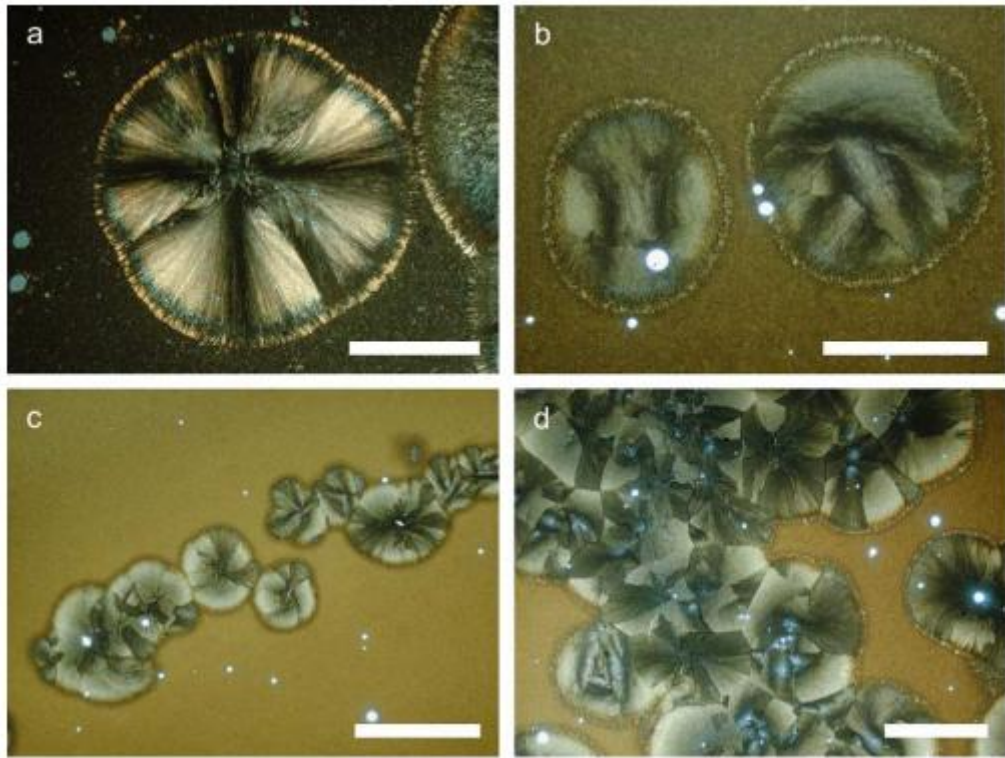


Figure 37. Photomicrograph of supercooling spherulitic textures forming within ocelli as presented by Monecke et al. (2004), scale bare 1 mm.

Geochemically, spherulitic crystallisation should manifest as enrichment in elements compatible in plagioclase and pyroxene, which intergrow to define the typical spherulitic texture. That the ocelli are enriched in all REE but show a negative Eu/Eu^* is not expected from a plagioclase bearing spherulite. Furthermore, that concentrations of both Cr and Sc, which are highly compatible in pyroxene, are indistinguishable between the ocelli and the host basalts argues against a pyroxene bearing spherulite.

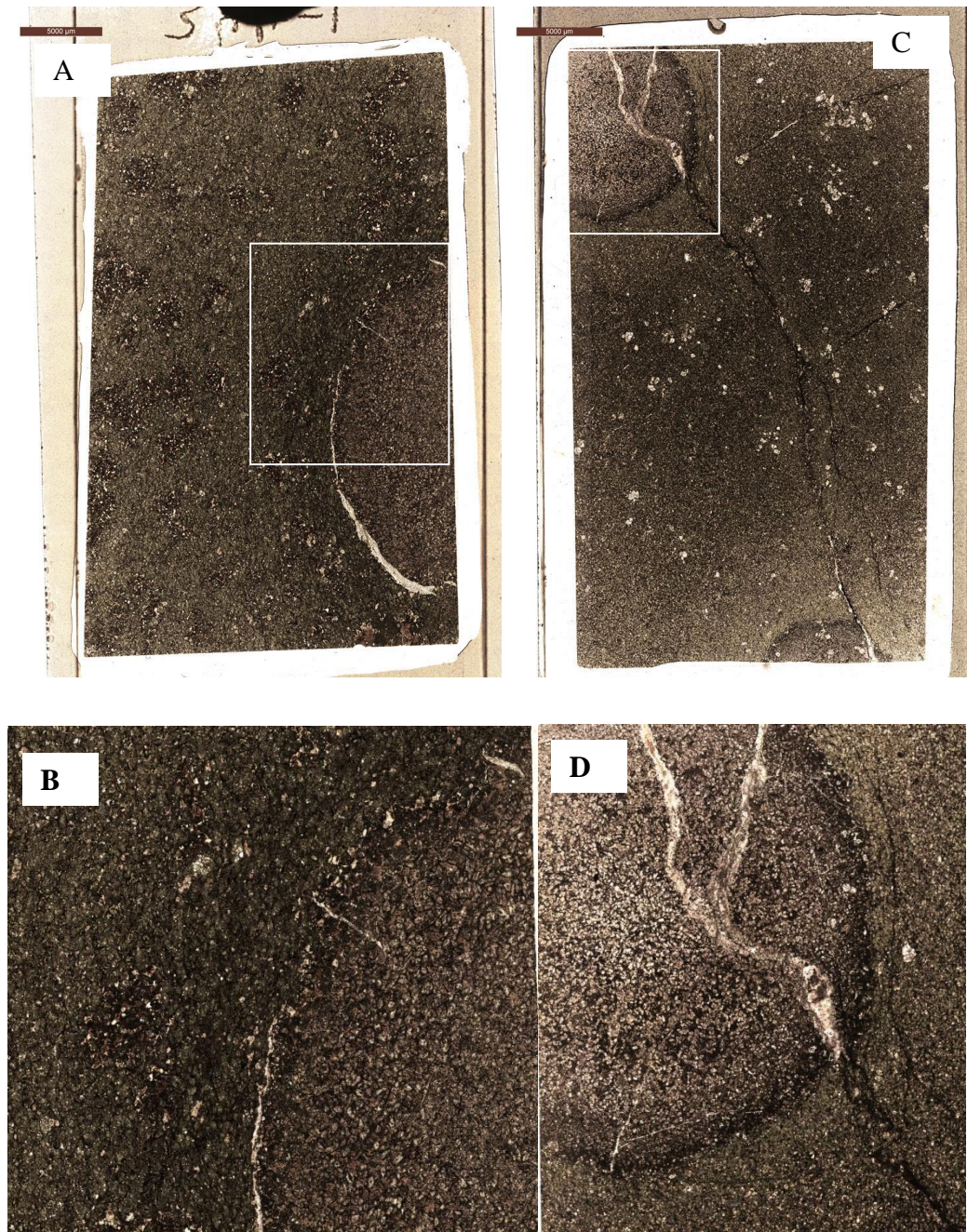


Figure 38. Digital mosaic image of ocelli bearing samples in plane polarised light (A & B) TS-334-1 where (B) is a close up of the ocelli host contact and (C & D) JDK 69 where (D) is a close up of the ocelli host contact. The images show the ocelli and host basalt relationship with very distinct rims. Both the host basalt and the ocelli contain pyroxene micro-phenocrysts. The preserved magmatic texture in the ocelli are not consistent with spherulitic textures.

Microprobe analysis revealed that the largest microphenocryst pyroxenes within the ocelli and the host basalt have a near identical geochemical signature. This would suggest that they both crystallised from the same source magma. This is not

consistent with the ocelli liquid being derived from a separate source such as mingling with a felsic melt (Appel et al., 2009; Gudin et al., 2012; Polat et al., 2009), but rather that the ocelli liquid and host basaltic liquid share a common parentage. Petrographically it was also observed that the well-preserved ocelli samples have coherent and distinct boundaries, whereas during magma mingling it is expected that there would be a reaction or diffusive rim. Furthermore, a crustal melt mingling origin of the ocelli predicts low Cr contents, a comparable enrichment in Zr and Hf relative to Sm and Nd and enrichment in Pb. In contrast, Cr, TiO₂, Zr and Hf concentrations in the ocelli are indistinguishable from their host basalts, suggesting that they have behaved conservatively during the formation of the ocelli.

The host rock shows enrichment in MgO, Fe₂O_{3T} and MnO, while the ocelli show enrichment of Na₂O, P₂O₅ and SO₃. While Na₂O, and SO₃ are often highly affected by alteration (Alt et al., 1986; Alt and Teagle, 2003), the distinct difference between the host basalt and ocelli samples from the same pillow would suggest that these differences are inherent to the original chemistry of the rock and not due to alteration. The ocelli show preferential enrichment of REE and, specifically, enrichment of Light REE relative to Heavy REE.

These major elemental differences have been shown in previous studies to be consistent with liquid immiscibility (Gélinas et al., 1976; Philpotts, 1982; Philpotts, 1979; Sandstå et al., 2011; Yoder, 1973). In tholeiitic compositions intrusive liquid immiscibility is commonly observed and consists of a felsic end-member that is enriched in alumina and alkalis and a mafic Fe rich end-member (Bogaerts and Schmidt, 2006; Philpotts, 1982). Such immiscible reactions commonly occur in relatively shallow magma chambers under pressures 650 Mpa to 0.1 Mpa and temperatures of 1050°C to 1240°C (Appel et al., 2009; Bogaerts and Schmidt, 2006;

Charlier and Grove, 2012; Freestone and Hamilton, 1980; Philpotts, 1982; Polat et al., 2009). Such pressure are equivalent to 25 km to <1 km of crustal depth, and at temperatures significantly below estimated ambient mantle temperature in the Archean.

However, these experimental studies have also shows that concentrations of P and REE partition into the Fe-rich immiscible liquid (Ripley et al., 1998; Jakobsen et al., 2005; VanTongeren and Mathez., 2012), which is the opposite of what is observed in the Central Pillow Basalt Unit samples. Other high field strength elements have also been shown to preferentially concentrate within the Fe-rich liquid along with Sr, Cr and Ni (Ripley et al., 1998; Jakobsen et al., 2005; VanTongeren and Mathez., 2012), however, as previously stated this has not been observed.

The petrological evidence indicates that the ocelli features within the pillow basalts of the central basalt unit are consistent with liquid immiscibility, discounting spherulitic crystallisation and magma mingling as the origin for the observed ocelli. The geochemical evidence also adds strength to liquid immiscibility for formation of ocelli, however, there were also inconsistencies relative to experimental immiscibility studies (Veksler, I.V., 2004) and relative to modern examples of tholeiite immiscibility (Veksler, I.V., 2004).

While it is not possible to conclusively demonstrate that the ocelli represent a liquid immiscibility feature without further data, for the remainder of the thesis the host and ocelli are considered to be reciprocal components of a common parental magma.

Petrogenesis of Central Pillow Basalt Unit

In the field, the majority of pillows were noted as having a moderate abundance (~10 - 20%) of ocelli. However, in thin sections, the ocelli make up less than 10% of the rock samples. Because of this, 10% was taken as the average weight percent of ocelli

in the whole rock. Using 10% of the total volume as ocelli chemistry, the ocelli and host basalt chemistry was recombined to approximate the composition of the parental magma.

The modelled parental magmas (Figure 39) show variable negative Nb and Ta anomalies with two groups evident, which are not related to MgO grouping and show no stratigraphic relationship, that reflect variable crustal contribution in melts (Arculus and Johnson, 1981; Briquet et al., 1984; Pearce and Cann, 1973).

Niobium depletion, low Nb/Th ratio and Pb enrichment as observed in Central Pillow basalt unit samples can be explained by either crustal contamination (Jolly and Hallberg, 1990) of the parent magma or that these magmas are derived by melting of a hydrated mantle source (Condie, 2015; Condie, 2001). However, a model invoking crustal contamination must take into account the scarce evidence for pre-Warrawoona felsic crust within the Pilbara (Kemp et al., 2015a; Kemp et al., 2015c). The presence of a crystalline basement material has been inferred from indirect evidence, including zircon dates from enclaves within granitic complexes, pre-Warrawoona detrital zircons in sediments and Sm-Nd isotopes (Bickle et al.; Green et al., 2000; Kemp et al., 2015b; Smithies et al., 2003; Van Kranendonk et al., 2007). However, the fact that there is no recorded preserved pre-Warrawoona group crust in the EPT does not preclude crustal contamination (Kemp et al. 2015). Modelling crustal contamination requires constraints on the nature of the uncontaminated melt and the contaminant, which are not available at present. It was concluded that distinguishing between crustal contamination and a primary feature associated with hydration of the melt source for the origin of low Nb/Th is not possible without radiogenic isotope data.

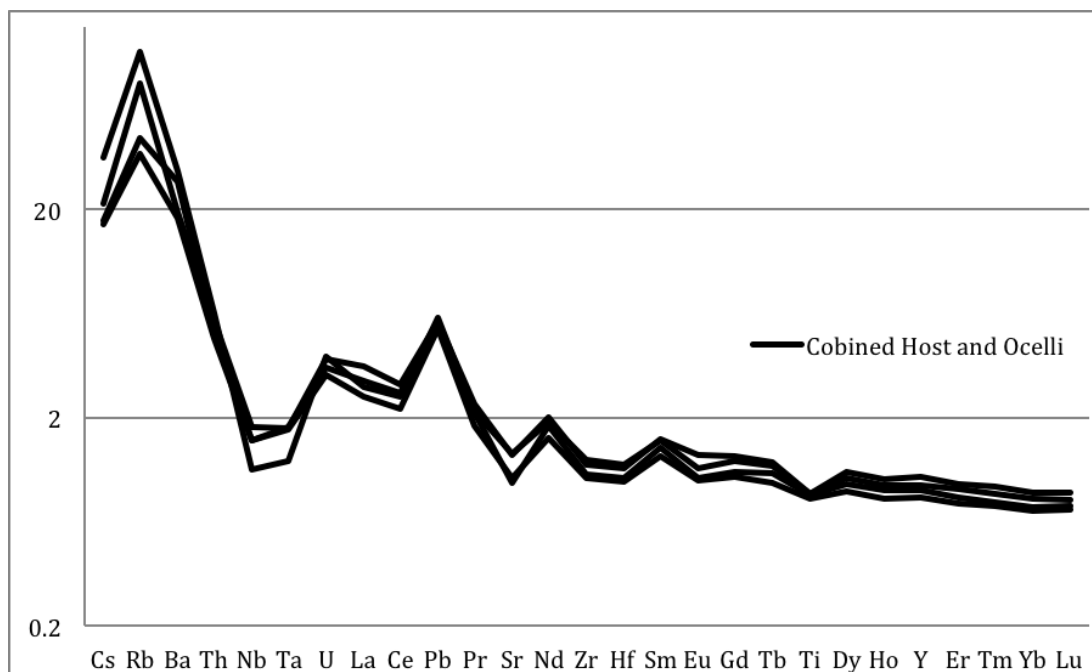


Figure 39, Multi elemental spider diagram of combined trace elements normalised to MORB, the defined negative and positive anomalies noted within the individual melts is consistent when compared to the combined elemental spider diagram.

Volcanic Conditions

The host basalts at the Warralong Greenstone belt had an estimated liquidus temperature based on the calculated liquidus at 40.3Mpa, which is equivalent to 4km deep in the ocean, to account for the lack of vesiculation in pHMELTS (*Ghiorso and Sack, 1995; Smith and Asimow, 2005*) of 1297.66°C (TS-22-1 host basalt) to 1202.93 °C (TS-53-1 host basalt). The ocelli sample had noticeably lower liquidus temperature of 1123.84°C (TS-31-1 Ocelli hosted in high MgO basalt) to 1116.21 °C (JDK-69 Ocelli hosted in low MgO basalt), assuming a bulk water content of 1.0 wt% for all samples. The calculated liquidus temperature is significantly lower than that of modelled Archean ambient mantle temperatures (Herberg and Asimow 2008) (Figure 38). Secular cooling models such as Richter (1988), suggest that ambient temperatures in the mantle range from 1670 (3.48Ga) to 1620°C (3.27Ga). However, recent studies by Korenaga (2008a, 2008b) have modelled temperatures of ~1680°C at 3.48-3.27Ga, which are supported by studies by Herzberg et al. (2010).

Petrogenetic studies into Archean mantle temperatures, such as those conducted by Puchtel et al. (2013), found that komatiites in the Barberton area had an eruption temperature of ~1600 °C and were derived from mantle melt temperatures of 1820°C (3.48 Ga) and 1830 °C (3.27 Ga) using the method for fresh olivine defined by McKenzie and Bickle (1988). However the same paper found that using a different method by Herzberg and Asimow (2008) achieved mantle temperatures of ~1740 °C and 1760 °C. Similar results were also found by a study by Connolly et al. (2011), who found that the komatiites from the Weltevreden (3.5Ga) were emplaced at a temperature of ~1600 °C and were a result of mantle melting temperatures of ~1830 °C using the McKenzie and Bickle (1988) protocols, and temperatures of ~1760 °C using the Herzberg and Asimow (2008). The higher than expected ambient mantle melt temperature of these studies are attributed to mantle plumes. Mantle plumes, or “hot spots” are suggested to be areas of hotter mantle material producing melts that form komatiites (Figure 40).

The Warralong samples liquidus temperature for the host basalts obtained from melts indicate significantly lower emplacement temperatures than what has previously been found for similar Greenstone belt basalts that are thought to be products of plume volcanism.

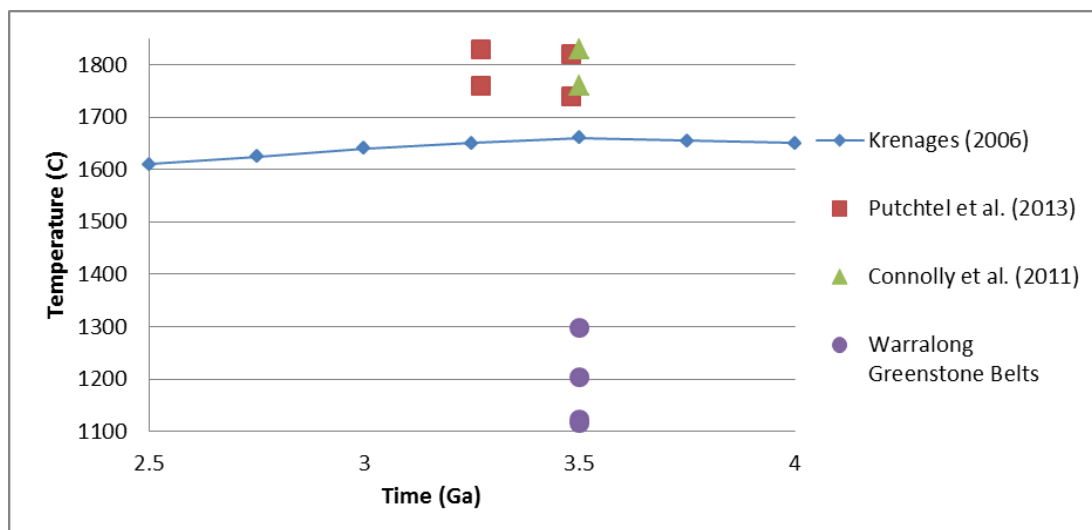


Figure 40. Archean mantle temperatures from a modelling and petrology perspective. Mantle temperatures from studies by Puchtel et al (2013) and Connolly et al. (2011) using protocols from both McKenzie and Bickle (1988) and Herberg and Asimow (2008) compared to Korenagas (2006) model for ambient mantle temperature and the recorded liquidus temperatures from the Warralong Greenstone belt.

Geodynamics of the Archaean

Previously, vertical tectonic models in a stagnant-lid geodynamic regime similar to what has been observed on modern-day Venus, have been proposed for the early Earth (Debaille et al., 2013; Solomatov and Moresi, 1996). They have been characterised as thick mafic sequences built up by episodic outpourings from massive plumes, resulting in whole-crustal resurfacing causing large amounts of heat dissipation (Kamber et al., 2005). The thick volcanic stratigraphic sequences observed in the major Greenstone sequences of Archaean terranes in Abitibi (Canada), Barberton (South Africa) and Pilbara (Western Australia) have been used to support this hypothesis (Debaille et al., 2013; Kamber et al., 2005). The Warralong Greenstone belt is interpreted to be associated with the Mt Ada mantle plume event within the East Pilbara Terrane (Smithies 2007). However the presented depositional environment and volcanism emplacement mechanism of slow effusion/flow rates and high cooling rate, as well as the modelled liquidus

temperatures, which are significantly lower than what would be expected from Early Archean plume volcanism (Campbell et al., 1989; Connolly et al., 2011; Dostal and Mueller, 2013; Puchtel et al., 2013; Van Kranendonk et al., 2007) all are inconsistent with plume magmatism. Most of the recent models rely on plumes as the cornerstone of the Earth's thermal evolution (Dostal and Mueller, 2013), however, with liquidus temperatures lower than modelled ambient Early Archean mantle temperatures it is hard to link the volcanism observed in the Warralong Greenstone belt with plume volcanism.

The presented low effusion rates have large implications on the interpretation of the Mt Ada sequence, which is thought to consist of a single large volcanic eruption covering a large area (Smithies et al., 2005; Van Kranendonk, 2006; Van Kranendonk et al., 2004a). The large volume and lateral continuity across five greenstone belts currently suggested for the Mount Ada basalt suggests a high effusion rate event that would have resulted in proximal sheet flows and pillow lavas only in distal environments.

The Greenstone belts within the East Pilbara terrane have previously been characterised as consisting of plume-related cycles of major basaltic and komatiitic to felsic volcanic rocks, interrupted by sedimentary deposition (Hickman, 1981; Hickman, 1983; Van Kranendonk et al., 2004a; Van Kranendonk et al., 2004b). Previously, it has been suggested that almost all plume-associated Archean volcanism produced komatiitic and basaltic lava flows (Arndt et al., 2008; Condie, 2001; Dostal and Mueller, 2013; Polat and Kerrich, 2000). However, the available geochemical data for basalts in the Mount Ada Basalts show that they are dominated by tholeiite to picrite basalts with variable contributions from both anhydrous to hydrous mantle sources (Smithies 2007 and this study). Therefore models on the

formation of the volcanic cycles within the East Pilbara Terrane need to consider tectonic scenarios where basaltic melting occurs at sub-ambient mantle temperatures and melting of both hydrated and anhydrous mantle.

Chapter 7: Conclusions

A petrological and geochemical study was undertaken on a stratigraphic sequence specifically investigating the Archean volcanic and sedimentary succession from the Warralong Greenstone belt (East Pilbara Craton, Western Australia). The study area has undergone regional metamorphism of lower to middle greenschist facies, and has been affected by deformation, alteration and weathering.

The sedimentary nature of the chert units present within the EWGB, as well as a lack of vesiculation, suggests that the volcano-sedimentary sequence was emplaced in deep water, below wave base and potential in a very deep (>4000 m) basin, if lack of vesiculation is due to pressure rather than degassing. The pillow morphology and lack of sheet flows suggest that the basalt had a low effusion rate, fast cooling rate and that the depositional environment was flat laying. The similarities in the lower and upper sediments suggest that this depositional environment did not change significantly throughout this period of volcanism and sedimentation.

Field observations coupled with petrographic analysis have raised many anomalies with current paleoenvironmental emplacement models from previous studies for the Mount Ada basalts. The presence of only pillowed basalt flows is evidence of low effusion and fast cooling rates, which would not facilitate the long flow distances needed to explain the presence of Mount Ada basalts in 6 other Greenstone belts. The extent of assumed lateral continuity of the Mount Ada basalt would suggest high effusion rate as well as a high ratio of sheet flows, to cover the area where it has been observed; however no evidence of this was found.

The basalts collected from the Warralong Greenstone belt have undergone a range of low to moderate degrees of alteration, as reflected by the low and high LOI and moderately to highly variable composition of fluid mobile elements such as Cs, Rb, K and Na. Two groups of host basalts were identified with bimodal distribution based on MgO wt% values. All samples contained leucocratic components manifested as ocelli. Some magmatic trends have been identified as well as well-preserved magmatic textures that have enabled the exclusion of spherulitic crystallisation and crustal contaminations for the formation of the ocelli. The mineralogy, texture and the chemistry of the ocelli is consistent with fractional crystallization liquid immiscibility as the formation mechanism for the ocelli melt.

The geochemical signature observed within the preserved pillow basalts, has also indicated that there are two possible mechanisms for the formation of the source magma. These two possibilities include either a hydrated mantle source, or crustal contamination. While both of these are possible mechanisms for the formation of the source magma, there has almost been no felsic crystalline basement material observed in the Pilbara and only previously has only been reported in indirect observation. However, Wiemer (in press) has dated a gneiss unit on the southern margin of the Muccan Granitoid Complex adjacent to the Doolena Gap Greenstone belt at 3.5 Ga, predating the deposition of the EWGB. This unit would suggest that there was felsic crustal basement present to contaminate the basalts of the EWGB. With this in consideration it is not possible to eliminate either options as possible sources for the parent magma of the EWGB central basalt unit. The lower modelled melt temperatures, below the komatiites observed in the Barberton Greenstones as well as the lower MgO Wt%. provides evidence that the basalt formed from mantle

at ambient to sub-ambient temperatures for the Archean and not likely from plume activity.

Further work is required within the East Pilbara Craton to determine if the same magmatic mechanism produces ocelli in other Greenstone belts, as well as to determine if the Mount Ada basalts within the Warralong Greenstone belt are petrogenetically related to other Mount Ada basalts within the East Pilbara craton.

Bibliography

- Alt, J.C., Honnorez, J., Laverne, C., Emmermann, R., 1986. Hydrothermal alteration of a 1 km section through the upper oceanic crust, Deep Sea Drilling Project Hole 504B: Mineralogy, chemistry and evolution of seawater-basalt interactions. *Journal of Geophysical Research: Solid Earth* (1978–2012) 91, 10309-10335.
- Alt, J.C., Teagle, D.A., 2003. Hydrothermal alteration of upper oceanic crust formed at a fast-spreading ridge: mineral, chemical, and isotopic evidence from ODP Site 801. *Chemical Geology* 201, 191-211.
- Anhaeusser, C.R., 1975. Precambrian tectonic environments. *Annual Review of Earth and Planetary Sciences*, 3, p.31.
- Appel, P.W., Polat, A., Frei, R., 2009. Dacitic ocelli in mafic lavas, 3.8–3.7 Ga Isua greenstone belt, West Greenland: geochemical evidence for partial melting of oceanic crust and magma mixing. *Chemical Geology* 258, 105-124.
- Arculus, R., Johnson, R., 1981. Island-arc magma sources: A geochemical assessment of the roles of slab-derived components and crustal contamination. *Geochemical Journal* 15, 109-133.
- Arndt, N., Leshner, M.C., Barnes, S.J., 2008. Komatiite.
- Arndt, N.T., 1977. Ultrabasic magmas and high-degree melting of the mantle. *Contributions to Mineralogy and Petrology* 64, 205-221.
- Arndt, N.T., Nisbet, E.G., 2012. Processes on the young Earth and the habitats of early life. *Annual Review of Earth and Planetary Sciences* 40, 521-549.
- Baker, E.T., Fox, C.G., Cowen, J.P., 1999. In situ observations of the onset of hydrothermal discharge during the 1998 submarine eruption of Axial Volcano, Juan de Fuca Ridge. *Geophysical Research Letters* 26, 3445-3448.
- Ballard, R.D., Holcomb, R.T., Andel, T.H., 1979. The Galapagos Rift at 86 W: 3. Sheet flows, collapse pits, and lava lakes of the rift valley. *Journal of Geophysical Research: Solid Earth* (1978–2012) 84, 5407-5422.
- Bickle, M.J., Bettenay, L.F., Chapman, H.J., Groves, D.I., McNaughton, N.J., Campbell, I.H., Laeter, J.R., The age and origin of younger granitic plutons of the Shaw Batholith in the Archaean Pilbara Block, Western Australia. *Contributions to Mineralogy and Petrology* 101, 361-376.
- Bogaerts, M., Schmidt, M., 2006. Experiments on silicate melt immiscibility in the system $\text{Fe}_2\text{SiO}_4\text{-KAlSi}_3\text{O}_8\text{-SiO}_2\text{-CaO-MgO-TiO}_2\text{-P}_2\text{O}_5$ and implications for natural magmas. *Contributions to Mineralogy and Petrology* 152, 257-274.
- Bonatti, E., Harrison, C., 1988. Eruption styles of basalt in oceanic spreading ridges and seamounts: Effect of magma temperature and viscosity. *Journal of Geophysical Research: Solid Earth* (1978–2012) 93, 2967-2980.
- Bouma, A., 1962. Sedimentology of some flysch deposits. Elsevier, Amsterdam. I68 pp. x975. Sedimentary structure of Philippine Sea and Sea of Japan sediments, DSDP, Leg 3, 489-497.
- Bouma, A., 1964. Turbidites. *Developments in sedimentology* 3, 247-256.
- Brown, A. J., Cudahy, T. J., & Walter, M. R. (2006). Hydrothermal alteration at the Panorama formation, North pole dome, Pilbara craton, Western Australia. *Precambrian Research*, 151, 211-223.
- Briqueu, L., Bougault, H., Joron, J.L., 1984. Quantification of Nb, Ta, Ti and V anomalies in magmas associated with subduction zones: petrogenetic implications. *Earth and Planetary Science Letters* 68, 297-308.

-
- Campbell, I., Griffiths, R., Hill, R., 1989. Melting in an Archaean mantle plume: heads it's basalts, tails it's komatiites. *Nature* 339, 697-699.
- Cawood, P.A., Hawkesworth, C., Dhuime, B., 2013. The continental record and the generation of continental crust. *Geological Society of America Bulletin* 125, 14-32.
- Chadwick Jr, W.W., Embley, R.W., Fox, C.G., 1991. Evidence for volcanic eruption on the southern Juan de Fuca Ridge between 1981 and 1987. *Nature* 350, 416-418.
- Chadwick, W., Cashman, K., Embley, R., Matsumoto, H., Dziak, R., De Ronde, C., Lau, T., Dearthorff, N., Merle, S., 2008. Direct video and hydrophone observations of submarine explosive eruptions at NW Rota-1 volcano, Mariana arc. *Journal of Geophysical Research: Solid Earth* 113.
- Charlier, B., Grove, T.L., 2012. Experiments on liquid immiscibility along tholeiitic liquid lines of descent. *Contributions to Mineralogy and Petrology* 164, 27-44.
- Clay, P., O'Driscoll, B., Gertisser, R., Busemann, H., Sherlock, S., Kelley, S., 2013. Textural characterization, major and volatile element quantification and Ar–Ar systematics of spherulites in the Rocche Rosse obsidian flow, Lipari, Aeolian Islands: a temperature continuum growth model. *Contributions to Mineralogy and Petrology* 165, 373-395.
- Coish, R., Hickey, R., Frey, F., 1982. Rare earth element geochemistry of the Betts Cove ophiolite, Newfoundland: complexities in ophiolite formation. *Geochimica et Cosmochimica Acta* 46, 2117-2134.
- Condie, K. C., 1981. *Archean greenstone belts* (Vol. 3). Elsevier.
- Condie, K., 2015. Changing tectonic settings through time: Indiscriminate use of geochemical discriminant diagrams. *Precambrian Research* 266, 587-591.
- Condie, K.C., 2001. *Mantle plumes and their record in Earth history*. Cambridge University Press.
- Connolly, B.D., Puchtel, I.S., Walker, R.J., Arevalo Jr, R., Piccoli, P.M., Byerly, G., Robin-Popieul, C., Arndt, N., 2011. Highly siderophile element systematics of the 3.3 Ga Weltevreden komatiites, South Africa: Implications for early Earth history. *Earth and Planetary Science Letters* 311, 253-263.
- de Wit, M.J., 2004. Archean greenstone belts do contain fragments of ophiolites. *Developments in Precambrian Geology* 13, 599-614.
- Debaille, V., O'Neill, C., Brandon, A.D., Haenecour, P., Yin, Q.-Z., Mattielli, N., Treiman, A.H., 2013. Stagnant-lid tectonics in early Earth revealed by ^{142}Nd variations in late Archean rocks. *Earth and Planetary Science Letters* 373, 83-92.
- Dostal, J., 2008. *Igneous Rock Associations 10. Komatiites*. 2008.
- Dostal, J., Mueller, W.U., 2013. Deciphering an Archean mantle plume: Abitibi greenstone belt, Canada. *Gondwana Research* 23, 493-505.
- Duzgoren-Aydin, N.S., Aydin, A., Malpas, J., 2002. Re-assessment of chemical weathering indices: case study on pyroclastic rocks of Hong Kong. *Engineering Geology* 63, 99-119.
- Foley, S.F., 1984. Liquid immiscibility and melt segregation in alkaline lamprophyres from Labrador. *Lithos* 17, 127-137.
- Fowler, A., Berger, B., Shore, M., Jones, M., Ropchan, J., 2002. Supercooled rocks: development and significance of varioles, spherulites, dendrites and spinifex in Archaean volcanic rocks, Abitibi Greenstone belt, Canada. *Precambrian Research* 115, 311-328.
- Fowler, A.D., Jensen, L.S., Peloquin, S.A., 1987. Varioles in Archean basalts: products of spherulitic crystallization. *Can Miner* 25, 275-289.

-
- Freestone, I.C., Hamilton, D.L., 1980. The role of liquid immiscibility in the genesis of carbonatites — An experimental study. *Contributions to Mineralogy and Petrology* 73, 105-117.
- Furnes, H., de Wit, M.J., Robins, B., Sandstå, N.R., 2011. Volcanic evolution of the upper Onverwacht Suite, Barberton greenstone belt, South Africa. *Precambrian Research* 186, 28-50.
- Furnes, H., Dilek, Y., de Wit, M., 2013. Precambrian greenstone sequences represent different ophiolite types. *Gondwana Research*.
- Furnes, H., Dilek, Y., de Wit, M., 2015. Precambrian greenstone sequences represent different ophiolite types. *Gondwana Research* 27, 649-685.
- Gélinas, L., Brooks, C., Trzcienski Jr, W., 1976. Archean variolites-quenched immiscible liquids. *Canadian Journal of Earth Sciences* 13, 210-230.
- Glikson, A.Y., 2013. Uniformitarian Models and the Role of Asteroid Impacts in Earth Evolution, *The Asteroid Impact Connection of Planetary Evolution*. Springer, pp. 129-136.
- Green, D., Nicholls, I., Viljoen, M., Viljoen, R., 1975. Experimental demonstration of the existence of peridotitic liquids in earliest Archean magmatism. *Geology* 3, 11-14.
- Green, M.G., Sylvester, P.J., Buick, R., 2000. Growth and recycling of early Archaean continental crust: geochemical evidence from the Coonterunah and Warrawoona Groups, Pilbara Craton, Australia. *Tectonophysics* 322, 69-88.
- Gregg, T.K., Fink, J.H., 1995. Quantification of submarine lava-flow morphology through analog experiments. *Geology* 23, 73-76.
- Gregg, T.K.P., Fink, J.H., 2000. A laboratory investigation into the effects of slope on lava flow morphology. *Journal of Volcanology and Geothermal Research* 96, 145-159.
- Griffin, W.L., Belousova, E.A., Shee, S.R., Pearson, N.J., O'Reilly, S.Y., 2004. Archean crustal evolution in the northern Yilgarn Craton: U–Pb and Hf-isotope evidence from detrital zircons. *Precambrian Research* 131, 231-282.
- Griffiths, R.W., Fink, J.H., 1992a. Solidification and morphology of submarine lavas: A dependence on extrusion rate.
- Griffiths, R.W., Fink, J.H., 1992b. Solidification and morphology of submarine lavas: A dependence on extrusion rate. *Journal of Geophysical Research: Solid Earth (1978–2012)* 97, 19729-19737.
- Grove, T.L., Parman, S.W., 2004. Thermal evolution of the Earth as recorded by komatiites. *Earth and Planetary Science Letters* 219, 173-187.
- Gudin, A., Dubinina, E., Nosova, A., 2012. Petrogenesis of variolitic lavas of the Onega structure, Central Karelia. *Petrology* 20, 255-270.
- Harrison, T.M., 2009. The Hadean crust: evidence from > 4 Ga zircons. *Annual Review of Earth and Planetary Sciences* 37, 479-505.
- Harrison, T.M., Schmitt, A.K., McCulloch, M.T., Lovera, O.M., 2008. Early (≥ 4.5 Ga) formation of terrestrial crust: Lu–Hf, $\delta^{18}\text{O}$, and Ti thermometry results for Hadean zircons. *Earth and Planetary Science Letters* 268, 476-486.
- Hawkesworth, C., Cawood, P., Dhuime, B., 2013. Continental growth and the crustal record. *Tectonophysics* 609, 651-660.
- Haymon, R.M., Carbotte, S., Wright, D., Beedle, N., Johnson, F., Fomari, D.J., Von Damm, K., Grebmeier, J., Lilley, M., McLaughlin, E., 1991. Active eruption seen on East Pacific Rise. *Eos, Transactions American Geophysical Union* 72, 505-507.

-
- Hepple, R.A., 2014. The effects of low degree alteration on Sm-Nd and U-Pb isotope systematics in Eoarchean basalts from the Doolena Gap and Warralong Greenstone belts, Pilbara Craton, Western Australia.
- Herzberg, C., Asimow, P.D., 2008. Petrology of some oceanic island basalts: PRIMELT2. XLS software for primary magma calculation. *Geochemistry, Geophysics, Geosystems* 9.
- Herzberg, C., Asimow, P.D., Arndt, N., Niu, Y., Leshner, C., Fitton, J., Cheadle, M., Saunders, A., 2007. Temperatures in ambient mantle and plumes: Constraints from basalts, picrites, and komatiites. *Geochemistry, Geophysics, Geosystems* 8.
- Herzberg, C., Condie, K., Korenaga, J., 2010. Thermal history of the Earth and its petrological expression. *Earth and Planetary Science Letters* 292, 79-88.
- Hickman, A., 1974. Precambrian structural geology of part of the Pilbara region. *West. Aust., Geol. Surv., Annu. Rep.*, 68-73.
- Hickman, A., 1981. Crustal evolution of the Pilbara block, Western Australia. *Spec. Publ. Geol. Soc. Aust* 7, 57-69.
- Hickman, A., 2004. Two contrasting granite– greenstone terranes in the Pilbara Craton, Australia: evidence for vertical< i> and</i> horizontal tectonic regimes prior to 2900Ma. *Precambrian Research* 131, 153-172.
- Hickman, A., 2009. Pilbara Supergroup of the East Pilbara Terrane. Pilbara Craton: updated lithostratigraphy and comments on the influence of vertical tectonics: Geological Survey of Western Australia, Annual Review 2010, 51-59.
- Hickman, A.H., 1983. Geology of the Pilbara Block and its environs. Geological Survey of Western Australia Perth, Western Australia.
- Hickman, A.H., 2008. Regional review of the 3426-3350 Ma Strelley Pool Formation, Pilbara Craton, Western Australia. Geological Survey of Western Australia.
- Hickman, A.H., 2011. Pilbara Supergroup of the East Pilbara Terrane, Pilbara Craton: Updated lithostratigraphy and comments on the influence of vertical tectonics. Geological Survey of Western Australia, Annual Review 2009-2010, 50-59.
- Hickman, A.H., 2012. Review of the Pilbara Craton and Fortescue Basin, Western Australia: crustal evolution providing environments for early life. *Island Arc* 21, 1-31.
- Hickman, A.H., Ladbrook, D., Australia, W., 2010a. Marble Bar. Geological Survey of Western Australia.
- Hickman, A.H., Smithies, R., Tyler, I., 2010b. Evolution of Active Plate Margins: West Pilbara Superterrane, De Grey Superbasin, and the Fortescue and Hamersley Basins—a Field Guide. Geological Survey of Western Australia.
- Hickman, A.H., Van Kranendonk, M.J., Grey, K., 2011. State Geoheritage Reserve R50149 (Trendall Reserve), North Pole, Pilbara Craton, Western Australia: Geology and Evidence for Early Archean Life. Geological Survey of Western Australia.
- Hickman, A.H., 2008. Archean crustal evolution and mineralization of the Northern Pilbara Craton : a field guide. Dept. of Industry and Resources, East Perth, W.A.
- Hofmann, A.W., 1988. Chemical differentiation of the Earth: the relationship between mantle, continental crust, and oceanic crust. *Earth and Planetary Science Letters* 90, 297-314.
- Jakobsen, J. K., Veksler, I. V., Tegner, C., & Brooks, C. K. 2005. Immiscible iron- and silica-rich melts in basalt petrogenesis documented in the Skaergaard intrusion. *Geology*, 33(11), 885-888.

-
- Jolly, W.T., Hallberg, J., 1990. Role of crustal contamination in heterogeneous Archean volcanics from the Leonora region, Western Australia. *Precambrian Research* 48, 75-98.
- Jones, J., 1969. Pillow lavas as depth indicators. *American journal of science* 267, 181-195.
- Kamber, B.S., Whitehouse, M.J., Bolhar, R., Moorbath, S., 2005. Volcanic resurfacing and the early terrestrial crust: zircon U–Pb and REE constraints from the Isua Greenstone Belt, southern West Greenland. *Earth and Planetary Science Letters* 240, 276-290.
- Kato, Y., Nakamura, K., 2003. Origin and global tectonic significance of Early Archean cherts from the Marble Bar greenstone belt, Pilbara Craton, Western Australia. *Precambrian Research* 125, 191-243.
- Kemp, A.I., Hickman, A.H., Kirkland, C.L., Vervoort, J.D., 2015. Hf isotopes in detrital and inherited zircons of the Pilbara Craton provide no evidence for Hadean continents. *Precambrian Research* 261, 112-126.
- Kloppenburg, A., White, S., Zegers, T., 2001. Structural evolution of the Warrawoona Greenstone Belt and adjoining granitoid complexes, Pilbara Craton, Australia: implications for Archean tectonic processes. *Precambrian Research* 112, 107-147.
- Kröner, A., Elis Hoffmann, J., Xie, H., Wu, F., Münker, C., Hegner, E., Wong, J., Wan, Y., Liu, D., 2013. Generation of early Archean felsic greenstone volcanic rocks through crustal melting in the Kaapvaal, craton, southern Africa. *Earth and Planetary Science Letters* 381, 188-197.
- Leverington, D.W., 2014. Did large volcanic channel systems develop on Earth during the Hadean and Archean? *Precambrian Research* 246, 226-239.
- Marshak, S., Alkmim, F., Jordt-Evangelista, H., 1992. Proterozoic crustal extension and the generation of dome-and-keel structure in an Archean granite-greenstone terrane. *Nature* 357, 491-493.
- McKenzie, D., Bickle, M., 1988. The volume and composition of melt generated by extension of the lithosphere. *Journal of petrology* 29, 625-679.
- Monecke, T., Renno, A.D., Herzig, P.M., 2004. Primary clinopyroxene spherulites in basaltic lavas from the Pacific–Antarctic Ridge. *Journal of volcanology and geothermal research* 130, 51-59.
- Moore, J.G., 1965. Petrology of deep sea basalt near Hawaii. *American Journal of Science* 263, 40-52.
- Nebel, O., Rapp, R.P., Yaxley, G.M., 2014a. The role of detrital zircons in Hadean crustal research. *Lithos* 190, 313-327.
- Nebel, O., Campbell, I.H., Sossi, P.A., Van Kranendonk, M.J., 2014b. Hafnium and iron isotopes in early Archean komatiites record a plume-driven convection cycle in the Hadean Earth. *Earth and Planetary Science Letters* 397, 111-120.
- Nelson, D.R., 2000. Metasandstone, Croydon Well. *Compilation of Geochronology Data 1999, June 2007 Update, Geochronology Dataset 327*. Geological Survey of Western Australia, Perth.
- Nelson, D.R., 2001. Crystal-lithic Tuff, Copper Hills. *Compilation of Geochronology Data 1999, June 2007 Update, Geochronology Dataset 222*. Geological Survey of Western Australia, Perth.
- Nelson, D.R., 2005. Lithic Quartz Sandstone, Mount Olive. *Compilation of Geochronology Data 1999, June 2007 Update, Geochronology Dataset 549*. Geological Survey of Western Australia, Perth.

-
- Nesbitt, R.W., Sun, S.-S., Purvis, A.C., 1979. KOMATIITES: GEOGHEMISTRY AND GENESIS. *Canadian Mineralogist* 17, 165-186.
- Pearce, J.A., Cann, J., 1973. Tectonic setting of basic volcanic rocks determined using trace element analyses. *Earth and planetary science letters* 19, 290-300.
- Philpotts, A., 1982. Compositions of immiscible liquids in volcanic rocks. *Contributions to Mineralogy and Petrology* 80, 201-218.
- Philpotts, A.R., 1979. Silicate liquid immiscibility in tholeiitic basalts. *Journal of Petrology* 20, 99-118.
- Philpotts, A.R., 2008. Comments on: Liquid immiscibility and the evolution of basaltic magma. *Journal of Petrology* 49, 2171-2175.
- Polat, A., Appel, P.W., Frei, R., Pan, Y., Dilek, Y., Ordóñez-Calderón, J.C., Fryer, B., Hollis, J.A., Raith, J.G., 2007. Field and geochemical characteristics of the Mesoarchean (~ 3075Ma) Ivisaartoq greenstone belt, southern West Greenland: Evidence for seafloor hydrothermal alteration in supra-subduction oceanic crust. *Gondwana Research* 11, 69-91.
- Polat, A., Frei, R., Appel, P., Dilek, Y., Fryer, B., Ordóñez-Calderón, J., Yang, Z., 2008. The origin and compositions of Mesoarchean oceanic crust: evidence from the 3075 Ma Ivisaartoq greenstone belt, SW Greenland. *Lithos* 100, 293-321.
- Polat, A., Frei, R., Fryer, B., Appel, P.W., 2009. The origin of geochemical trends and Eoarchean (ca. 3700Ma) zircons in Mesoarchean (ca. 3075Ma) ocelli-hosting pillow basalts, Ivisaartoq greenstone belt, SW Greenland: Evidence for crustal contamination versus crustal recycling. *Chemical Geology* 268, 248-271.
- Polat, A., Kerrich, R., 2000. Archean greenstone belt magmatism and the continental growth-mantle evolution connection: constraints from Th-U-Nb-LREE systematics of the 2.7 Ga Wawa subprovince, Superior Province, Canada. *Earth and Planetary Science Letters* 175, 41-54.
- Polat, A., Kerrich, R., 2001. Geodynamic processes, continental growth, and mantle evolution recorded in late Archean greenstone belts of the southern Superior Province, Canada. *Precambrian Research* 112, 5-25.
- Puchtel, I., Blichert-Toft, J., Touboul, M., Walker, R., Byerly, G., Nisbet, E., Anhaeusser, C., 2013. Insights into early Earth from Barberton komatiites: Evidence from lithophile isotope and trace element systematics. *Geochimica et Cosmochimica Acta* 108, 63-90.
- Rakovan, J., 2005. Pillow Basalt. *Rocks & Minerals* 80, 287-287.
- Richter, F.M., 1988. A major change in the thermal state of the Earth at the Archean-Proterozoic boundary: consequences for the nature and preservation of continental lithosphere. *Journal of Petrology*, 39-52.
- Ripley, E. M., Severson, M. J., & Hauck, S. A. 1998. Evidence for sulfide and Fe-Ti-P-rich liquid immiscibility in the Duluth Complex, Minnesota. *Economic Geology*, 93(7), 1052-1062.
- Robin-Popieul, C.C., Arndt, N.T., Chauvel, C., Byerly, G.R., Sobolev, A.V., Wilson, A., 2012. A new model for Barberton komatiites: deep critical melting with high melt retention. *Journal of Petrology* 53, 2191-2229.
- Sandstå, N.R., Robins, B., Furnes, H., De Wit, M., 2011. The origin of large varioles in flow-banded pillow lava from the Hoogenoeg Complex, Barberton Greenstone Belt, South Africa. *Contributions to Mineralogy and Petrology* 162, 365-377.
- Satkoski, A. M., Lowe, D. R., Beard, B. L., Coleman, M. L., & Johnson, C. M., 2016. A high continental weathering flux into Paleoproterozoic seawater revealed by strontium isotope analysis of 3.26 Ga barite. *Earth and Planetary Science Letters*, 454, 28-35

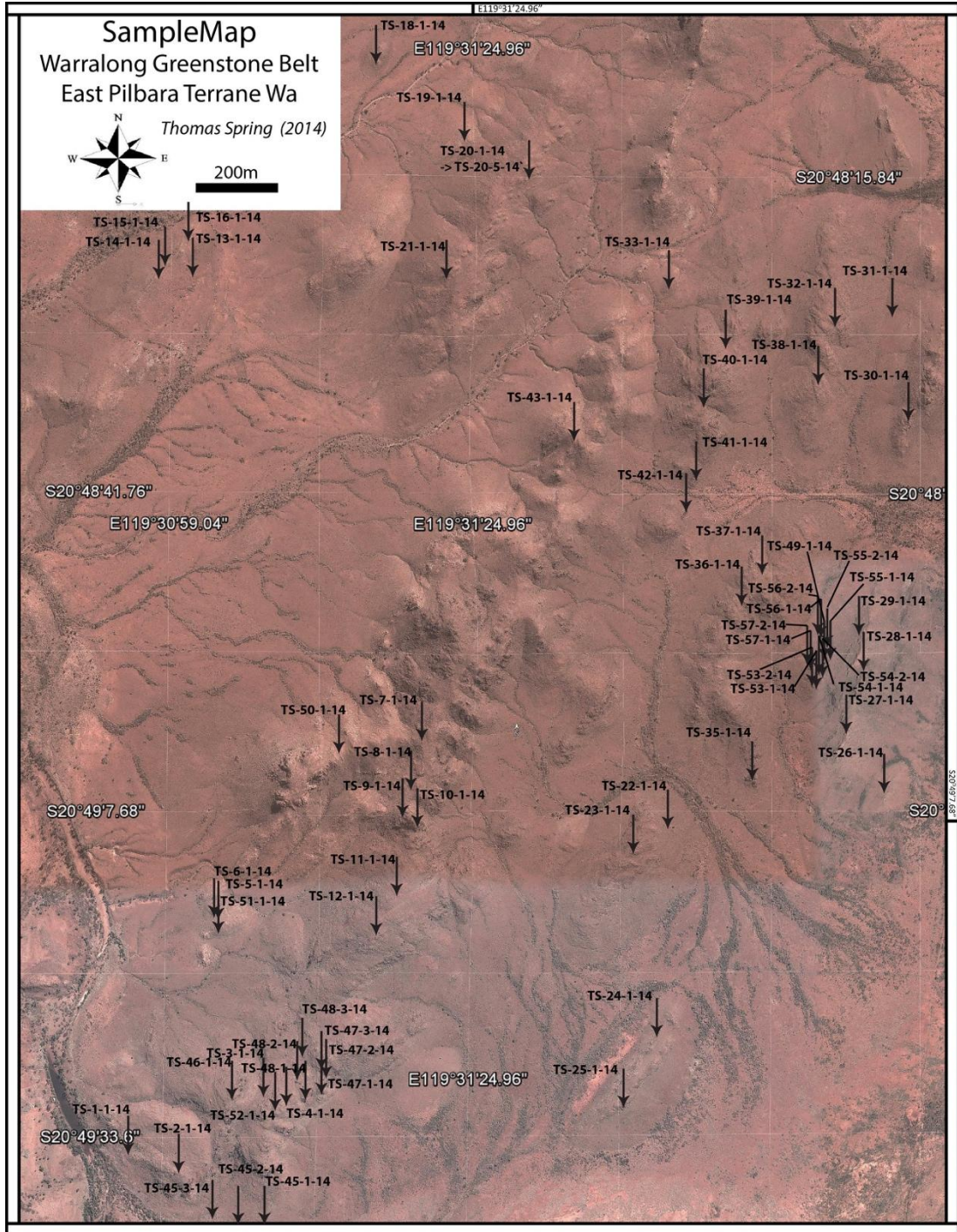
-
- Smithies, R., Champion, D., Cassidy, K., 2003. Formation of Earth's early Archaean continental crust. *Precambrian Research* 127, 89-101.
- Smithies, R., Champion, D., Van Kranendonk, M., 2009. Formation of Paleoproterozoic continental crust through infracrustal melting of enriched basalt. *Earth and Planetary Science Letters* 281, 298-306.
- Smithies, R., Van Kranendonk, M., Champion, D., 2005. It started with a plume—early Archaean basaltic proto-continental crust. *Earth and Planetary Science Letters* 238, 284-297.
- Smithies, R., Van Kranendonk, M., Champion, D., 2007. The Mesoproterozoic emergence of modern-style subduction. *Gondwana Research* 11, 50-68.
- Smithies, R.C., DC; Van Kranendonk, MJ and Hickman, AH. , 2007. **GEOCHEMISTRY OF VOLCANIC ROCKS OF THE NORTHERN PILBARA CRATON WESTERN AUSTRALIA**, in: Resources, G.S.o.W.A.D.o.I.a. (Ed.), .
- Solomatov, V., Moresi, L.N., 1996. Stagnant lid convection on Venus. *Journal of Geophysical Research: Planets (1991–2012)* 101, 4737-4753.
- Sossi, P.A., Eggins, S.M., Nesbitt, R.W., Nebel, O., Hergt, J.M., Campbell, I.H., O'Neill, H.S.C., Van Kranendonk, M., Davies, D.R., 2016. Petrogenesis and Geochemistry of Archean Komatiites. *Journal of Petrology* 57, 147-184.
- Sproule, R., Leshner, C., Ayer, J., Thurston, P., Herzberg, C., 2002. Spatial and temporal variations in the geochemistry of komatiites and komatiitic basalts in the Abitibi greenstone belt. *Precambrian research* 115, 153-186.
- Sugitani, K., 1992. Geochemical characteristics of Archean cherts and other sedimentary rocks in the Pilbara Block, Western Australia: evidence for Archean seawater enriched in hydrothermally-derived iron and silica. *Precambrian Research* 57, 21-47.
- Sugitani, K., Yamashita, F., Nagaoka, T., Yamamoto, K., Minami, M., Mimura, K., & Suzuki, K. 2006. Geochemistry and sedimentary petrology of Archean clastic sedimentary rocks at Mt. Goldsworthy, Pilbara Craton, Western Australia: evidence for the early evolution of continental crust and hydrothermal alteration. *Precambrian Research*, 147(1), 124-147.
- Sugitani, K., Mimura, K., Takeuchi, M., Lepot, K., Ito, S., Javaux, E., 2015. Early evolution of large micro-organisms with cytological complexity revealed by microanalyses of 3.4 Ga organic-walled microfossils. *Geobiology* 13, 507-521.
- Sun, S.-s., McDonough, W.F., 1989. Chemical and isotopic systematics of oceanic basalts: implications for mantle composition and processes. Geological Society, London, Special Publications 42, 313-345.
- Takahashi, E., 1990. Speculations on the Archean mantle: missing link between komatiite and depleted garnet peridotite. *Journal of Geophysical Research: Solid Earth (1978–2012)* 95, 15941-15954.
- Tribble, G.W., 1991. Underwater observations of active lava flows from Kilauea volcano, Hawaii. *Geology* 19, 633-636.
- Van Den Boorn, S. H., van Bergen, M. J., Nijman, W., & Vroon, P. Z. 2007. Dual role of seawater and hydrothermal fluids in Early Archean chert formation: evidence from silicon isotopes. *Geology*, 35(10), 939-942.
- Van Kranendonk, M., 2001. Stratigraphic and tectonic significance of eight local unconformities in the Fortescue Group, Pear Creek Centrocline, Pilbara Craton, Western Australia. *Geological Survey of Western Australia Annual Review* 2002, 70-79.
- Van Kranendonk, M., Hickman, A., Collins, W., 2001. Comment on "Evidence for multiphase deformation in the Archaean basal Warrawoona group in the Marble

-
- Bar area, East Pilbara, Western Australia” by van Haaften, WM, White, SH, 1998: Precambrian Research 88, 53–66. Precambrian Research 105, 73-78.
- Van Kranendonk, M., Morant, P., 1997. Revised Archaean stratigraphy of the NORTH SHAW 1: 100 000 sheet, Pilbara Craton. Western Australia Geological Survey, Annual Review 98, 55-62.
- Van Kranendonk, M.J., 2006. Revised lithostratigraphy of Archean supracrustal and intrusive rocks in the northern Pilbara Craton, Western Australia. Geological Survey of Western Australia.
- Van Kranendonk, M.J., 2010. Geology of Coongan, 1:100 000 Sheet, in: Australia, G.S.o.W. (Ed.).
- Van Kranendonk, M.J., 2001. Archaean Geology of the East Pilbara Granite-greenstone Terrane, Western Australia: A Field Guide. Geological Survey of Western Australia.
- Van Kranendonk, M.J., Bodorkos, S., Wingate, M.T.D., Strong, C., Loan, G., Ladbrook, D., Greenberg, K., Australia, W., 2004a. Coongan. Geological Survey of Western Australia.
- Van Kranendonk, M.J., Collins, W., 1998. Timing and tectonic significance of late Archaean, sinistral strike-slip deformation in the central Pilbara structural corridor, Pilbara Craton, Western Australia. Precambrian Research 88, 207-232.
- Van Kranendonk, M.J., Collins, W., Hickman, A., Pawley, M.J., 2004. Critical tests of vertical vs. horizontal tectonic models for the Archaean East Pilbara granite–greenstone terrane, Pilbara craton, western Australia. Precambrian Research 131, 173-211.
- Van Kranendonk, M.J., Hickman, A.H., Smithies, R.H., Nelson, D.R., Pike, G., 2002. Geology and tectonic evolution of the archaean North Pilbara terrain, Pilbara Craton, Western Australia. Economic Geology 97, 695-732.
- Van Kranendonk, M.J., Philippot, P., Lepot, K., Bodorkos, S., Pirajno, F., 2008. Geological setting of Earth's oldest fossils in the ca. 3.5 Ga Dresser Formation, Pilbara Craton, Western Australia. Precambrian Research 167, 93-124.
- Van Kranendonk, M.J., Pirajno, F., 2004. Geochemistry of metabasalts and hydrothermal alteration zones associated with c. 3.45 Ga chert and barite deposits: implications for the geological setting of the Warrawoona Group, Pilbara Craton, Australia. Geochemistry: Exploration, Environment, Analysis 4, 253-278.
- Van Kranendonk, M.J., Smithies, H.R., Bennett, V., 2007. Earth's oldest rocks. Elsevier.
- Van Kranendonk, M.J., Smithies, R.H., Griffin, W.L., Huston, D.L., Hickman, A.H., Champion, D.C., Anhaeusser, C.R., Pirajno, F., 2015. Making it thick: a volcanic plateau origin of Palaeoarchean continental lithosphere of the Pilbara and Kaapvaal cratons. Geological Society, London, Special Publications 389, 83-111.
- VanTongeren, J.A. and Mathez, E.A., 2012. Large-scale liquid immiscibility at the top of the Bushveld Complex, South Africa. Geology, 40(6), pp.491-494.
- Veksler, I.V., 2004. Liquid immiscibility and its role at the magmatic–hydrothermal transition: a summary of experimental studies. Chemical Geology, 210(1), pp.7-31.
- Veksler, I.V., Dorfman, A.M., Borisov, A.A., Wirth, R., Dingwell, D.B., 2007. Liquid immiscibility and the evolution of basaltic magma. Journal of Petrology 48, 2187-2210.
- Viljoen, M., Viljoen, R., 1969a. Evidence for the existence of a mobile extrusive peridotitic magma from the Komati Formation of the Onverwacht Group. Geological Society of South Africa Special Publication 2, 87-112.

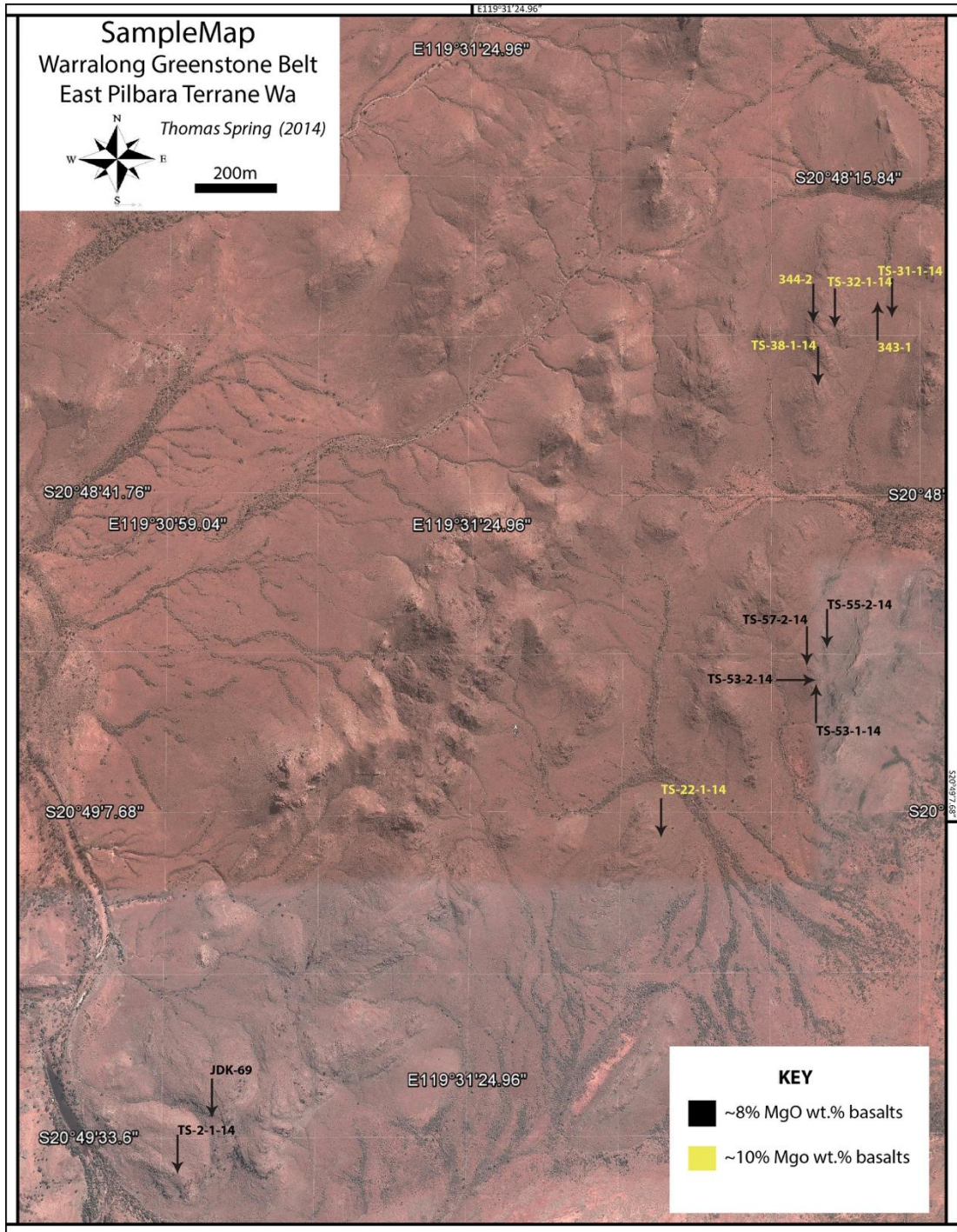
-
- Viljoen, M., Viljoen, R.P., 1969b. The geology and geochemistry of the lower ultramafic unit of the Onverwacht Group and a proposed new class of igneous rocks. Geological Society of South Africa Special Publication 2, 55-86.
- Walter, M.J., 1998. Melting of garnet peridotite and the origin of komatiite and depleted lithosphere. *Journal of Petrology* 39, 29-60.
- Wells, G., Bryan, W.B., Pearce, T.H., 1979. Comparative Morphology of Ancient and Modern Pillow Lavas. *The Journal of Geology* 87, 427-440.
- White, S.M., Haymon, R.M., Fornari, D.J., Perfit, M.R., Macdonald, K.C., 2002. Correlation between volcanic and tectonic segmentation of fast-spreading ridges: Evidence from volcanic structures and lava flow morphology on the East Pacific Rise at 9–10 N. *Journal of Geophysical Research: Solid Earth* (1978–2012) 107, EPM 7-1-EPM 7-20.
- Wiemer, D., Schrank, C. E., Murphy, D. T., & Hickman, A. H. 2016. Lithostratigraphy and structure of the early Archaean Doolena Gap greenstone belt, East Pilbara Terrane, Western Australia. *Precambrian Research*, 282, 121-138.
- Wyman, D.A., 2013. A critical assessment of Neoproterozoic “plume only” geodynamics: Evidence from the Superior Province. *Precambrian Research* 229, 3-19.
- Yoder, H., 1973. Contemporaneous basaltic and rhyolitic magmas. *American Mineralogist* 58, 153-171.
- Yuan, H., 2015. Secular change in Archaean crust formation recorded in Western Australia. *Nature Geoscience*, 8(10), 808-813.
- Zegers, T., White, S., De Keijzer, M., Dirks, P., 1996. Extensional structures during deposition of the 3460 Ma Warrawoona Group in the eastern Pilbara Craton, Western Australia. *Precambrian Research* 80, 89-105.

Appendices

Appendix A Sample Locations



Appendix B High MgO vs Lower MgO Basalt Sample Locations



Appendix C
LOI Results of Basalts and Ocelli from the Eastern Warralong green stone belt

Sample Label	LOI %	Sample Label	LOI%
343-1 Basalt	1.816218	TS-31-1 Ocelli	3.97032
343-1 Ocelli	5.310063	TS-32-1	2.768695
344-2 Basalt	2.649037	TS-37-1	10.65184
344-2 Ocelli	9.012149	TS-38-1	5.242384
69 Basalt	1.653314	TS-39-1	12.02168
69 Ocelli	3.017394	TS-4-1	11.12222
Sample 1 (TS-8-1 duplicate)	13.66849	TS-48-1	12.10918
Sample 2 (TS-53-1 duplicate)	1.944903	TS-52-1	6.172434
Sample 4 (TS-32-2 duplicate)	2.871411	TS-53-1	1.884825
TS-10-1	13.46068	TS-53-2	1.310723
TS-11-1	8.454155	TS-55-2	1.406935
Ts-2-1 Basalt	1.901997	TS-57-2	1.547806
TS-2-1 Ocelli	6.940978	TS-7-1	14.19142
TS-22-1	3.414004	TS-8-1	13.73867
TS-23-1	18.57405	TS-9-1	8.871088
TS-31-1 Basalt	1.527736		

Appendix D
Trace Element Composition of Basalts and Ocelli from the Eastern Warralong green stone belt (ppm).

Element	TS-53-2	TS-55-2	TS-53-1	TS-57-2	JDK 69 Basalt	TS-2-1 Basalt	TS-31-1 Basalt	343-1 Basalt	344-2 Basalt	TS-32-1	TS-22-1	TS38-1	JDK 69 Ocelli	TS-31-1 Ocelli	343-1 Ocelli	TS-2-1 Ocelli	344-2 Ocelli
7 Li	6.82	6.53	6.51	5.82	10.65	9.54	9.07	10.34	10.75	15.09	33.23	21.13	2.29	1.39	1.70	2.32	0.76
45 Sc	30.58	30.68	29.74	31.25	30.90	28.25	33.45	34.19	34.92	35.68	32.50	33.96	29.15	27.91	30.53	30.07	34.72
51 V	215.39	218.11	208.52	217.11	228.24	224.99	248.28	243.89	241.68	275.88	250.01	266.21	130.98	219.33	219.03	187.06	218.44
52 Cr	375.69	444.29	493.95	447.51	504.92	407.80	741.97	762.69	628.64	596.69	544.31	459.19	482.52	748.36	803.20	427.92	646.81
59 Co	49.74	52.08	55.80	53.24	66.23	55.76	65.20	62.63	58.06	64.43	64.77	63.35	36.26	46.37	42.36	42.90	44.05
60 Ni	107.98	114.79	120.31	115.20	160.76	128.45	199.33	188.41	149.87	170.05	159.71	150.35	110.71	143.15	143.95	82.28	45.63
63 Cu	136.79	114.59	122.43	133.73	143.22	141.01	146.76	136.75	117.47	173.50	124.93	177.26	140.41	115.49	109.23	134.55	105.66
66 Zn	65.47	72.61	63.97	65.67	87.53	83.42	87.27	91.03	88.18	113.11	113.57	129.16	53.60	18.42	26.72	78.54	12.88
71 Ga	10.15	10.87	9.78	10.71	11.07	12.14	12.25	12.69	13.16	15.50	15.52	15.19	13.43	12.64	11.26	12.63	14.61
72 Ge	1.65	1.55	1.46	1.67	1.49	1.66	1.47	1.63	1.67	1.58	0.97	1.59	1.68	1.67	1.30	1.02	2.36
85 Rb	13.63	22.65	38.54	9.30	63.70	54.53	24.48	20.81	45.08	52.47	55.91	30.89	66.61	26.84	21.32	47.04	46.79
88 Sr	35.64	33.91	74.38	41.08	117.18	204.50	81.04	89.83	104.26	114.37	28.74	43.30	148.03	143.91	121.51	135.80	256.98
89 Y	20.53	19.97	19.47	19.83	22.88	23.48	22.61	21.85	23.66	26.88	23.41	26.71	58.73	48.14	34.86	44.66	76.64
90 Zr	80.21	77.24	71.82	76.48	93.91	90.48	80.73	76.26	88.54	97.63	86.00	101.55	83.65	67.77	71.29	82.42	82.41
93 Nb	3.02	3.83	2.55	2.05	2.41	1.40	3.63	3.65	4.22	4.48	2.23	4.26	4.39	3.61	3.69	4.15	4.29
95 Mo	0.24	0.22	0.19	0.23	3.38	0.22	1.07	0.19	0.41	0.47	0.27	0.55	0.34	0.43	0.32	0.28	0.33
107 Ag	0.04	0.04	0.04	0.04	0.04	0.04	0.04	0.03	0.04	0.05	0.04	0.05	0.04	0.03	0.03	0.04	0.04
111 Cd	0.07	0.11	0.07	0.06	0.09	0.09	0.12	0.09	0.07	0.09	0.08	0.07	0.10	0.06	0.10	0.14	0.08
118 Sn	0.93	1.00	0.44	0.48	0.86	0.97	1.03	0.81	0.94	1.21	0.00	1.33	0.69	1.05	0.86	0.18	0.94
121 Sb	0.42	0.68	0.23	0.10	0.02	0.05	0.21	0.29	0.30	0.41	0.06	0.20	0.04	0.13	0.13	0.03	0.19
133 Cs	0.54	0.47	0.40	0.90	0.24	0.21	0.12	0.12	0.13	0.15	0.21	0.17	0.33	0.14	0.15	0.31	0.30
137 Ba	101.00	190.86	827.08	45.57	204.74	191.53	148.84	95.12	94.86	178.13	190.72	122.32	86.40	368.57	287.01	61.41	369.48

139 La	6.74	4.87	5.80	5.93	4.58	4.78	5.24	4.98	5.17	5.97	6.07	7.44	28.86	28.29	18.32	21.18	42.21
140 Ce	16.67	12.95	14.19	14.78	13.05	13.53	14.07	13.46	13.83	15.83	15.32	18.75	70.42	68.82	45.25	45.55	91.47
141 Pr	2.44	1.99	2.07	2.17	2.10	2.14	2.12	2.06	2.14	2.43	2.24	2.73	9.28	8.76	5.76	6.09	11.42
146 Nd	11.67	9.97	10.03	10.40	10.80	10.79	10.55	10.31	10.86	12.22	10.94	13.20	41.33	37.61	24.87	26.87	49.46
147 Sm	3.23	2.98	2.92	2.98	3.38	3.31	3.26	3.18	3.31	3.86	3.27	3.91	10.32	8.60	5.80	6.67	11.54
153 Eu	1.02	0.94	1.02	0.91	0.99	1.15	0.96	1.00	1.17	1.42	1.05	1.35	2.71	1.75	1.31	1.72	2.97
157 Gd	3.65	3.40	3.25	3.25	3.86	3.97	3.55	3.62	3.94	4.29	3.74	4.23	10.79	8.67	6.00	7.30	12.80
159 Tb	0.60	0.57	0.57	0.56	0.68	0.69	0.65	0.63	0.69	0.76	0.64	0.76	1.72	1.35	0.95	1.16	1.97
47 Ti	5762.87	5620.41	4957.38	5428.00	6493.94	6002.20	6466.15	6232.98	6557.72	7187.04	6099.72	7245.30	6808.96	6439.03	6166.69	6613.32	6679.40
163 Dy	3.65	3.57	3.47	3.52	4.08	4.14	3.98	3.89	4.22	4.74	4.18	4.68	10.12	7.82	5.57	7.41	11.92
165 Ho	0.77	0.74	0.72	0.73	0.84	0.86	0.83	0.80	0.86	0.97	0.88	0.95	1.99	1.54	1.13	1.55	2.44
166 Er	2.16	2.12	2.02	2.06	2.37	2.42	2.25	2.22	2.42	2.67	2.47	2.67	5.50	4.26	3.15	4.32	6.84
169 Tm	0.31	0.31	0.30	0.31	0.35	0.36	0.33	0.34	0.36	0.40	0.37	0.41	0.78	0.59	0.45	0.61	0.99
172 Yb	1.98	1.94	1.90	1.95	2.27	2.25	2.12	2.13	2.31	2.46	2.27	2.35	4.59	3.47	2.83	3.76	5.98
175 Lu	0.31	0.30	0.28	0.30	0.33	0.35	0.32	0.32	0.34	0.38	0.32	0.37	0.69	0.51	0.43	0.56	0.89
178 Hf	2.00	1.99	1.91	1.99	2.45	2.42	2.13	2.06	2.35	2.59	2.25	2.54	2.36	1.86	1.86	2.19	2.25
181 Ta	0.14	0.24	0.17	0.14	0.15	0.01	0.24	0.24	0.23	0.29	0.14	0.29	0.27	0.20	0.22	0.24	0.26
182 W	0.07	0.11	0.07	0.06	0.00	0.02	0.14	0.00	0.15	0.11	0.05	0.44	0.07	0.26	0.12	0.25	0.09
204 Pb	1.75	1.98	2.60	1.66	1.84	2.52	1.69	1.59	1.60	1.99	0.88	2.03	1.59	2.04	1.77	1.58	2.85
205 Tl	0.11	0.17	0.26	0.08	0.50	0.42	0.19	0.16	0.31	0.33	0.38	0.21	0.50	0.31	0.22	0.37	0.38
232 Th	0.81	0.78	0.72	0.76	0.77	0.77	0.62	0.59	0.71	0.78	0.67	0.79	0.70	0.52	0.53	0.65	0.67
238 U	0.19	0.19	0.18	0.19	0.17	0.17	0.16	0.14	0.17	0.19	0.17	0.19	0.30	0.23	0.23	0.21	0.29
Ti/Dy	1579.47	1572.30	1429.20	1542.07	1593.47	1450.40	1625.91	1600.52	1553.40	1514.69	1457.80	1547.98	672.59	823.48	1107.15	892.55	560.58
Zr/Hf	40.01	38.80	37.51	38.44	38.29	37.45	37.83	37.07	37.61	37.67	38.27	39.96	35.47	36.41	38.39	37.59	36.62
Nb/Ta	20.90	15.82	14.95	15.09	15.97	109.76	15.07	15.51	18.18	15.70	15.73	14.51	16.52	17.70	16.74	17.35	16.30

Th/Nb	0.27	0.20	0.28	0.37	0.32	0.55	0.17	0.16	0.17	0.17	0.30	0.19	0.16	0.14	0.14	0.16	0.16
Nd/Pb	6.69	5.05	3.86	6.27	5.88	4.29	6.25	6.50	6.77	6.14	12.49	6.50	26.00	18.45	14.07	17.04	17.38
Sm/Nd	0.28	0.30	0.29	0.29	0.31	0.31	0.31	0.31	0.30	0.32	0.30	0.30	0.25	0.23	0.23	0.25	0.23
Eu/Eu*	0.90	0.90	1.01	0.89	0.84	0.97	0.86	0.89	0.99	1.06	0.92	1.01	0.78	0.61	0.67	0.75	0.74

Appendix E
Major Element Composition of Basalts and Ocelli from the Eastern Warralong green stone belt (w%)

Element	TS-53-2	TS-55-2	TS-53-1	TS-57-2	JDK 69 Basalt	TS-2-1 Basalt	TS-31-1 Basalt	343-1 Basalt	344-2 Basalt	TS-32-1	TS-22-1	TS-38-1	JDK 69 Ocelli	TS-31-1 Ocelli	343-1 Ocelli	TS-2-1 Ocelli	344-2 Ocelli
SiO ₂	53.89	53.39	54.42	52.72	53.92	52.34	52.13	51.06	51.61	51.60	50.85	52.29	60.97	62.78	59.07	56.70	55.27
TiO ₂	1.02	1.01	1.03	0.99	1.16	1.14	1.07	1.09	1.13	1.15	1.16	1.18	1.16	1.13	1.07	1.15	1.14
Al ₂ O ₃	10.12	10.03	10.28	9.79	9.15	9.69	9.10	9.13	9.66	9.85	9.66	10.08	15.33	12.56	11.93	12.24	12.30
Fe ₂ O ₃	14.04	13.45	13.23	13.23	12.66	12.92	13.90	14.43	13.65	14.50	16.79	15.01	2.74	3.11	3.77	3.76	4.23
MnO	0.19	0.17	0.18	0.18	0.22	0.22	0.22	0.25	0.24	0.26	0.30	0.27	0.10	0.07	0.10	0.26	0.12
MgO	7.99	7.51	7.60	7.80	8.18	8.14	9.79	10.20	9.90	10.31	11.13	10.56	1.61	2.64	4.01	2.98	1.17
CaO	7.55	9.56	8.41	9.91	11.12	12.22	10.48	11.10	10.57	9.25	7.22	8.40	8.47	10.16	12.51	15.20	17.68
Na ₂ O	3.85	4.31	3.97	2.99	0.71	0.65	2.15	1.72	1.63	1.23	0.35	1.02	6.27	5.70	5.94	4.87	4.88
K ₂ O	1.14	0.36	0.69	2.16	2.68	2.48	0.95	0.83	1.43	1.69	2.38	1.00	2.37	1.08	0.86	1.92	1.70
P ₂ O ₅	0.10	0.10	0.10	0.10	0.09	0.09	0.11	0.11	0.10	0.09	0.11	0.11	0.57	0.45	0.43	0.46	0.83
SO ₃	0.10	0.10	0.09	0.12	0.10	0.10	0.07	0.07	0.07	0.05	0.04	0.06	0.38	0.32	0.31	0.44	0.67
LOI	1.31	1.41	1.88	1.55	1.65	1.90	1.53	1.82	2.65	2.77	3.41	5.24	3.02	3.97	5.31	6.94	9.01

Appendix F
Micro Probe analysis of host basalts and ocelli from the Eastern Warralong green stone belt (ppm)

	TS-2-1-14	TS-2-1-14	TS-2-1-14	TS-2-1-14	TS-2-1-14	TS-2-1-14	TS-2-1-14	TS-2-1-14	344	344	TS-31-1-14	TS-31-1-14	TS-31-1-14	TS-31-1-14	TS-31-1-14	TS-31-1-14	TS-31-1-14	TS-31-1-14	TS-31-1-14	TS-31-1-14
	Ocelli	Ocelli	Ocelli	Ocelli	Basalt	Basalt	Basalt	Basalt	Ocelli	Ocelli	Ocelli	Ocelli	Ocelli	Basalt	Basalt	Basalt	Basalt	Ocelli	Ocelli	Basalt
SiO2 WT%	52.59	53.23	51.57	53.16	53.16	53.05	53.67	51.82	50.60	48.31	53.85	49.78	51.86	53.15	53.18	52.61	51.95	51.09	49.95	50.76
TiO2 WT%	0.38	0.22	0.55	0.27	0.32	0.22	0.20	0.53	0.65	0.96	0.15	0.92	0.44	0.34	0.24	0.35	0.57	0.20	0.59	0.70
Al2O3 WT%	2.04	1.37	2.82	1.21	1.46	1.35	0.87	2.21	2.87	4.72	0.76	3.76	2.18	1.51	1.48	1.76	2.25	0.97	2.38	3.09
Cr2O3 WT%	1.16	0.95	0.36	0.88	0.98	0.81	0.73	0.17	0.08	0.01	0.49	0.02	0.42	0.41	1.01	0.47	0.28	0.59	0.10	0.09
FeO WT%	6.65	6.53	8.84	5.99	6.15	6.29	6.60	8.66	9.10	13.36	7.57	12.10	7.19	6.86	6.54	6.52	7.26	5.85	8.40	9.37
MnO WT%	0.15	0.21	0.20	0.18	0.19	0.16	0.20	0.21	0.21	0.33	0.22	0.27	0.23	0.17	0.21	0.18	0.20	0.22	0.22	0.20
MgO WT%	16.15	16.94	15.38	16.55	16.60	16.70	17.91	15.80	14.77	12.30	19.60	13.67	16.74	17.03	18.33	17.18	16.53	18.47	16.58	15.13
CaO WT%	19.61	18.61	18.41	20.08	19.75	19.64	18.05	18.45	18.70	17.88	15.47	17.73	18.17	19.07	17.24	18.87	19.18	18.42	17.75	18.49
Na2O WT%	0.25	0.29	0.31	0.26	0.28	0.26	0.24	0.24	0.27	0.30	0.19	0.30	0.21	0.20	0.20	0.19	0.20	0.21	0.20	0.20
BaO WT%	0.00	0.02	0.00	0.02	0.00	0.09	0.03	0.10	0.00	0.08	0.00	0.00	0.08	0.05	0.00	0.06	0.00	0.08	0.08	0.00
SrO WT%	0.04	0.00	0.00	0.02	0.00	0.00	0.00	0.03	0.03	0.00	0.00	0.00	0.00	0.00	0.00	0.00	0.00	0.00	0.00	0.00
NiO WT%	0.06	0.05	0.00	0.01	0.06	0.08	0.00	0.03	0.03	0.05	0.02	0.03	0.00	0.05	0.14	0.04	0.03	0.06	0.08	0.03
ZnO WT%	0.11	0.07	0.18	0.02	0.04	0.00	0.17	0.16	0.00	0.00	0.00	0.12	0.10	0.12	0.00	0.00	0.08	0.00	0.01	0.04
Total WT%	99.18	98.48	98.63	98.67	99.00	98.64	98.65	98.41	97.30	98.31	98.32	98.69	97.63	98.95	98.57	98.23	98.51	96.16	96.34	98.09
P2O5 WT%	0.00	0.00	0.00	0.01	0.00	0.00	0.00	0.00	0.04	0.04	0.01	0.01	0.01	0.01	0.01	0.01	0.00	0.02	0.03	0.00
SO3 WT%	0.01	0.02	0.00	0.01	0.01	0.00	0.00	0.00	0.00	0.00	0.02	0.02	0.02	0.02	0.04	0.00	0.01	0.01	0.00	0.00
K2O WT%	0.00	0.00	0.00	0.00	0.00	0.00	0.01	0.00	0.00	0.00	0.00	0.00	0.00	0.00	0.00	0.00	0.00	0.00	0.00	0.00